Silver Transport in CVD Silicon Carbide

by

Heather J. MacLean

B.S. Nuclear Engineering
University of Wisconsin-Madison, 1996

SUBMITTED TO THE DEPARTMENT OF NUCLEAR ENGINEERING
IN PARTIAL FULLFILLMENT OF THE REQUIREMENTS FOR THE DEGREE OF

DOCTOR OF PHILOSOPHY IN NUCLEAR ENGINEERING
AT THE
MASSACHUSETTS INSTITUTE OF TECHNOLOGY

June 2004

Signature of Author: _____
Heather J. MacLean
May 24, 2004

Certified by: _____
Ronald G. Ballinger
Associate Professor of Nuclear Engineering
Associate Professor of Materials Science and Engineering
Thesis Supervisor

Accepted by: _____
Dr. Scott A. Simonson
Manager, Space Reactors
Lockheed Martin Corporation
Thesis Reader

Accepted by: _____
Jeffrey A. Coderre
Associate Professor of Nuclear Engineering
Chairman, Department Committee on Graduate Students

Silver Transport in CVD Silicon Carbide

by

Heather J. MacLean

Submitted to the Department of Nuclear Engineering
on May 24, 2004, in partial fulfillment of the requirements
for the degree of Doctor of Philosophy in Nuclear Engineering
at the Massachusetts Institute of Technology

Abstract

Ion implantation and diffusion couple experiments were used to study silver transport through and release from CVD silicon carbide. Results of these experiments show that silver does not migrate via classical diffusion in silicon carbide. Silver release is, however, likely dominated by vapor transport through cracks in SiC coatings.

The results of silver ion implantation in silicon carbide and subsequent annealing at 1500°C place an upper limit on the silver diffusion coefficient in SiC of 5×10^{-21} m^2/s, a value which is roughly 6 orders of magnitude less than the previous values reported in the literature. Silver diffusion should have been easily observable, but was not detected in SiC plates after heat treatments at 1500°C for times ranging between 200 h and 500 h. A detailed investigation of the silver morphology within the SiC both before and after heating showed that silver was immobilized at SiC grain boundaries and did not diffuse along them as expected.

Novel spherical diffusion couples were fabricated containing silver inside shells of either graphite or SiC which were coated with CVD SiC. Mass measurements clearly revealed silver release from the diffusion couples after heating, but no silver was detected during concentration profile measurements in the SiC. Leak testing results, however, gave evidence of the presence of cracks in many of the SiC coatings, which may have provided pathways for silver escape. A simple vapor flow model was applied to estimate crack sizes that would account for silver release from SiC coatings in the current diffusion couples and coated fuel particle tests from the literature. These calculated crack sizes are small enough that they would not have been detected during normal investigation or post-irradiation examination.

A diffusive mechanism has been assumed to control silver transport in silicon carbide based on silver release observations reported previously in the literature, but no direct evidence of silver diffusion has been offered. Additionally, variations in silver release from particle to particle indicate that silver transport does not occur equally in all silicon carbide samples and is not consistent with diffusion. The findings presented in this dissertation are important to coated particle fuel design and fabrication because they indicate that SiC can successfully retain silver but that some SiC coatings permit silver release. Future work must be directed at identifying the pathways for silver release and their root causes in order to prevent silver release from coated fuel particles.

Thesis Supervisor: Ronald G. Ballinger
Title: Associate Professor of Nuclear Engineering and Materials Science Engineering

Acknowledgments

Many people have helped me during my time at MIT. From technical discussions and meetings to lunch breaks and trips away from Cambridge, I owe many thanks to the colleagues and friends who have made the past years memorable.

My advisor, Prof. Ballinger, supported my work at MIT and always had many ideas to share and suggestions to try. I have explored many new paths while working on this project. I would also like to thank the members of my committee, Prof. Kadak, Dr. Kolaya, Dr. Simonson, and Prof. Todreas, for their direction and support. My work was funded, in part, by a research assistantship through the Idaho National Engineering and Environmental Laboratory.

The U.S. Department of Energy sponsored much of this work through the Nuclear Engineering/Health Physics Fellowship program. I would like to thank Lockheed Martin for hosting me during my DOE Fellowship internship. My internship experience introduced me to the national labs and the great people who work at them. The opportunity to work at a national lab and to work with so many incredible people was the highlight of my graduate career and played an important role in my decision to select the national labs at the beginning of my professional career.

I am also grateful for the technical assistance I received from the ATLAS group at Argonne National Laboratory. Dr. Richard Pardo and Rick Vondrasek guided me through ion implantation and made my experiments possible. In addition, Dr. Timothy Antaya at MIT introduced me to ATLAS and helped design the ion implantation rig.

I would like to thank all of the people who made the analysis of my experiments possible. Nathan Lewis performed the AEM analyses; Mike Hanson provided XPS and Auger analyses; and Tony Garrett-Reed performed the STEM analysis and taught me how to use the SEM.

I owe special thanks to my reader and mentor Dr. Scott Simonson. His guidance from the beginning of this project was invaluable and his attention to the "big picture" helped the end of this project become a reality. I can't begin to express my gratitude to my mentor Dr. Lynne Kolaya. She spent countless hours helping me with all manner of questions and helping me learn how to ask the right questions. Lynne's encouragement and reassurance made even the most difficult tasks seem possible.

I have the fondest memories of the friends I've made while at MIT. I would like to thank all of the friends who shared their experiences, their advice, and their lunches with me during my time here. I am deeply indebted to Sara, who welcomed me into her home and was always there to share stories. I am also grateful to have shared many years with Sanjay, a fantastic roommate and a wonderful friend.

None of this would have been possible without the support of my family, who impressed upon me, at an early age, the importance and value of education. Their support, emotionally and, often, financially, helped me achieve my goals through this long process. Their joy in my accomplishments and excitement about the future have sustained me during this process.

My Dad has probably learned more about silver transport than he ever expected to know, but I owe him sincere thanks for his thorough editing of my dissertation and for trying to teach me all of the English I'd forgotten since high school. Any remaining errors are solely mine. Thank you, Dad and Marilyn, for your support and understanding.

I don't think I would have attempted this monumental effort had I not seen my Mom do it first, and I know I would not have succeeded had it not been for her help. Always ready with advice, encouragement, and rewards, my Mom pulled me through the tough times and helped celebrate my achievements.

Though many miles away, David stood by me through the hard times, day by day, always trying to share the load. Thank you, David, for your love and support. As this chapter closes I look forward to starting our new life, together.

Table of Contents

List of Figures

List of Tables

1. Introduction

High efficiency, modular design, and improved safety characteristics are some of the features sparking a renewed interest in high-temperature gas reactors (HTGRs) to generate nuclear power. Higher efficiency reactors provide more power per unit of fuel and produce less spent fuel requiring ultimate disposal in geologic repositories. A modular reactor design allows for shorter construction times, decreasing the cost and economic risk associated with new nuclear power plant construction. As with any nuclear power plant design, safety is of paramount importance and including passive safety features improves plant stability during postulated accident scenarios.

One key feature of the HTGR design is the use of ceramic-coated particle fuel. In this type of fuel a small fuel kernel, typically on the order of 500 μm in diameter, is surrounded by coatings of pyrocarbon (PyC) and silicon carbide (SiC). The set of coatings is designed to retain all of the fission products produced in the individual fuel kernels. In the HTGR then, each coated fuel particle acts as a containment for all of the fission products produced within it and forms the primary defense against fission product release.

Since each fuel particle is important to the integrity of the entire system against fission product release, any fission product release from the coated fuel particle system concerns the reactor designers. Although the evolution of coated fuel particle design has produced a fuel particle that retains most of the fission products, silver release has been observed during operation and testing of apparently intact, coated fuel particles.

Although silver release from SiC-coated fuel particles has been studied for nearly three decades, the mechanisms governing silver transport are not currently understood in detail. An improved knowledge of these mechanisms will lead to a more focused approach to eliminate silver release.

1.1 THE ROLE OF SILICON CARBIDE IN COATED FUEL PARTICLES

Although HTGRs vary in the details of their fuel and plant designs, they share in common a graphite moderated core, helium gas coolant, and fuel elements composed of ceramic-coated fuel particles contained within a graphite matrix. The use of ceramic-coated fuel allows HTGRs to take advantage of higher operating temperatures and improved efficiencies. The basic fuel design employed in HTGRs is the TRISO concept consisting of a fuel kernel surrounded by successive layers of a buffer, inner pyrocarbon (IPyC), silicon carbide (SiC), and outer pyrocarbon (OPyC).[1] The individual layers of the TRISO fuel particle have the following primary characteristics:

Fuel kernel The fuel kernel is typically 250-600 μm in diameter and can consist of any of a variety of fuel materials, the most common being UO_2 and UCO.

Buffer Typical buffer layers are approximately 100 μm thick and consist of low-density pyrocarbon designed to accommodate both fission product release from the fuel kernel as well as fuel kernel swelling during irradiation. Typical buffer densities fall in the range 0.9-1.1 g/cm^3 with the theoretical pyrocarbon density of 2.26 g/cm^3.

IPyC The inner pyrocarbon layer is the first of three dense layers at the heart of the TRISO fuel design, forming the basis of the structural integrity of the fuel particle. The IPyC, on the order of 35-40 μm thick, is the first line of defense against fission product release and is effective at retaining the gaseous fission products (e.g., krypton and xenon). Additionally, the IPyC layer protects the fuel kernel from interactions with the precursors used during SiC deposition.

SiC The silicon carbide layer, on the order of 35 μm thick, provides the primary fission product boundary, included in the TRISO particle fuel design to retain cesium and silver. CVD (chemical vapor deposition) of SiC from the precursor MTS (methyltrichlorosilane, CH_3SiCl_3) at specified conditions results in SiC with densities near the theoretical density of 3.21 g/cm^3.

OPyC The outer pyrocarbon is the same material as the IPyC. In addition to providing a last line of defense against fission product release from the fuel particle, the OPyC also protects the brittle SiC layer during the fuel fabrication process. Furthermore, shrinkage of the IPyC and the OPyC layers during irradiation puts the SiC layer into compression, improving the mechanical stability of the fuel particle during operation.

In the pebble bed reactor, one type of HTGR, usually 11,000-15,000 fuel particles are mixed with a graphite matrix material and formed into 60-mm diameter fuel spheres, also known as pebbles. These fuel pebbles flow through the core, from top to bottom, and are recirculated until they reach a maximum burnup level. Figure 1-1 shows a schematic of the fuel sphere and coated fuel particle system.

In the coated fuel particle system, the PyC and SiC coatings form the first line of defense against fission product release. The PyC coating tends to retain the noble fission gases and the SiC coating is designed to retain the metallic fission products, including cesium and silver.

Silver transport through SiC, long assumed to be controlled by grain boundary diffusion, has been thought to depend on the SiC microstructure. Accordingly, fuel designers have preferred an SiC microstructure with small grains, resulting in tortuous grain boundary paths through the coating, to a microstructure with long columnar grains where a single grain boundary may extend straight through the SiC coating. A single grain boundary connecting the inner and outer SiC surfaces could potentially aid fission product transport through the SiC coating.

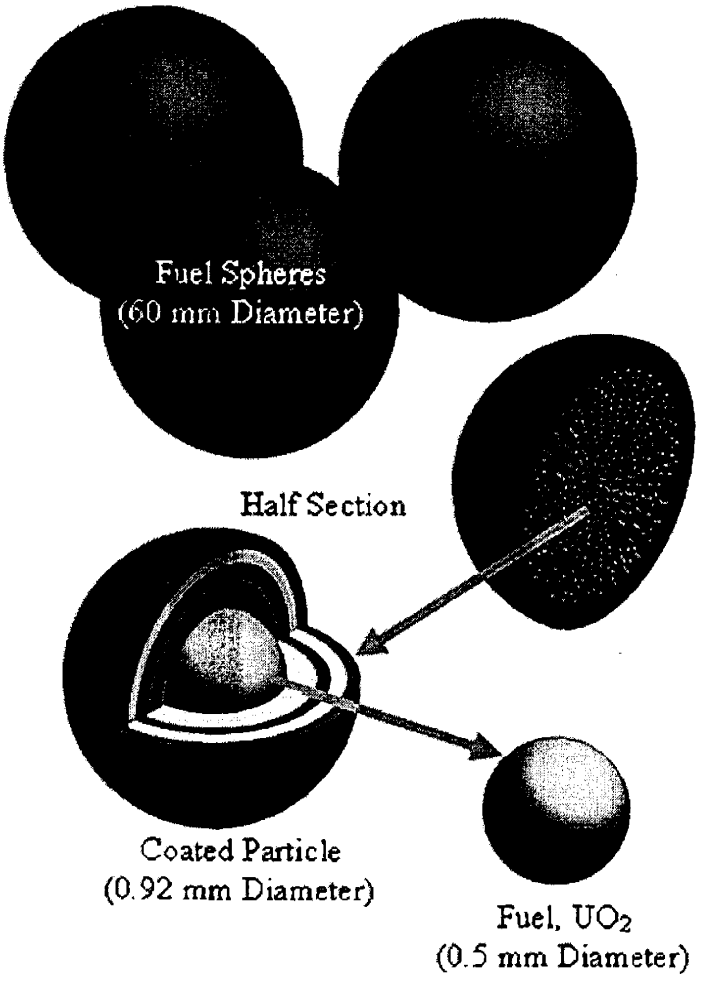

Figure 1-1. Schematic of the coated particle and fuel sphere system (courtesy of Eskom, South Africa).

1.2 SILVER BACKGROUND

The isotope ^{110m}Ag, produced by neutron capture in ^{109}Ag, is the principal long-lived silver nuclide used to monitor release of silver from coated particle fuel.[2] The release of ^{110m}Ag, which has a 253-day half-life, creates concern because it increases the radiation levels in the primary system and increases maintenance complexity. The precursor to ^{109}Ag is the fission product ^{109}Pd with a 13.5-hour half-life which decays to ^{109}Ag via β decay.[3,4] Although both ^{109}Ag and ^{110m}Ag are actually activation products, rather than direct fission products, they are commonly categorized as fission products for convenience in the literature and will be done so here.[5] The fission yield of ^{109}Ag from ^{239}Pu (produced by neutron capture in ^{238}U) is more than one order of magnitude greater than for ^{235}U, so that the production of ^{110m}Ag is greater in low-enriched fuels compared to high-enriched fuels.[2] Table 1-1 shows the ^{109}Ag fission yield from some fissile isotopes.

Table 1-1. ^{109}Ag production from plutonium fuels is much greater than from uranium.[6]

Isotope	^{233}U	^{235}U	^{239}Pu
Effective Fission Yield (%)	0.04	0.03	1.2

Silver release from TRISO fuel particles poses a concern to reactor designers because any silver that escapes from fuel particles will condense on the structural materials or equipment within the reactor. Silver release will, therefore, increase activity levels inside HTGR systems, creating potential health and safety hazards to plant personnel during system maintenance.

Previous experiments, reported in the literature, focused on the total release of silver from coated particle fuel. The overall goal of many of these experiments was to characterize the effective silver release for safety calculations and plant dose levels. Many of the previous experiments measured silver release from fuel elements or large batches of particles, and calculated effective diffusion coefficients. Only a few of these experiments, however, have looked at the release of silver from individual particles and none has focused directly on the fundamental mechanism of silver transport through silicon carbide. The ability of coated fuel particles to retain metallic fission products, notably silver and cesium, during HTGR operation is a significant concern because release of these fission products to the reactor coolant system and the absorption or condensation of them in other plant components can create health and safety hazards to plant personnel.[7]

Under typical Dragon reactor and AVR operating conditions, only 0.1% of the ^{109}Ag atoms are converted to ^{110m}Ag, but with a gamma-ray dose rate five times higher than that for ^{137}Cs, ^{110m}Ag is considered a "key fission product."[6] In addition to preventing the release of ^{131}I, ^{134}Cs, and ^{137}Cs for radiological health reasons, a criterion in reactor design is the accessibility and maintainability of reactor components. Release of ^{110m}Ag increases activity levels of reactor components resulting in higher doses to maintenance workers and requiring more decay time before work on reactor components can begin after a shutdown.

By demonstrating the integrity of the TRISO fuel particle, HTGR designers hope to avoid the need for a full containment building. In order to satisfy the safety requirements, each fuel particle must retain its inventory of fission products. The potential for release of any fission products, including silver, may contribute to the requirement of an expensive containment building.

Results of previous experiments, reported in the literature, clearly show silver release from apparently intact SiC-coated fuel particles. These results have often been explained in terms of diffusion with the range of silver diffusion coefficients in SiC spanning almost 2 orders of magnitude. Although diffusion provides a convenient form for representing silver release results and comparing different fuels and different experiments, there is disagreement within the community as to the exact cause of silver transport in SiC.

Efforts to reduce and eliminate silver release from SiC-coated fuel particles rely on an accurate understanding of the transport mechanisms governing silver release. A better understanding of silver transport pathways through silicon carbide will allow a more focused effort at preventing silver release.

1.3 THESIS OBJECTIVE

The goal of this dissertation is to develop a better understanding of the mechanisms governing silver transport in CVD silicon carbide. No previous studies have positively witnessed the silver transport mechanism in SiC but authors have attributed silver release to diffusion. New evidence, however, from the work in this dissertation questions the mechanism of diffusion. A better

understanding of which phenomena govern silver transport and which do not is vital to improving SiC performance and silver retention. Many observations of silver release from SiC-coated fuel particles have been reported, but measurements of characteristic concentration profiles, expected as a result of diffusion, have not been attempted.

1.4 OUTLINE AND KEYPOINTS

Chapter 2 presents a detailed assessment of the silver diffusion and release data available in the literature, reviewing the types of experiments performed, their results, and uncertainties. A comprehensive examination of the experimental arrangements and assumptions in the previous studies is included in this chapter. The literature review highlights the uncertainty within the community regarding the exact silver transport mechanism. Additionally, the literature suggests that variations in reported diffusion coefficients are due to variations in the total silver path length through the individual SiC coatings. An examination of the relationship between the diffusion coefficient and the path length, however, shows unreasonable path lengths would be required to explain the 2 orders of magnitude variation in the silver diffusion coefficient. A reassessment of some of the literature data shows that total silver inventory release from a few particles within a batch is a plausible alternative to the assumed small and uniform releases from all of the particles within a batch.

The results of silver ion implantation in silicon carbide and subsequent heating are presented in Chapter 3. Silver diffusion should have been easily observable, but was not detected in SiC after heat treatments at 1500°C for times ranging between 200 h and 500 h. The lack of any measurable silver concentration profile change places an upper limit on the silver diffusion coefficient in SiC of approximately 5×10^{-21} m^2/s, roughly 6 orders of magnitude less than the previous values reported in the literature. Furthermore, the silver diffusion path was expected to be visible in the SiC after heating. The results of the silver concentration profiles both before and after heating are presented along with a detailed investigation of the silver morphology within the SiC both before and after heating.

The results of spherical diffusion couple experiments are presented in Chapter 4. A novel spherical diffusion couple contained silver inside shells, either graphite or SiC, which were coated with CVD SiC. Mass measurements clearly revealed silver release from the diffusion couples after heating, but concentration profiles did not detect any silver. Leak testing results, however, gave evidence of the presence of cracks in many of the SiC coatings, which may have provided pathways for silver escape.

Chapter 5 takes a new look at both the current experimental data and previous silver release data reported in the literature. A simple vapor flow model provides estimates of crack sizes that would account for silver release from SiC coatings in the current diffusion couples and coated fuel particle tests from the literature. These crack sizes are small enough that they would not have been detected during normal investigation or post-irradiation examination. Silver release is, therefore, concluded to be most likely dominated by vapor transport through cracks in the SiC coating. Improved retention of other fission products, such as cesium, krypton, and xenon, relative to silver, in fuel kernels and PyC coatings provides a possible explanation of why those fission products are not released even when cracks in the SiC coating are present.

Finally, Chapter 6 summarizes the findings of this dissertation and presents some ideas for future work to further enhance understanding of silver transport and improve silver retention in CVD SiC.

1.5 REFERENCES

[1] G.H. Reynolds, J.C. Janvier, J.L. Kaae, J.P. Morlevat, "Irradiation Behavior of Experimental Fuel Particles Containing Chemically Vapor Deposited Zirconium Carbide Coatings," *J. Nucl. Mater.* **62** (1976) 9-16.

[2] P.E. Brown, R.L. Faircloth, "Metal Fission Product Behaviour in High Temperature Reactors—UO_2 Coated Particle Fuel," *J. Nucl. Mater.* **59** (1976) 29-41.

[3] D. Kocher, *Radioactive Decay Data Tables: A Handbook of Decay Data for Application to Radiation Dosimetry and Radiological Assessments*, Technical Information Center, U.S. Department of Energy, 1981.

[4] C.M. Lederer, V.S. Shirley, *Table of Isotopes*, 7th ed., New York: John Wiley and Sons, Inc., 1978.

[5] R.E. Bullock, "Fission-Product Release During Postirrdiation Annealing of Several Types of Coated Fuel Particles," *J. Nucl. Mater.* **125** (1984) 304.

[6] H. Nabielek, P.E. Brown, P. Offermann, "Silver Release from Coated Particle Fuel," *Nucl. Tech.* **35**, 483-493 (1977).

[7] J.W. Ketterer, M.J. Kania, R.E. Bullock, I.I. Siman-Tov, *Capsule HRB-15A Postirradiation Examination Report*, GA-A16758, July 1984.

2. Silver Transport Literature Review and Assessment

A review of the literature on the topic of silver transport in CVD silicon carbide reveals a wide range of experiments and results. Many authors have interpreted silver release as diffusion through SiC coatings and have reported effective diffusion coefficients. No direct evidence, however, of diffusion has been presented (for example, characteristic concentration profiles). The following review highlights the variation and uncertainty in the literature regarding the results of silver release tests and the exact mechanisms governing silver transport in SiC.

2.1 INTRODUCTION

In many previous tests, coated fuel particles were irradiated, often at low temperatures to prevent fission product migration, and then heated, out-of-pile, to measure fission product release. Various measurement techniques were used to evaluate fission product migration and release including on-line gas measurement systems, gamma counting for fission product inventory, periodic analysis of fission product plate-out on cold traps, and electron microscopy.

Experimenters often selected heating temperatures to represent typical HTGR operating conditions. However, some experiments were conducted at elevated temperatures to either simulate accident conditions or to accelerate fission product release. Bullock selected annealing temperatures between 1200°C and 1500°C, above those expected during operation, in order to accelerate the diffusive release of fission products.[1] While high-temperature testing may be more aggressive than typical operating temperatures during irradiation, it does allow experimenters the ability to obtain relative comparisons between different fuel types in a more efficient manner.

Fuel particles retain fission products either by forming chemically stable compounds in the fuel kernel or in one of the coating layers or by preventing diffusion through the coating layers. Fission products that do not form stable compounds in the fuel particle are thought to diffuse through the coating layers. If the diffusion rate is sufficiently slow, the fission products will remain in the fuel particle during operation. If the diffusion rates are fast enough, however, fission products may escape, depending on the temperature and duration of operation.

Diffusion is generally reported as an Arrhenius equation of the form:

$$D = D_o \cdot \exp\left(\frac{-Q}{R\,T}\right) \tag{2-1}$$

where D = diffusion coefficient (m^2/s),
D_o = pre-exponential constant (m^2/s),
Q = activation energy (J/mol),
R = universal gas constant (8.314 J/mol·K), and
T = absolute temperature (K).

The two most common types of silver experiments encountered in the literature are batch experiments in which the total fission product release from a population of particles is measured,

and individual experiments in which the fission product inventory of each fuel particle is measured before and after heating.

In batch experiments, cold plates typically collect metallic fission products released from a large population of fuel particles or even whole fuel elements (pebbles or compacts). Periodic analysis, typically gamma-counting, of the cold plates reveals any condensed metallic fission products released from the entire population of particles. Sweep gas monitoring during these heating experiments detects catastrophic particle failure by detecting pulses in release in the sweep gas stream characteristic of fission gas release accompanying through-coating particle failure.

Although batch measurements during heating experiments can document the overall behavior of a large population of fuel particles, these measurements do not give any insight into individual particle behavior. Attempts to measure individual fuel particle inventories are reported in the literature, but are limited by the time and resources required to separately examine each individual particle. For this reason, individual fission product inventory measurements tend to only survey a limited number of fuel particles, on the order of 10-25 per test. While these individual measurements may supply more detailed information about particle performance, they are hampered by poor statistics, using only a small number of particles to characterize large batches of fuel with greater than 3×10^9 particles proposed for a single HTGR core. Similar to bulk measurements, individual particle inventory measurements also do not reveal the specific release pathway.

2.2 BATCH MEASUREMENTS

Many experiments have used fission product release measurements from a large batch of particles during post-irradiation heating to gather information on overall fuel performance. Common measurements include on-line monitoring of fission gas release in the sweep gas system and periodic gamma counting of the metallic fission products condensed on a cold plate assembly. In batch testing, large populations of fuel particles, either loose or bonded in fuel elements, are heated together and the total amount of released fission products is measured. Using analytical and numerical solutions for diffusion and release from spherical shells, researchers calculate effective diffusion coefficients in the different layers.

2.2.1 Assumptions

An inherent assumption when evaluating fuel performance from batch measurements is that all of the fuel particles within the batch behave the same. Fission gas release values can be used to estimate the number of individual failed particles by comparing the amount of fission gas released to the estimated average particle inventory. In most cases, however, solid fission product collection on cold plates is attributed to all particles equally.

2.2.2 Silver Diffusion in UO_2

Silver release from fuel kernels in coated particles via diffusion largely determines the amount of silver available to escape through the rest of the coatings. Any silver retained in the fuel kernel itself will not be released from the fuel particle. Several studies have measured silver diffusion from UO_2 fuel kernels either from bare kernels or from BISO particles coated with a buffer and a single pyrocarbon layer.

Nabielek et al. determined the diffusion coefficient of silver in UO_2 as:

$$D'_{UO_2} = 5.49\times10^{-2}\cdot\exp\left(\frac{-213\,\frac{kJ}{mol}}{RT}\right)s^{-1}$$
$$D'_{UO_2}\left(1500^oC\right) = 2.68\times10^{-8}\ s^{-1} \tag{2-2}$$

where D' is the reduced diffusion coefficient, equal to the diffusion coefficient divided by the grain size, a, squared.[2]

$$D' = \frac{D}{a^2} \tag{2-3}$$

From a separate set of experiments, Nabielek et al. determined a slightly lower silver diffusion coefficient in UO_2 at 1500°C:

$$D'_{UO_2}\left(1500^oC\right) = 9.3\times10^{-9}\ s^{-1} \tag{2-4}$$

Brown and Faircloth also measured silver diffusion in UO_2 using radiochemical analysis to measure the silver content of fuel kernels after irradiation and comparison to the calculated inventory based on the irradiation conditions.[3] Testing fuel irradiated between 1000°C and 1400°C, Brown and Faircloth derived the following reduced diffusion coefficient for silver in UO_2 fuel:

$$D'_{UO_2} = 3.80\cdot\exp\left(\frac{-269\,\frac{kJ}{mol}}{RT}\right)s^{-1} \tag{2-5}$$

Since the buffer and pyrocarbon layers do not retain silver (as discussed in section 2.2.3), Förthmann et al. measured silver release from PyC-coated particles at 1400°C and determined the kernel release using the equivalent sphere model.[4] In this model, also known as the Booth model, the fuel kernel is assumed to consist of spherical grains of equal radius. The equivalent sphere model also assumes that when diffusing atoms reach the surface of a spherical grain they are able to move rapidly along grain boundaries; only the spherical grains, not the grain boundaries, slow atom transport in this model.

$$D_{UO_2}\left(1400°C\right) = 6.9\times10^{-15}\ \frac{m^2}{s} \tag{2-6}$$

According to Förthmann et al. the time dependence of fractional release from SiC-coated particles contains two contributions: 1) spontaneous release described by the Booth model, and 2) diffusion-controlled release starting after a breakthrough time. No explanation is offered for the observation of spontaneous silver release.

2.2.3 No Silver Retention in PyC

It is well accepted in the literature that pyrocarbon layers do not retain silver. Nabielek et al. compared silver release from bare kernels and BISO particles, those containing a fuel kernel surrounded only by buffer and PyC layers. From these results Nabielek et al. concluded there is no silver holdup in low-density graphite buffers or in any type of pyrocarbon.[2] Additionally,

Nabielek et al. found that graphite matrix materials also do not retard silver at temperatures above 850°C.

Offermann derived the following diffusion coefficient for silver in pyrocarbon after implanting silver in flat pyrocarbon samples and heating at constant temperatures between 450°C and 800°C:[5]

$$D_{PyC} = 1.00 \times 10^{-8} \cdot \exp\left(\frac{-164 \frac{kJ}{mol}}{RT}\right) \frac{m^2}{s} \tag{2-7}$$

McCardell et al. extrapolated this fit to 1250°C, typical of fuel operating temperatures, and determined that breakthrough times for silver in pyrocarbon are on the order of hours.[6] This indicates that PyC does not function as a barrier to silver release during normal operation.

Verfondern et al. summarized the diffusion coefficients reported from a variety of sources.[7] Two diffusion coefficients for silver in pyrocarbon are listed below with the source country (research program) in brackets:

$$D_{PyC} = 5.3 \times 10^{-9} \cdot \exp\left(\frac{-154 \frac{kJ}{mol}}{RT}\right) \frac{m^2}{s} \text{ [FRG, USA]} \tag{2-8}$$

$$D_{PyC} = 5.3 \times 10^{-4} \cdot \exp\left(\frac{-193 \frac{kJ}{mol}}{RT}\right) \frac{m^2}{s} \text{ [Russian Fed.]} \tag{2-9}$$

The three diffusion coefficients for silver in PyC discussed above are plotted as a function of temperature in Figure 2-1.

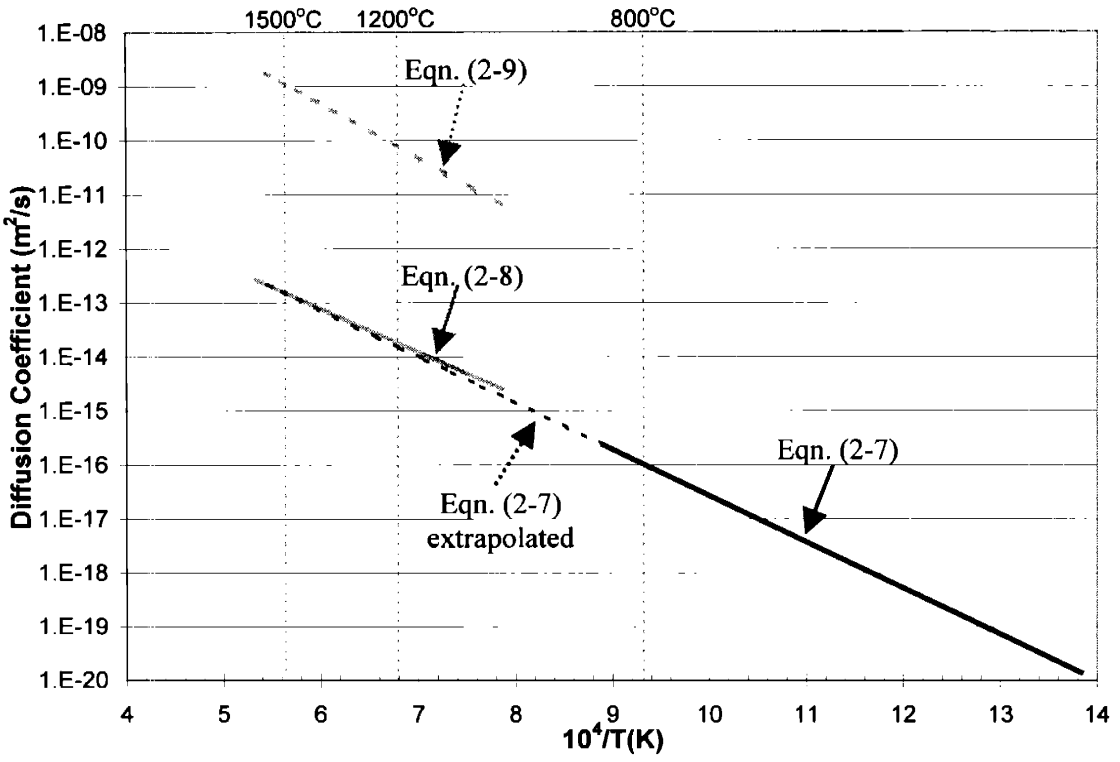

Figure 2-1. Diffusion coefficients for silver in pyrocarbon.

The breakthrough time through a thin spherical shell can be approximated from the following relationship:

$$D = \frac{x^2}{6t_o} \tag{2-10}$$

where D is the diffusion coefficient (m^2/s), x is the shell thickness (m), and t_o is the breakthrough time (s) (the time when the diffusing atoms reach the outer surface of the shell).[1] At 1500°C, the relationship shown in Equation (2-10) predicts silver breakthrough from a 40-μm thick PyC shell in approximately 30 min using the diffusion coefficients in Equations (2-7) and (2-8) and in less than 1 s using the diffusion coefficient shown in Equation (2-9). These estimated breakthrough times through PyC coatings are short enough that diffusion through PyC layers is usually neglected; any silver released from the fuel kernel is assumed to migrate directly to the inner surface of the SiC coating.

2.2.4 Silver Transport in Silicon Carbide

Observations recorded during previous testing have suggested that silver migration in coated fuel particles is governed by diffusion through intact silicon carbide layers. This conclusion has been driven by results of silver release from coated particles while the volatile fission gases and cesium are still retained. Through-coating failures, where both pyrocarbon layers and the silicon carbide layer have failed and the fuel kernel is exposed, result in the release of the fission gases and any other mobile fission product. At typical operating and testing temperatures cesium and silver escape from fuel particles with through-coating failures.

To date, the literature data has been interpreted as representing diffusion-controlled release of silver through intact silicon carbide layers. Observations of silver release with cesium retention suggest rapid silver diffusion through intact silicon carbide layers. If the silicon carbide layer were not intact, both cesium and silver should escape. Additionally, activation energies calculated for silver diffusion coefficients in silicon carbide (derived from silver release measurements) fall in the same range as activation energies for grain boundary diffusion of other fission products.[8] Thus, the current interpretation of silver migration data indicates that silver diffuses along grain boundaries in intact silicon carbide at typical operating temperatures. Variations in the diffusion coefficients reported, however, are not consistent with grain boundary diffusion and other observations, described below, raise doubts about diffusion as the dominant silver transport mechanism.

Nabielek et al. measured silver release from a variety of fuel particles during irradiations and posit-irradiation anneals. Silver detected by gamma-ray spectrometric measurements in fuel tubes and other graphite components was interpreted as release due to diffusion. By measuring the fractional release of silver from a variety of coated particle types, in both loose and elemental form, between 850°C and 1500°C, Nabielek et al. derived an upper limit of the effective diffusion coefficient for silver in silicon carbide:[2]

$$D_{SiC} = 6.76\times10^{-9}\cdot\exp\left(\frac{-213\,\frac{kJ}{mol}}{RT}\right)\frac{m^2}{s} \qquad (2\text{-}11)$$

Nabielek et al. also heated 170 previously irradiated TRISO fuel particles at 1500°C and measured the total fission product release every 10 days. While cesium and strontium were retained in the TRISO particles, silver release began after 10 days. According to the authors, however, the shape of the release curve with heating time is not consistent with silver diffusion in SiC. At the beginning of the heat treatment silver release matched the characteristic release curve corresponding to a diffusion coefficient of 10^{-16} m^2/s, but as the heat treatment progressed the silver release corresponded to a diffusion coefficient of 10^{-15} m^2/s. The authors suggested instead that the silicon carbide became gradually "transparent" during heating allowing increased silver release. Although a physical mechanism for this apparent change in the SiC properties during the heat treatment was not proposed, this finding suggests that silver release is not dominated by a classical diffusion mechanism

In other irradiation experiments performed by Nabielek et al. a very steep increase in silver release was noted between 1140°C and 1240°C in both the shorter and longer duration experiments.[2] These results indicate that SiC may only perform as an effective barrier to silver release at temperatures below 1200°C.

Brown and Faircloth compared silver release behavior from BISO and TRISO particles. While the BISO particles exhibited rapid silver release starting at the beginning of the annealing period, the silicon carbide layer in the TRISO particles prevented silver breakthrough for 16 days at 1500°C.[3] Brown and Faircloth determined an effective diffusion coefficient for silver in SiC from the breakthrough time:

$$D_{SiC}(1500°C) = 1.5\times10^{-16}\,\frac{m^2}{s} \qquad (2\text{-}12)$$

Amian and Stöver measured silver and cesium release from loose particles that had been previously irradiated at temperatures varying from <<400°C to 1050°C. Other irradiation parameters included a burnup range between 2.3% and 12.1% FIMA and a fast fluence range from $<0.5\times10^{23}$ n/m^2 to 8.2×10^{23} n/m^2. Different particle types had different fuel kernel materials with slight variations in coating dimensions. Water-cooled cold plates in the furnace collected released silver and were removed and counted periodically during heat treatments. Fractional release results were interpreted using Fickian diffusion theory and evaluated with a simple diffusion model with multizone geometry to estimate diffusion coefficients for each heat treatment. Combining all of the results, Amian and Stöver derived a diffusion coefficient for silver in silicon carbide[8]:

$$D_{SiC} = 4.5\times10^{-9}\cdot\exp\left(\frac{-218\,\frac{kJ}{mole}}{RT}\right)\frac{m^2}{s} \qquad (2\text{-}13)$$

Figure 2-2 shows this diffusion coefficient along with the diffusion coefficients listed for each batch test. The diffusion coefficients cover a span greater than one order of magnitude at any given temperature. At 1000°C, the 95% confidence region for this diffusion coefficient is between 2×10^{-18} m^2/s and 1.5×10^{-17} m^2/s.

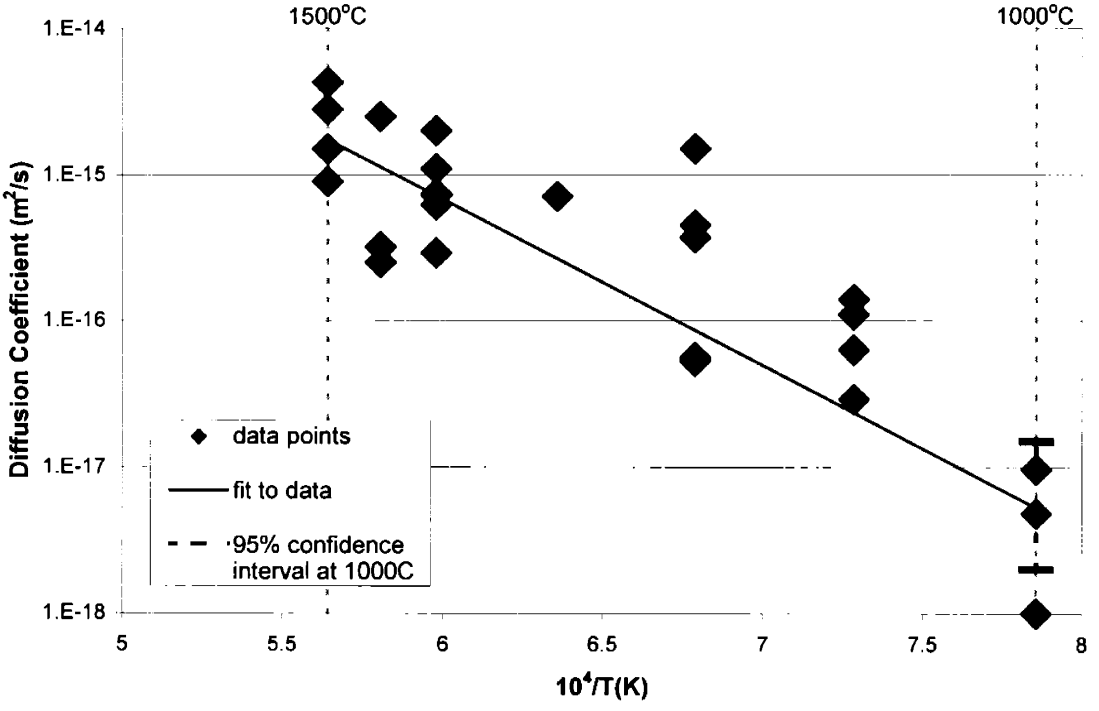

Figure 2-2. The calculated diffusion coefficients from Amian and Stöver's post-irradiation annealing tests exhibit scatter up to a factor of 30.

Total silver release values were normalized to the estimated silver inventory before heating to calculate the fractional release. Amian and Stöver attribute scatter in the diffusion coefficient results to variations in the specific silicon carbide microstructure, which varies from coating to coating. Within the range of burnup and fast fluence of the tested fuels, the authors found no dependence of silver diffusion on those variables within the intrinsic scatter of the data.[8]

According to Amian and Stöver, activation energies for diffusion in pyrolytically deposited SiC coatings are approximately 200 kJ/mol while the activation energies for diffusion in single crystals are about 450 kJ/mol.[8] Given the results of the experiments performed by these authors, these data (and the diffusion coefficient proposed) suggest that the mechanism responsible for silver diffusion in SiC is grain boundary diffusion in the polycrystalline material, not volume diffusion through grains. A grain boundary diffusion mechanism also accounts for the large scatter in the data, according to the authors. Grain boundary diffusion depends on the exact microstructure of the sample, which varies from sample to sample. Grain boundary diffusion is a collection of "different elementary processes" with different activation energies. Since each sample has a different microstructure, there will be scatter in the data reflecting the exact microstructure of each sample (the exact path of Ag transport through a given set of SiC grains). As discussed in Section 2.4.1, however, the scatter in the reported data exceeds the expected variations in SiC structure and the silver path length traveled through the SiC coatings.

Bullock measured the cumulative release of silver and other fission products at three temperatures from five types of previously irradiated fuel. TRISO coatings formed the basis of the five types of fuel, but three variations in the fuel kernel material and two variations to the TRISO coating constituted the experimental base. The five types of fuel denoted by their fuel kernel material include UO_2; UC_2; UCO, a mixture of UO_2 and UC_2; $UO_2^*(1)$, UO_2 with a solid ZrC overcoating on the kernel; and $UO_2^*(2)$, UO_2 with ZrC dispersed in the buffer layer. Three sets of ten particles of each fuel type were selected to be heated at three temperatures: 1200°C, 1350°C, and 1500°C. Fission products released during annealing condensed on the mullite sleeve or tantalum tube in the furnace. By periodically removing these components from the furnace and counting them with a gamma detector, Bullock collected fission product release data as a function of time during the greater than 10,000-hour tests.[1]

These heating experiments revealed a strong temperature dependence: as the temperature increased, the fission product breakthrough times decreased dramatically. The breakthrough times also appeared to depend on the type of fuel particle tested. The $UO_2^*(1)$ particles did not release any fission products during the annealing tests while the other particle types all released silver with breakthrough times varying from about 30 h to 8,000 h. Each batch, however, consisted of only ten particles and one must exercise caution when drawing conclusions about large population behavior from only a few particles.

The fairly long delay times, in general, before silver release do suggest that no silver escaped during irradiation. Silver escape during irradiation would have (most likely) required silver distribution throughout the particle. If that were the case, silver escape during heating would have occurred much sooner. This does raise concern about the knowledge of the silver distribution before heating began. The silver concentration at the beginning of heating must be assumed in order to accurately calculate the diffusion coefficients from release measurements. If these data are uncertain, however, the uncertainty of the diffusion coefficient will increase.

Schenk and Nabielek conducted post-irradiation annealing of 60 mm diameter spherical fuel elements, with 16,400 particles per element, between 1600°C and 1800°C. Seven fuel elements with low-enriched UO_2 with TRISO coatings were irradiated and heated. During irradiation these elements experienced a range of burnup from 3.5% to 10.6% FIMA, fast fluence from 0.2×10^{23} n/m^2 to 5.9×10^{23} n/m^2, a mean irradiation temperature of 700°C to less than 1280°C, and durations from 350 to 1200 full power days.[9] The fission product content of each spherical element was measured before and after heating. In addition, electrolytic deconsolidation of the elements after heating exposed individual fuel particles, which could be selected from specific locations of the element and further analyzed.

During heating, a water-cooled cold finger with a removable condensation plate collected released fission products. Analysis of the condensation plate determined the quantities of ^{137}Cs, ^{90}Sr, and ^{110m}Ag. Analysis of the matrix graphite from the fuel elements after electrolytic deconsolidation also determined fission product release. All seven fuel elements released a greater fraction of their silver inventory than any other fission product. The high release of silver from these fuel elements was attributed to its high mobility in silicon carbide, but Schenk and Nabielek did not calculate any diffusion coefficients from these results.

Schenk and Nabielek derived the fractional release values by comparing the total amount of silver released during heating (as trapped on the cold plate) with the measured inventory before heating. If one looks, however, at the reported values from a different perspective, one can calculate the number of failed particles necessary to release the same amount of silver. With 16,400 particles per element, if one particle lost its entire silver inventory, the effective fractional release would be 6.1×10^{-5}. Using this base value, the fractional release values are converted to an equivalent number of failed particles as listed in Table 2-1.

Table 2-1. ^{110m}Ag fractional release increases with heating temperature.

Heating Temperature (°C)	Heating Time (h)	^{110m}Ag Fractional Release	Equivalent Failures
1600	138	2.8×10^{-3}	46
	500	9.0×10^{-4}	15
	500	2.7×10^{-2}	443
1700	185	4.8×10^{-2}	787
1800	100	0.17	2788
	100	0.67	10988
	200	0.62	10168

Although an increase in silver release would be expected to accompany an increase in temperature, according to the Arrhenius form of diffusion, seen in Equation (2-1), other mechanisms may also produce these results. Measurements of silver release from the collection of coated fuel particles inside an element do not provide any insight to the mechanism controlling silver transport. The equivalent failures calculated from the fractional release values shown in Table 2-1 indicate that a mechanism resulting in complete silver loss from a fraction of the particles in the element could produce the same observed quantities of silver release. As the temperature increases the number of particles releasing their entire silver inventory would also increase if silver transport were dominated by cracks in the SiC layer whose formation was exacerbated by higher temperatures.

Förthmann et al. also measured the fractional release of silver from UO_2 TRISO-coated fuel particles in post-irradiation heating at 1400°C, but they focused on the variation in the calculated diffusion coefficient with variations in SiC coating parameters.[4] While such variables as the SiC density, grain size, microstructure, and light reflectivity had no apparent correlation with silver release the authors did report a range of diffusion coefficients corresponding to the range of deposition temperatures and carrier gas used during SiC deposition.

Seven types of fuel, compressed with matrix graphite to form compacts, were heated at 1400°C after irradiation. A cold plate collected silver released from the fuel particles. Silver was leached off the cold plate and counted after different annealing periods.

In an effort to account for multiple contributions to silver release Förthmann et al. modeled the results with a spontaneous release portion, described by the Booth model for release from the kernel, along with the more complicated diffusion-controlled release after a breakthrough time.[4] The spontaneous release portion of the silver release curve provides a steady contribution of silver before the general breakthrough of silver and is most likely due to uranium contamination outside of the silicon carbide layer. Any silver born outside the silicon carbide layer will be released almost immediately and contribute to the overall silver deposition on the cold plate.

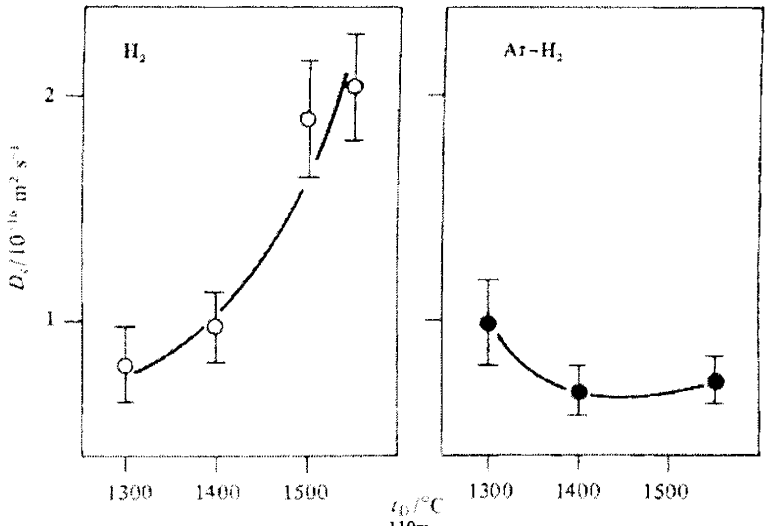

Figure 2-3. Diffusion coefficients at 1400°C for ^{110m}Ag in SiC deposited by H_2 and $Ar+H_2$ have opposite trends with deposition temperature.[4]

The diffusion coefficient increased from 8.0×10^{-17} m^2/s to 2.0×10^{-16} m^2/s as the deposition temperature increased from 1300°C to 1550°C for SiC deposited in pure hydrogen.[4] Förthmann et al. also noted that the SiC microstructure consisted of striated structure with free silicon when the deposition temperature was 1300°C, crystalline structure with small crystallite sizes when the deposition temperature was 1400°C, and large columnar crystals when the deposition temperature was 1500°C. The presence of free silicon in the SiC deposited at 1300°C does not result in increased silver diffusion as suggested by Nabielek et al.[2] For SiC deposited in pure hydrogen, it appears that the silver diffusion coefficient increases as the SiC microstructure becomes more columnar, but the total change in the diffusion coefficients with SiC deposition temperature is much smaller than the range observed in the literature that a definite trend cannot be verified. Additionally, the residual stress state within the SiC coatings is different for different SiC grain structures and those stresses may play a role in the ability of SiC to retain silver.

For SiC deposited in a mixture of argon and hydrogen, the diffusion coefficient decreased from 9.9×10^{-17} m^2/s to 7.3×10^{-17} m^2/s as the deposition temperature increased from 1300°C to 1550°C.[4] Förthmann et al. observed less variation in the SiC appearance with temperature for the SiC deposited in an argon-hydrogen mixture. The SiC consisted of crystalline structure with small crystallite sizes when the deposition temperature was 1300°C, small and uniformly distributed crystallites when the deposition temperature was 1400°C, and coarse-grained but not columnar grains when the deposition temperature was 1550°C. No correlation between the SiC microstructure and silver release could be determined from these data.

Although the trend of diffusion coefficient change with respect to deposition temperature appears fairly clear (at least for SiC deposited in pure hydrogen), as shown in Figure 2-3, and the

uncertainty bands are fairly small, the values reported here are all within the range of diffusion coefficient reported by other authors. Based on the small variation in Förthmann et al.'s data relative to the other data reported in the literature, one cannot conclude that the change in SiC microstructure associated with the change in SiC deposition temperature is a primary contributor to silver transport in SiC.

A collaboration between JAERI (Japanese Atomic Energy Research Institute) and ORNL (Oak Ridge National Laboratory) irradiated and heated UO_2 TRISO-coated particles. Capsule HRB-22 contained 12 annular fuel compacts composed of 32,200 UO_2 TRISO-coated particles dispersed in a graphite matrix. The irradiation of capsule HRB-22 lasted 88.8 effective full power days with a maximum burnup of 6.7% FIMA, maximum fast fluence of 2.8×10^{25} n/m^2, and the maximum fuel compact temperature maintained below 1300°C.[10]

The sweep gas monitoring system examined fission gas release during irradiation with coating failures causing a distinctive pulse in the ion chamber signal. Four pulses in the sweep gas monitoring system indicated single particle failures at 29.57, 32.52, 56.91, and 83.07 effective full power days.[10] These through-coating failures suggest a failure fraction during irradiation of 1.2×10^{-4}. The release-to-birth ratio (R/B) was also monitored during irradiation. The R/B results suggest that there were two through-coating failures at the beginning of the irradiation. Silver release was not measured during irradiation, but further heating tests on this fuel are discussed below and in section 2.3.2.

Accident condition testing on the irradiated fuel subjected one intact compact to 219 h at 1600°C. Krypton gas release was monitored continuously during the heating test and silver release was monitored periodically by measuring collection on a removable deposition cup in the furnace. High gas release measurements during the test indicate that there may have been two or three failed particles at the beginning of the heating test. The rapid krypton release indicative of an additional particle failure caused a spike in the gas monitoring system about 49 h into the test. According to the measurements of the deposition cup, the fuel particles in the element released 38% of their silver while only releasing 1% of their cesium inventory.[10] Measurements of the remaining solution after deconsolidation suggested there were at least two failed particles in the compact. As in many other tests reported in the literature, silver release significantly exceeded cesium release. The release information, however, does not provide any insight regarding the mechanism governing silver transport in SiC.

Verfondern et al. summarized silver diffusion coefficients in SiC from a number of sources. The diffusion coefficients reported are listed below:[7]

$$D_{SiC} = 3.6\times10^{-9}\cdot\exp\left(\frac{-215\,\frac{kJ}{mole}}{RT}\right)\frac{m^2}{s} \tag{2-14}$$

$$D_{SiC} = 6.8\times10^{-11}\cdot\exp\left(\frac{-177\,\frac{kJ}{mole}}{RT}\right)\frac{m^2}{s} \tag{2-15}$$

between 1200°C and 1400°C

$$D_{SiC} = 3.5\times10^{-10}\cdot\exp\left(\frac{-213\,\frac{kJ}{mole}}{RT}\right)\frac{m^2}{s} \qquad (2\text{-}16)$$

between 1200°C and 2300°C

$$D_{SiC} = 5.0\times10^{-10}\cdot\exp\left(\frac{-182\,\frac{kJ}{mole}}{RT}\right)\frac{m^2}{s} \qquad (2\text{-}17)$$

The diffusion coefficients calculated from the experiments described in this section are displayed in Figure 2-4. The diffusion coefficients span more than an order of magnitude at most temperatures and more than 2 orders of magnitude at 1200°C.

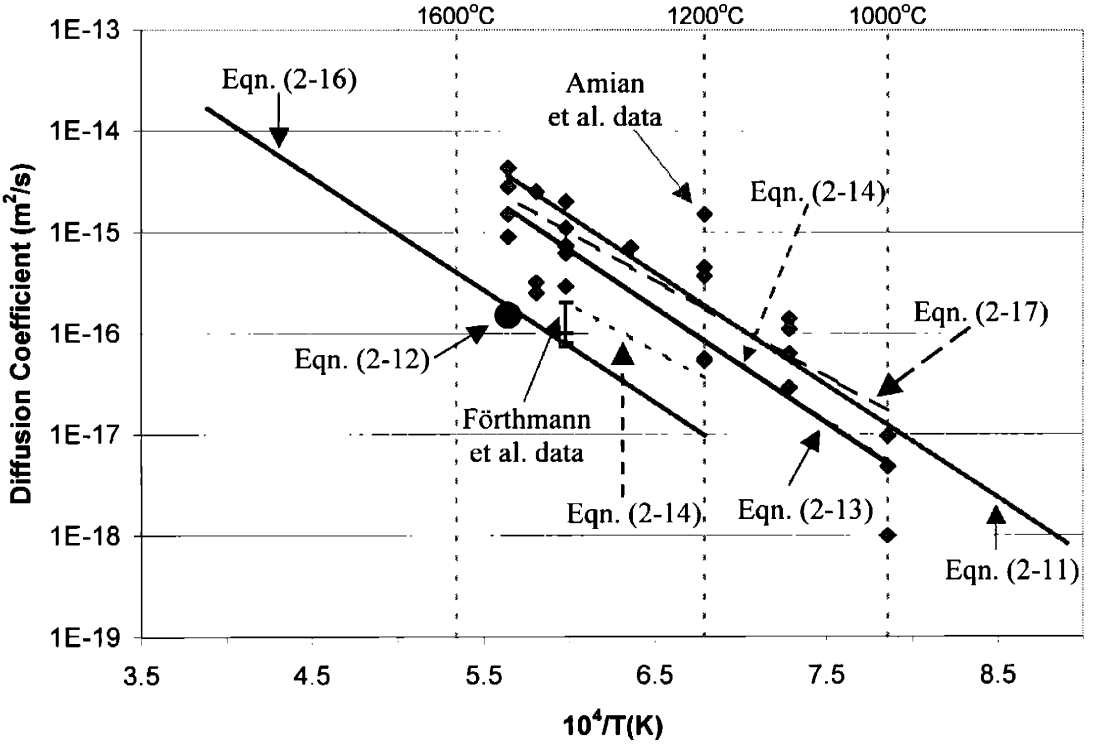

Figure 2-4. Silver diffusion coefficients derived from irradiation and annealing experiments span more than an order of magnitude.

2.3 INDIVIDUAL INVENTORY

Whereas fission product release measurements on large batches of fuel provide useful information on overall performance, individual particle measurements attempt to develop a more detailed image of fission product transport. Individual particle measurements include techniques such as gamma counting of fission product inventory measurements and electron microscopy.

2.3.1 Assumptions

One of the primary challenges with conducting measurements on individual particles is the time required to count each particle. Counting times up to 8 h have been required to obtain reasonable counting statistics. This demand on resources limits the number of particles that can be individually counted to evaluate fission product release. Therefore, small populations of particles, sometimes just 10 to 25, are investigated and assumed to be representative of much larger batches, on the order of tens of thousands of particles.

2.3.2 Silver Migration in Silicon Carbide

In addition to batch testing, Nabielek et al. measured the individual silver content of particles. Although the particles selected appeared intact and had retained all of their cesium and other fission products, the authors noted "drastic variations" in silver content.[2] They attributed the scatter in particle silver release to variations in availability and accessibility of free silicon on the silicon carbide grain boundaries as the presence of free silicon on the SiC grain boundaries facilitates silver migration.

After heating ten selected particles from the capsule HRB-15B irradiation, Bullock examined each particle individually and measured the silver, cesium, europium, and cerium contents. From each of the five different irradiated fuel types, Bullock selected ten particles for each of the three annealing experiments. Intermediate counting of mullite collector sleeves and tantalum tubes during heating measured fission product release during the test. In addition, the fission product inventory of each particle was counted using gamma spectrometry before and after heating.

The individual fission product inventories after irradiation but before heating were normalized to the ^{106}Ru inventory, a chemically stable fission product in the fuel particle, and the experimental and calculated values were compared. These measurements and calculations indicate whether any of the fission products were released during irradiation. Good matching between the experimental and theoretical values for the ^{134}Cs and ^{137}Cs inventories indicate no cesium release during irradiation. The experimental measurements showed about 25% less silver, 15% less cerium, and 25% more europium than predicted. However, uncertainties in the variables used to calculate these fission product inventories can account for the discrepancies.

The silver release per particle during heating was "highly nonuniform."[1] Many of the heated particles released more than 50% of their silver, but in seven out of the eight batches experiencing silver release, at least one particle retained all of its silver. Cesium, on the other hand, appeared to be mostly retained with only three particles from two of the batches losing their entire cesium inventory. Partial cesium release was not observed in any particle. The range of observed silver release, from complete retention to complete release, casts doubt on diffusion as the governing mechanism. In identical particles in the same test, a diffusion process should have produced similar release results. The fact that some of particles retained their entire silver inventory while others experienced total release indicates that the release mechanism for silver is not intrinsic to all SiC coatings; rather, SiC can be an effective barrier to silver even at temperatures up to 1500°C.

Silver release occurred in four of the particle types: UO_2, UC_2, UCO, and $UO_2^*(2)$ (ZrC dispersed in the buffer). No silver release was observed from the $UO_2^*(1)$ (ZrC coating around the fuel kernel) during the almost 3000-hour test. The SiC microstructures varied considerably from laminar to large columnar grains among these four fuel types. The UO_2 particles, suffering the greatest silver release, consisted of columnar, large-grained SiC. The $UO_2^*(1)$ particles retained all their silver and other fission products and had laminar structured SiC, but the presence of the

solid ZrC coating on the fuel kernel may have also aided retention. The UCO particles also had laminar SiC and good silver retention. However, the UC_2 particles, also with laminar SiC, readily released silver indicating that laminar SiC is not the sole reason, if at all, for silver retention.

Silver breakthrough times increased significantly as the heating temperature decreased. Figure 2-5 shows the silver fractional release curves for the UO_2*(2) particles during heat treatments at three temperatures. Measurements of the fission product inventory before the heat treatments provide the total amount of silver in each particle at the beginning of each test, but do not reveal the exact location or distribution of the silver. Any silver not already released from the fuel kernel into the coating layers must diffuse through at least part of the fuel kernel and the coatings before it reaches the silicon carbide. For particles irradiated under the same conditions the location and distribution of silver should be similar, but without knowing the exact initial condition it is impossible to know the contribution of silver retention due to holdup in the fuel kernel versus the silicon carbide layer.

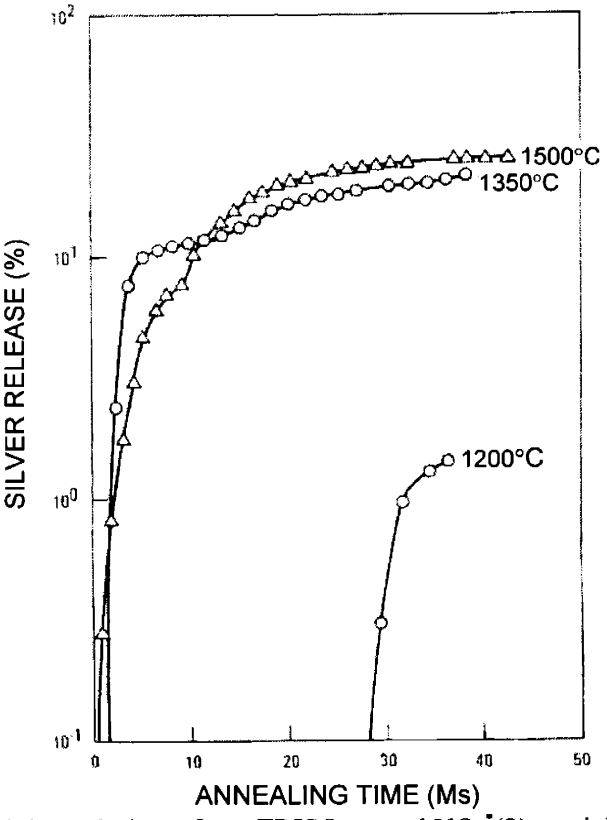

Figure 2-5. Silver breakthrough times from TRISO-coated UO_2*(2) particles increase as the heating temperature decreases.[1]

Silicon carbide microstructures within a given batch of fuel appeared similar after etching, but silver release varied from particle to particle within a batch. While variations in SiC microstructure may appear to play a role in silver release between batches, SiC microstructure does not, by itself, explain the large variations in silver release within the batches. Short-circuit paths or cracks in the SiC layers, however, could explain the large variations in silver release with flawed particles losing silver while truly intact SiC coatings retain silver. Silver must diffuse through the fuel kernels within coated particles before release is observed. The time and

temperature dependence of silver diffusion through fuel kernels contributes to the apparent time and temperature dependence of overall silver release.

Experiments conducted at the Oak Ridge National Laboratory studied the interaction of silver in UO_2 TRISO-coated particle in out-of-pile testing. Silver was mixed with UO_2 during fuel kernel fabrication and the standard TRISO coatings were applied.[11, 12] The silver-doped fuel particles were not irradiated, but were heated on a graphite wafer in a 27.8°C/mm temperature gradient so that the particles were exposed to a range of temperatures during each test.

The samples contained 3.3 wt % silver in the fuel kernel, about 100 times more silver than expected during normal operation of medium-enriched UO_2 to 20% FIMA. This increased silver concentration ensured detectability after heating while accounting for any silver loss from the fuel kernel during the coating process. The heating conditions for the first set of silver-doped tests are shown in Table 2-2. Pearson et al. mounted the particles after heating and then polished them to the midplane. X-ray analysis in either an SEM (scanning electron microscopy) or an EMP (electron microprobe) identified several locations of silver interaction with the SiC in many of the particles. A distribution of silver in the SiC coatings consistent with a diffusion process was not reported. Additionally, the silver lay along the PyC-SiC interface on the cold side of the particles.[11]

Table 2-2. Heating temperature ranges silver-doped fuel heating tests.[11]

Wafer #	Heating Temperature Range (°C)		Time (h)
	minimum	maximum	
1	1550	1900	25
2	1400	1750	260
3	1250	1500	3528

In further testing of silver interaction, Pearson et al. heated TRISO particles with 1.26 wt% silver mixed in with the UO_2 fuel kernel. These tests were conducted at a maximum temperature of 1500°C with particles on graphite wafers heated in a 27.8°C/mm temperature gradient. No silver penetration into the SiC layer could be observed during SEM examination.[12] The authors did, however, note occasional large nodules in the SiC layer where silver had completely replaced the silicon carbide. If diffusion controlled silver transport in SiC, one would expect to observe silver distributed uniformly around the particle and a silver concentration gradient through the SiC layer. Pearson et al.'s observations continue to indicate that silver migration is not dominated by diffusion, but rather is dominated by localized interactions where discrete pockets of phase-separated silver are observed in the SiC coating.

Transmission electron microscopy after 2000 h of heating revealed no microstructural changes either on the hot or cold side of the particles, no second-phase nodules, and no obvious grain boundary films.[12] Particle silver inventories were not measured and no discussion of silver release was included. It is not clear whether the silver was retained or if release accompanied the findings.

Further work by the JAERI/ORNL collaboration, discussed in section 2.2.4, examined particles that were deconsolidated from irradiated fuel elements.[10] The IMGA (Irradiated Microsphere Gamma Activity) system measured the fission product inventory of the individual particles before and after heating. The predominant gamma rays after irradiation were from ^{95}Zr, ^{106}Ru, ^{134}Cs, ^{137}Cs, and ^{144}Ce. Activity ratios of mobile fission products, such as cesium, cerium, and silver, to chemically stable fission products, such as zirconium and ruthenium, allowed comparisons between fuel particle inventories while accounting for individual variations in fuel kernel size and

burnup. During accident condition testing (ACT) solid fission products released from the fuel particles were collected on deposition cups, which were removed periodically and counted. Charcoal traps connected to the flowing helium monitored the amount of ^{85}Kr release as a sign of through-coating particle failure during heating.

ACT-1 heated 100 deconsolidated particles at 1600°C for 73.6 h. The test, initially planned for 1000 h, was stopped short due to the high number of particle failures and the contamination caused by fission product release. Online gas monitoring of ^{85}Kr during heating indicated four through-coating particle failures after 5 h, 28 h, 44 h, and 50 h at 1600°C.[10] Based on the IMGA results, five particles lost significant cesium during heating. A total of 22 particles lost part of their OPyC layers. Three of the five particles that lost significant cesium also lost part of or had hair line cracks in their OPyC layers. Only six of the 100 particles were counted for silver; two of those six lost more silver than cesium. The fission product release curves evaluated from seven measurements of the deposition cups during heating have similar shapes for both silver and cesium indicating that silver and cesium were released within the same 5-20 h windows. Silver and cesium fractional release curves as measured by accumulation on the deposition cups are shown in Figure 2-6*a* and *b*, respectively. While suggesting that silver and cesium may have been released at the same time, presumably from the same particles, the long gap between deposition cup readings leaves uncertainty about the individual behavior of silver and cesium.

The goal of the following two tests, ACT-3 and ACT-4, was to measure silver diffusion through intact SiC layers. Each test was limited to 25 particles to accommodate the long counting times, 8 h, to measure silver inventories. Minato et al. selected a compact with a lower burnup, 4.79±0.11% FIMA, for deconsolidation to provide more safety margin during heating and avoid through-coating failures.[10] Particle identities were maintained during heating so that fission product inventories measured by IMGA could be compared before and after heating. The fractional release curves for silver and cesium during ACT-3 and ACT-4 heating are shown in Figure 2-6*a* and *b*, respectively.

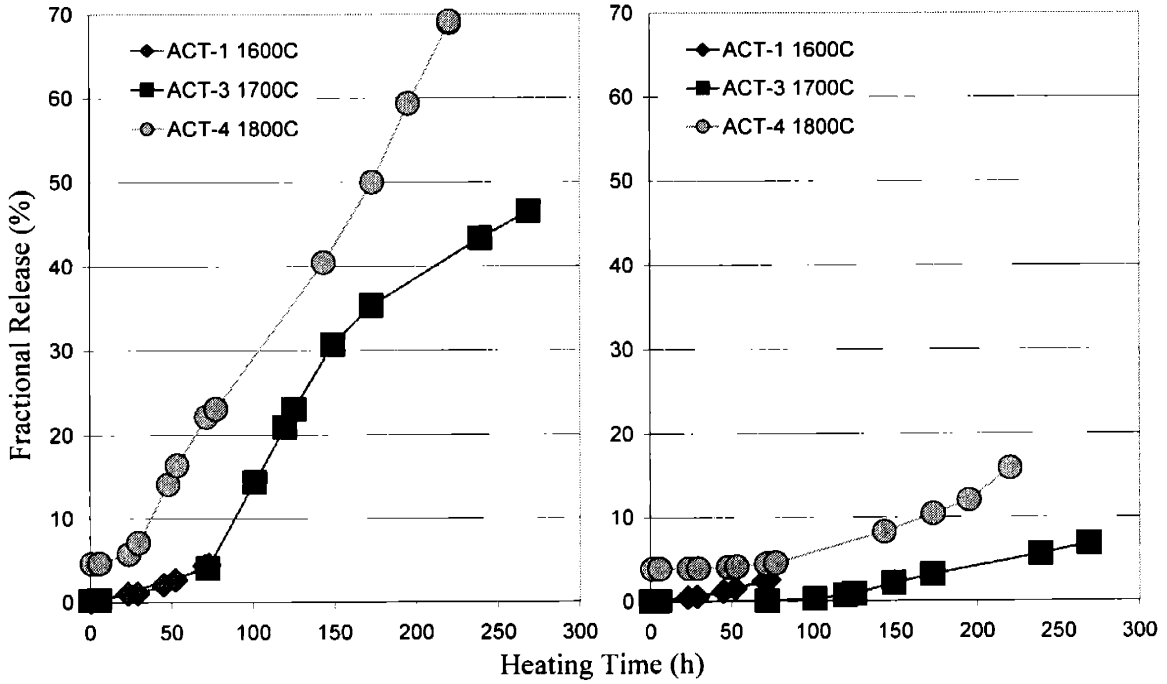

a) Fractional release of silver *b*) Fractional release of cesium

Figure 2-6. Fractional release of silver is greater than cesium during accident condition testing.[10]

The gas monitoring system detected no significant fission gas release indicating no through-coating failures during ACT-3 heating for 270 h at 1800°C. However, IMGA counting detected "considerable variation" in the retention of silver, cesium, and europium among the particles, as shown in Figure 2-7. It appears that there was much more silver release than cesium, but the accuracy of the measurements and calculations is not known. Based on the total inventory measurements of the 25 particles before and after heating, the particles lost an average of about 47% of their silver and about 7% of their cesium during ACT-3.

The 25 particles heated in ACT-4 at 1800°C for 222 h again exhibited "considerable variation" in the retention of the fission products silver, cesium, and europium, as shown in Figure 2-8. As with ACT-3, the 25 particles together released more silver than cesium, losing about 69% of their silver and 16% of their cesium. Visual examination of the particles after heating revealed one particle with completely fragmented coatings and an exposed fuel kernel (noted as a failed particles in Figure 2-8).

The fractional release of cesium is, again, lower than the fractional release of silver. This feature has been interpreted to mean that silver diffuses faster than cesium through SiC. Although the pyrocarbon layers are generally not credited with retaining cesium, they do slow cesium transport more than they slow silver transport contributing to the lower observed releases. Again, the variation in fractional release among the 25 particles in each of the ACT-3 and ACT-4 tests argues against diffusion as the controlling silver transport mechanism.

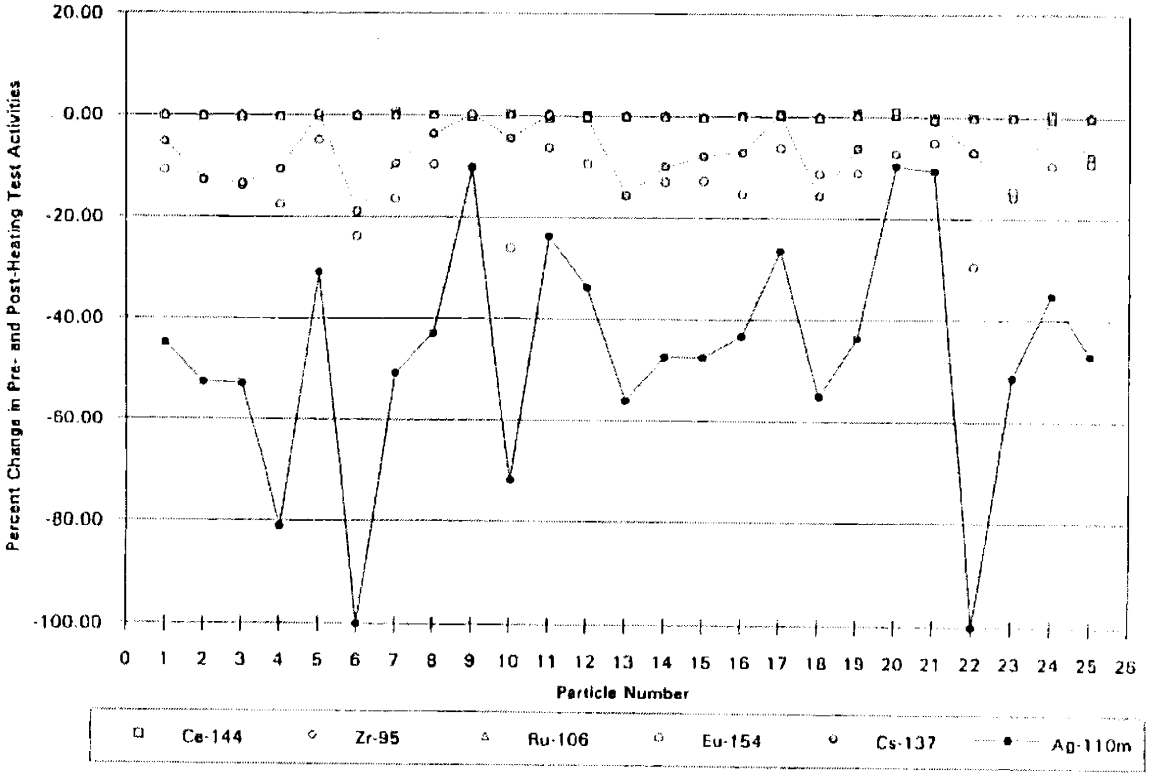

Figure 2-7. Individual particle fission product retention varies significantly during ACT-3 heating at 1700°C.[10]

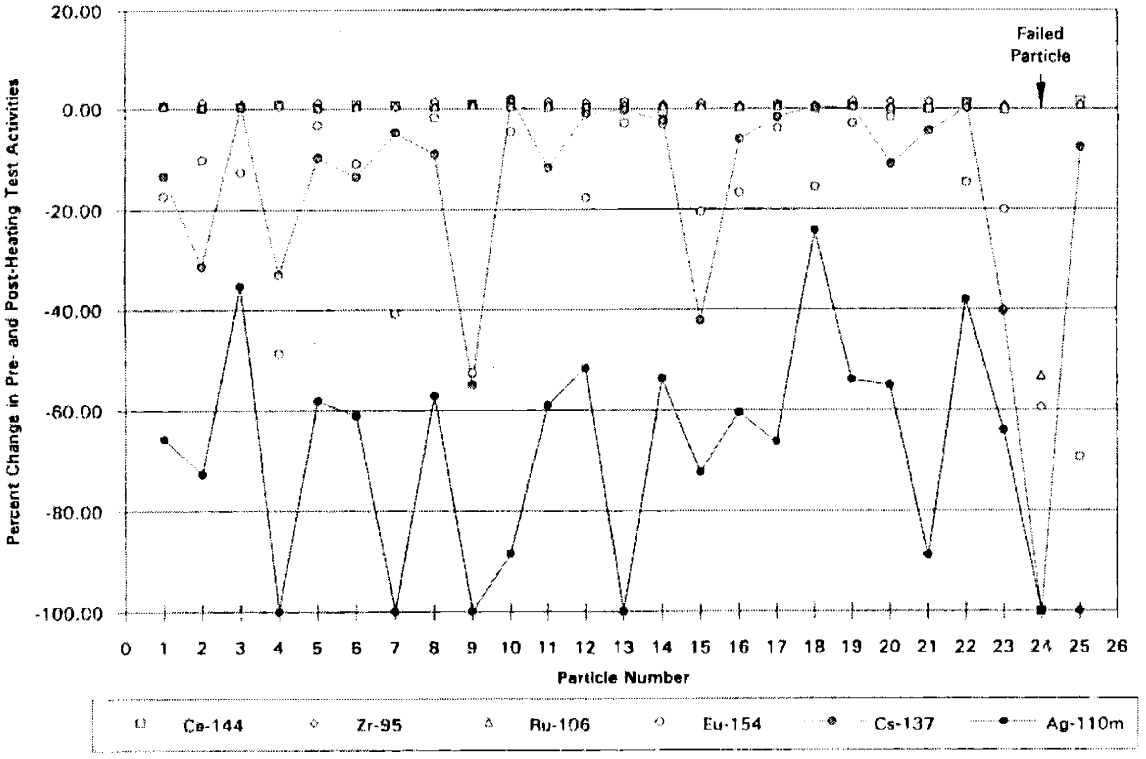

Figure 2-8. Individual particle fission product retention varies significantly during ACT-4 heating at 1800°C.[10]

Ketterer and Bullock examined loose particles for silver and cesium release after irradiation in capsule HRB-15B.[13] During irradiation, the low-enriched fuel, approximately 19.5% ^{235}U, achieved a peak exposure of 6.6×10^{25} n/m^2 fast fluence and about 27% FIMA fissile burnup with nominal time average temperatures between 815°C and 915°C. The TRISO-coated particles retained all of their fission products except for small quantities of silver. Different fissile and fertile fuel types were tested. The TRISO-coated fissile fuels included UO_2, UC_2, UCO, and two types of UO_2 fuels with either ZrC dispersed in the buffer or a ZrC coating over the fuel kernel.

IMGA measurements of the particles after irradiation generally indicate complete retention of ^{137}Cs, but "significant loss" of ^{110m}Ag.[13] Uncertainties for IMGA results are on the order of 9%-15% for the ^{137}Cs /^{106}Ru inventory ratio and 10%-16% for the ^{110m}Ag/^{106}Ru ratio. The 0%-8% ^{137}Cs release indicated by IMGA measurements falls within the uncertainty of the measurement and is, therefore, not sufficient evidence of cesium release during irradiation.

There is some confusion about the meaning of the silver release measurements. IMGA results and the ^{110m}Ag/^{106}Ru ratio indicate that, on average, 27% of the silver inventory was released during irradiation. Gamma-counting measurements on the empty graphite trays indicated only 2%-13% silver release. Even considering the uncertainties of both types of measurements, the release values from IMGA on particle and gamma-counting of empty trays do not agree. While this discrepancy is a source of concern for the authors, other work on silver migration in graphite materials indicate that they do not retain silver. Although silver is expected to condense on cold (significantly less than silver's melting temperature, 960°C) components in the system, it should not be surprising that silver was not detected on the graphite trays.

IMGA measurements on particles after irradiation showed no cesium loss and unquantified silver release. However, gamma-counting of empty trays detected ^{134}Cs, ^{137}Cs, and ^{110m}Ag. Of the trays with significant autoradiograph patterns, two trays had silver but no cesium and two trays had cesium but no silver. While gamma scans of empty particle trays suggest that the particles released 2%-13% of their theoretical silver inventory, the uncertainty of approximately 13%-15.6% for ^{137}Cs and 21.6%-23.3% for ^{110m}Ag means that cesium and silver release cannot be confirmed.

The fuel temperatures were greater than the graphite tray temperatures. While the graphite tray mean temperatures were approximately 840°C, the actual temperatures were greater than the mean for a significant time during irradiation. Although even the mean fuel temperatures may have been relatively low during irradiation, fuel temperatures exceeded the melting temperature of silver, 960°C, for a significant portion of the irradiation. At these temperatures, any silver escaping the fuel particles would be a vapor and would not likely condense on the graphite trays.

The SiC layers of the TRISO-coated UC_2 and UCO fuels contained some flaws and porosity that may have degraded their performance. Short, lenticular flaws observed during metallography are purported to be associated with areas of free silicon in the SiC layer.[13] Porosity found in the UCO particles was randomly dispersed in the silicon carbide and was observed both before and after irradiation.

In another irradiation test, fission gas release measurements and gamma-ray analysis of fuel particles and structural components provided means for Ketterer et al. to compare fuel performance of different fuel kernel materials and the effect of replacing SiC with ZrC in the TRISO coating. The irradiation at ORNL in capsule HRB-15A included fuel particles in fuel rods, bonded trays, and unbonded particle trays. Fission gas release measurements during irradiation and end-of-life release-to-birth ratios indicated some fuel failure, about 2% average in-service particle failure.[14] Fuel in capsule HRB-15A experienced burnup between 20% and 29% FIMA and fast fluence between 3.3 n/m^2 and 6.5×10^{25} n/m^2. Time-averaged temperatures for the fuel rods and bonded and unbonded particle wafers all fell in the 1000°C-1100°C range.

Two batches of fuel with $UC_{0.5}O_{1.5}$ kernels were the least retentive of silver and experienced severe SiC degradation by fission product (e.g. palladium) attack in 70% of those particles observed with ceramography. Degradation of the SiC coating by palladium or interactions with other fission products may provide pathways for silver release. Two batches of ZrC-TRISO (ZrC instead of SiC layer) exhibited better resistance to fission product attack, but the batch with UC_2 fuel still had poor silver retention. It is not yet clear whether ZrC retains silver better than SiC does.

Gamma counting of particles, particle trays, the graphite sleeve, and the stainless steel primary tube all provided data on fuel performance during the irradiation. The empty particle trays contained no silver after irradiation, but cesium, cerium, and europium were detected on some of the trays. Cobalt, cesium, silver, and europium were found on the graphite sleeve surrounding the fuel rods and trays with 60% of the silver detected occurring at the elevations of the $UC_{0.5}O_{1.5}$ fuels. Silver was also leached off the stainless steel primary containment tube indicating that silver passed through the graphite sleeve while the other fission products remained inside the sleeve.

Deconsolidation of the fuels rods provided fuel particles for gamma counting after irradiation. Analysis of the electrolytic solution after deconsolidation indicated a significant number of failed particles per rod. By measuring the amount of uranium contained in the solution after

deconsolidation and comparing that to the calculated inventory per particle, Ketterer et al. calculated the number of failed particles per rod. Gamma analysis of the ^{134}Cs, ^{137}Cs, ^{110m}Ag, ^{95}Zr, and ^{106}Ru inventories per particle and the ratios of mobile (cesium and silver) to stable (zirconium and ruthenium) fission products provided insight into cesium and silver and, in some cases, cerium and europium release during irradiation.

Table 2-3. Silver retention is less than cesium retention in HRB-15A fuels.[14]

Fuel	Coating	Number of Particles	Failure Fraction	Silver Retention (%)		Cesium Retention (%)	
				Mean	Range	Mean	Range
UO_2	TRISO	467	6.5×10^{-3}	48	26-71	94	90-99
UO_2	TRISO	201	2.5×10^{-3}	44	0-69	91	75-95
UO_2^*	TRISO ZrC in buffer	365	1.5×10^{-2}	56	35-80	96	69-100
UC_2	ZrC-TRISO	342	6×10^{-2}	47	0-66	90	0-97
UC_2	TRISO	184	1.8×10^{-2}	55	40-73	92	89-96
UCO	TRISO	345	3×10^{-2}	15	0-72	91	24-98

As shown in Table 2-3, silver is generally released more readily from all fuels from the HRB-15A irradiation than cesium.[14] In the UO_2 TRISO fuels, high silver release was observed in some of the same particles with high cesium retention. The UC_2 fuel with ZrC-TRISO coating experienced poor silver retention with the best particle only retaining 62% of its silver. Release values, however, for both silver and cesium vary significantly within a single batch and single fuel rod. Ketterer et al. suggest that variations in the microstructures of the barrier layers (SiC and ZrC) within and between batches are responsible for the variations in fission product release. Differences in individual SiC grain structures, however, are not sufficient to account for the scatter in the release values.

Cesium releases were significantly greater than expected and Ketterer et al. suggest this is due to particles with failed SiC but intact OPyC layers. According to Ketterer et al., with lower average fuel temperatures during expected HTGR operation, cesium diffusion through OPyC layers would be hindered and holdup in the core graphite would limit cesium release even with failed SiC layers.

Particles with failed SiC coatings and intact OPyC coatings would release silver and cesium while retaining the noble fission gases krypton and xenon. An intact OPyC layer would retard cesium release, explaining lower observed releases of cesium relative to silver. Although path length variations due to individual SiC microstructures are insufficient to explain the range of release values, failed SiC layers in some of the particles does account for observations of silver release from some particles (the ones with failed SiC coatings) with silver retention in others (those with intact SiC coatings).

2.3.3 Ion Implantation

In addition to studying total silver release from fuel particles, Nabielek et al. examined the migration of silver implanted in a silicon carbide disk. Using SiC chemically vapor deposited on a plane graphite disk, silver was implanted with a peak concentration equivalent to 2×10^{-3} mole ^{109}Ag per mole SiC. After heating the sample at 1180°C for only 30 minutes, the authors reported that the "mobility of silver was too small to be detectable."[2]

The silicon carbide contained some pores and had a density of 3.18 g/cm^3, within the range of typically characterized SiC and fairly close to the theoretical SiC density of 3.21 g/cm^3. The

implanted silver concentration was in the range typical of in-pile concentrations reached at 12% FIMA of 2×10^{-4} to 4×10^{-3} mole ^{109}Ag per mole SiC. The authors hypothesize that the silver was trapped inside the SiC grains hence the lack of migration is attributable to the extremely low silver diffusion rate within SiC grains, not a measure of silver grain boundary diffusion. The ion implantation used in this experiment resulted in a shallow silver concentration profile with the peak silver concentration occurring approximately 80 nm, or 0.08 μm, below the SiC surface. Typical SiC grain dimensions on the order of 0.5-1 μm are common, and grain sizes are often larger. The implanted silver, therefore, was probably contained within the first row of grains in the SiC plate. The width of the implanted area, however, was most certainly larger than a single SiC grain, probably on the order of millimeters. The silver implantation beam most likely spanned many SiC grains and their associated grain boundaries. The silver ions were, therefore, not completely contained within SiC grains and those on the grain boundaries should have been free to diffuse, but no evidence of silver transport was observed.

From the small movement of silver atoms in the ion implantation experiment Nabielek et al. derived an upper limit for the diffusion coefficient of silver in silicon carbide at 1180°C as:

$$D_{SiC}(1180°C) << 10^{-19}\,\frac{m^2}{s} \tag{2-18}$$

This value is much lower, approximately 3 orders of magnitude lower, than the other diffusion coefficients for silver in silicon carbide reported in the literature and discussed in Section 2.2.4. Compared to other experiments reported in the literature, the heat treatment used here, 30 min at 1180°C, is quite short and at a much lower temperature. Although estimates for silver migration in the ion implantation sample using average diffusion coefficient values in the literature predicted measurable silver movement, given sufficient accuracy of the silver concentration measurement technique, the duration and temperature of the heat treatment may not have been enough to generate silver diffusion.

2.4 DISCUSSION

The lack of cesium release during various irradiation and heating tests argues that most of the fuel particles tested were intact. Thus, it seems reasonable that, in order to escape, silver must have diffused through intact silicon carbide. This view of effective silver release has allowed many authors to compare results from different types of fuels and to categorize their results with diffusion coefficients, useful for estimating total silver release from future operating cores.

Although the reported silver diffusion coefficients agree with each other within about 2 orders of magnitude, the specific path of grain boundary diffusion has been assumed from a comparison of activation energies and not from direct observation. A few observations among the diffusion coefficient experiments and simple calculations aim to look at the process of silver migration in silicon carbide from a different perspective.

2.4.1 Scatter in the Data

Amian and Stöver and other authors propose that the scatter observed in calculated silver diffusion coefficients stems from variations in the silicon carbide microstructure. If silver diffuses along silicon carbide grain boundaries, as commonly suggested, then different microstructures in different particles would produce different total path lengths through each

silicon carbide layer. While this explanation makes intuitive sense, it does not represent the available data well.

Given a specific heat treatment duration and silver concentration at the inner SiC surface, the amount of silver released through the SiC coating can be calculated from the analytical solution through a spherical shell, shown in Equation (2-19). Equating the mass release from two different scenarios and allowing the overall thickness to vary to represent the total silver path length along SiC grain boundaries, one can calculate the effective change in SiC thickness to match a change in the diffusion coefficient. The maximum and minimum diffusion coefficient values at selected temperatures were taken from the literature values shown in Figure 2-4.

$$Q_r = 4\pi ab(b-a)C_1 \cdot \left[\frac{D \cdot t}{(b-a)^2} - \frac{1}{6} - \frac{2}{\pi^2} \cdot \sum_{n=1}^{\infty} \frac{(-1)^n}{n^2} \exp\left[-\frac{Dn^2\pi^2 t}{(b-a)^2} \right] \right] \qquad (2\text{-}19)$$

where Q_r = mass released (g),
a = inner radius of spherical shell (m),
b = outer radius of spherical shell (m),
C_1 = source concentration of silver at $r = a$ (g/m^3),
D = diffusion coefficient of silver in SiC (m^2/s), and
t = duration of heat treatment (s).

In previous work, authors measured silver release from fuel particles and then calculated effective diffusion coefficients using the duration of the heat treatment and the dimensions of the SiC coating. In either analytical or numerical solutions used to determine the diffusion coefficients, the silver path length is assumed to be, simply, the thickness of the SiC coating. But, if silver travels along a tortuous path through the SiC coating before it escapes, the path length would be longer than the SiC coating thickness and the diffusion coefficient required to "push" the same amount of silver through the coating would have to be greater. If, therefore, the lowest diffusion coefficients are associated with the shortest diffusion paths (i.e., a single SiC grain boundary extending radially from the inner surface to the outer surface of the SiC coating), then one can calculate the total effective path length required to result in a higher diffusion coefficient for the same mass loss.

Equating the silver release using the maximum diffusion coefficient value at a given temperature with the silver release using the minimum diffusion coefficient at the same temperature, on can calculate the difference in effective path length. The values for the effective silver path length required to result in the reported range of diffusion coefficient are listed in Table 2-4. The range in values, however, is greater than that expected based on typical SiC grain structures. As discussed above, one SiC grain structure extreme is the case of long, columnar grains with single grains extending through the entire SiC coating. At the other end of the spectrum is a SiC coating with small, equiaxed grains, on the order of 0.5 μm per side, for example. If for every grain-width a silver atom moves in the radial direction it also moves one grain-width in the tangential direction, then the effective path length traveled by the silver atom is twice the SiC coating thickness. For the diffusion coefficient values at 1200°C and 1500°C, where the values differ by more than 1 order of magnitude, the effective path length changes by a factor of roughly 8-10. Although silver would be expected to follow a tortuous path as a result of grain boundary diffusion, a total path length greater than twice the SiC thickness is not likely. From this assessment of the variation in reported diffusion coefficients, the argument that silver diffusion varies because of the individual SiC microstructures does not reflect the actual data. Another mechanism, therefore, must govern silver transport through silicon carbide coatings resulting in

the large variations observed in silver release, both in individual particle measurements and in large batch testing.

Table 2-4. The calculated path lengths necessary to explain the range of diffusion coefficients is larger than reasonable tortuous paths through SiC layers.

Temperature (°C)	Lower D (m^2/s)	Assumed Thickness (μm)	Upper D (m^2/s)	Calculated Thickness (μm)	Thickness Ratio (Calculated: Assumed)
1000	1.0E-18	35	1.7E-17	105	3.0
1200	9.8E-18	35	1.5E-15	470	13.4
1500	1.5E-16	35	4.3E-15	290	8.3

2.4.2 Silicon Carbide Diffusion vs. Particle Failure

Most of the silver diffusion coefficients reported in the literature were derived from batch testing of a population of fuel particles. In general, these diffusion coefficients were calculated assuming the collected silver release was due equally to all particles in the batch. But what if the silver release was not uniform? If just a few particles in a batch had a short-circuit diffusion path or connected porosity in the silicon carbide layer, a large portion of that particle's silver inventory could escape. It is possible that almost total release of silver from a few particles in a batch of fuel particles with almost complete retention in the rest would produce the same silver deposition on a cold plate during heating as those previously assumed due to diffusion from the entire batch.

Take, for example, the data reported by Amian and Stöver for a number of post-irradiation anneals.[8] The authors report the diffusion coefficient calculated from release measurements during post-irradiation anneals. The geometry of the fuel and anneal conditions are given, along with the calculated values of fractional release. The number of fuel particles per element tested is not included, but the following demonstration remains instructive.

If the procedure applied to calculate the diffusion coefficients from release measurements is reversed, an estimate of the release detected and silver mass per particle (element) can be determined. The following analysis assumes that there are 250 particles in each element tested. Using the reported diffusion coefficient for each anneal (D) and the anneal conditions (T, t), the amount of silver released from each element (Q) was calculated using the analytical solution for diffusive release from a thin spherical shell. The total amount of silver released (Q_{total}) from each element was also calculated (using the original assumption that the release was evenly attributed to all of the particles in the element). The total amount of silver in each particle at the beginning of the heat treatment (M_{Ag}) was calculated given the fractional release values listed by Amian and Stöver.[8] The results of this analysis are shown in Table 2-5. A comparison of the calculated amount of silver per particle to the calculated amount of silver released from the element shows that it is feasible that in some elements the release is due to a nearly complete loss of silver from a few particles and almost complete retention in the rest.

Table 2-5. Equivalent number of failed particles given the fractional release for the batch and assuming 250 particles per batch.

Temp. (K)	Time (h)	D (m^2/s)	FR	Q (g) (particle)	M_{Ag} (g) (particle)	Q_{total} (g) (element)	Failed SiC
1273	2340	4.8E-18	4.0E-03	2.35E-09	5.87E-07	5.87E-07	1.00
1273	700	9.6E-18	4.1E-03	9.53E-12	2.32E-09	2.38E-09	1.03
1273	1000	1.0E-18	7.0E-04	3.34E-21	4.77E-18	8.34E-19	0.18
1373	543	1.4E-16	5.0E-02	1.08E-05	2.16E-04	2.70E-03	12.50
1373	294	1.1E-16	5.3E-03	9.73E-07	1.84E-04	2.43E-04	1.33
1473	162	4.5E-16	3.0E-02	9.84E-06	3.28E-04	2.46E-03	7.50
1473	240	5.6E-17	2.4E-03	9.67E-09	4.03E-06	2.42E-06	0.60
1673	40	7.4E-16	5.3E-03	6.94E-07	1.31E-04	1.74E-04	1.33
1673	75	6.2E-16	9.8E-03	3.19E-06	3.25E-04	7.97E-04	2.45
1673	30	2.0E-15	1.1E-02	6.27E-06	5.70E-04	1.57E-03	2.75
1673	45	1.1E-15	5.0E-03	3.80E-06	7.60E-04	9.50E-04	1.25
1773	30	9.0E-16	4.1E-03	4.77E-07	1.16E-04	1.19E-04	1.03
1773	225	1.5E-15	1.5E-01	1.06E-04	7.09E-04	2.66E-02	37.50
1773	183	2.8E-15	2.9E-01	1.72E-04	5.92E-04	4.29E-02	72.50

* assuming 250 particles per fuel element

Rearranging the numbers somewhat, for a batch of 250 particles, the release of 30% of the silver inventory of just four particles would produce the same results as 0.5% release from each particle, the value attributed to diffusion by Amian and Stöver. This calculation, once again, suggests that silver release could result from a short-circuit path or silicon carbide failure in a few particles per batch rather than diffusion.

2.4.3 Other Possible Silver Migration Pathways

With a melting temperature of 960°C, silver exists as a vapor when released from fuel particles. Nabielek et al. cite previous work when they report that silver is "trapped, nearly quantitatively" when particle surface temperatures are below 1000°C.[2] For all of the results reported in the literature, the fuel surface temperatures exceeded, at least for some portion of the test, 1000°C, so the retention of silver at low temperature cannot be confirmed. This does, however, leave open the possibility that paths allowing the transport of a vapor through the silicon carbide layer may play a role in silver release.

A number of authors have advised some caution relative to the silver diffusion coefficients. Nabielek et al. conclude that migrating fission products will follow grain boundaries in poly-crystalline SiC "through disorganized material via traces of free silicon".[2] If free silicon is present in the silicon carbide layer, Nabielek et al. suggested that it will be stored at the grain boundaries and will aid in silver migration. Additionally, other authors have suggested looking for short-circuit diffusion paths as they may provide significant contributions to enhanced fission product release.

Schenk and Nabielek report that an intermediate stage of silicon carbide failure, beginning around 1600°C, is characterized by non-uniform porosity and cracks.[9] These features could certainly lead to fast silver release from silicon carbide, appearing as diffusion through intact material as long as the pyrocarbon layers are undamaged and still retaining the fission gases and some of the cesium. Nabielek et al. also suggest a deterioration of silicon carbide occurring during operation when fuel temperatures are above 1200°C leading to increased silver release at higher temperatures.[2] Although the assessment of the quality of the fuel used by Nabielek et al. has been

challenged in the literature, it is important to note that other pathways and mechanisms resulting in silver release have been suggested and may explain some of the variation in the data.

Although pressure vessel failure (failure of all three structural layers) has been a concern for fuel performance, silicon carbide failure next to intact pyrocarbon layers can occur. During HRB-22 post-irradiation examination, Minato et al. found a partial crack in a single SiC layer. Cracks like this one do not extend completely through the SiC coating so they are not detected by standard burn/leach methods used to detect coating failures. The authors suggest that the crack formed either from mechanical shocks after SiC deposition or during the compact fabrication process.[10] Pathways like this one would provide paths for silver vapor release.

2.4.4 Other Fission Product Behavior

The retention and release of other fission products, namely the noble gases krypton and xenon, and other metallics, primarily cesium, plays an important role in judging the performance of the fuel particles. Intact pyrocarbon layers retain the noble fission gases. As long as either the inner or outer pyrocarbon layer is undamaged, fission gas release will not be observed and this fact is used to categorize fuel as, generally, intact or failed.

One of the initial drivers for adding a silicon carbide layer to coated particle fuels was to improve cesium retention. Cesium escaped from the original pyrocarbon coatings of the BISO particles, but the degree to which pyrocarbon or graphite materials can retain or retard cesium migration is not completely clear.

Brown and Faircloth state that cesium seems to be well retained by the particle coatings, "principally in the inner pyrocarbon layer".[3] Amian and Stöver also had a similar finding stating the "cesium is effectively retained in the HTI-PyC coatings" and that there was no distinct improvement for cesium retention in SiC relative to PyC.[8] Schenk and Nabielek reported that cesium was found mainly in the buffer layer and the matrix graphite around the fuel particles provided enough retention to prevent rapid cesium release from the fuel element.[9] Ketterer et al. found cesium throughout the buffer layer in the particles from the HRB-15B irradiation, indicating some solubility or adsorption of cesium in the low-density graphite buffer and also stated that cesium was retained by the OPyC layer.[14]

These findings suggest that both the pyrocarbon layers and the low-density buffer and matrix materials may provide some retention for cesium, possibly through adsorption in the low-density materials. If cesium is retained, at least somewhat, by the PyC layers or the other graphite materials, then failure of a silicon carbide layer would not automatically result in cesium release. In this way silver release from particles with intact PyC layers and failed SiC layers could be observed while the cesium was still retained.

2.5 CONCLUSIONS

Although the Arrhenius form of the diffusion equation appears to cover the observed temperature trends regarding silver release from coated fuel particles, other observations suggest that silver release may depend on mechanisms other than classical diffusion.

Nablielek et al. calculate silver diffusion coefficients based on release data, but also caution that the shapes of some of the release curves are not consistent with diffusion. They further propose that silver release may be due to a degradation of the silicon carbide with irradiation and heating.

Amian and Stöver attribute the greater than one order of magnitude scatter in their data to variation in the specific microstructure in each silicon carbide layer. However, as seen in section 2.4.1, variations in microstructure alone cannot account for the large range of diffusion coefficients. If silver release from particles is driven by SiC integrity rather than by grain boundary diffusion along specific grain paths, large variations in release per particle and per batch would still be observed with corresponding variations in the calculated effective diffusion coefficient.

Variations in silver release would be expected given a grain boundary diffusion mechanism from individual particles based on specific microstructures and irradiation conditions. However, the large variations observed by Amian and Stöver, Bullock, and Ketterer et al. are greater than can be explained by SiC microstructure and irradiation conditions and do not appear characteristic of a diffusion pathway. When testing particles from a single fabrication batch with nearly identical dimension and irradiation parameters, release due to diffusion should not vary by orders of magnitude. Diffusion does not explain why some particles in Bullock's study released 100% of their silver while others from the same batch in the same test retained all of their silver. These observations suggest that mechanisms other than diffusion are involved with silver release.

The assumption that silver release is governed by grain boundary diffusion attempts to explain a range of data whose span is larger than expected based on typical grain boundary path variations. Without measuring silver concentration profiles or observing direct evidence of diffusion, one must still consider other transport mechanisms. Various authors have expressed doubts about the specific silver migration mechanism and have offered some suggestions of alternative possibilities contributing to silver release, but these paths have not yet been followed.

There is ample uncertainty in the current data to suggest that silver may not only diffuse through silicon carbide, but may escape through failed silicon carbide layers or other defects in the coating. If this is the case, identifying those flawed particles and removing them from operation would decrease silver release. Additional work to identify the specific silver transport mechanism is important for developing methods to reduce or mitigate silver release.

2.6 REFERENCES

[1] R.E. Bullock, "Fission-Product Release During Postirradiation Annealing of Several Types of Coated Fuel Particles," *J. Nucl. Mater.* **125** (1984) 304-319.

[2] H. Nabielek, P.E. Brown, P. Offermann, "Silver Release from Coated Particle Fuel," *Nucl. Tech.* **35** (1977) 483-493.

[3] P.E. Brown, R.L. Faircloth, "Metal Fission Product Behavior in High Temperature Reactors – UO2 Coated Particle Fuel," *J. Nucl. Mater.* **59** (1976) 29-41.

[4] R. Förthmann, E. Gyarmati, J. Linke, E. Wallura, "Influence of Material Properties on the Retention of Fission Products by Silicon Carbide Coatings," *High Temp.-High Press.* 14 (1982) 477.

[5] P. Offermann, "Ag-Diffusion in PyC," *J. Nucl. Mater.* **64** (1977) 249.

[6] R.K. McCardell, R.L. Downs, E.L. Shaber, R.R. Hobbins, W.D. Wagner, M.J. Kania, B.F. Myers, O.M. Stansfield, D.L Hanson, W.J. Scheffel, *NP-MHTGR Fuel Development Program Plan*, EGG-NPR-8971 Rev. C, September 1992.

[7] K. Verfondern, R.C. Martin, R. Moormann, *Methods and Data for HTGR Fuel Performance and Radionuclide Release Modeling during Normal Operation and Accidents for Safety Analysis*, Jül-2721, Forschungszentrum Jülich GmbH, January 1993.

[8] W. Amian, D. Stöver, "Diffusion of Silver and Cesium in Silicon-Carbide Coatings of Fuel Particles for High-Temperature Gas-Cooled Reactors," *Nucl. Tech.* **61** (1983) 475.

[9] W. Schenk, H. Nabielek, "High-Temperature Reactor Fuel Fission Product Release and Distribution at 1600 to 1800°C," *Nucl. Tech.* **96** (1991) 323.

[10] K. Minato et al. *HRB-22 Capsule Irradiation Test for HTGR Fuel (JAERI/USDOE Collaborative Irradiation Test)*, JAERI-Research 98-021, March 1998.

[11] R.L. Pearson, T.B. Lindemer, E.C. Beahm, *Simulated Fission Product-SiC Interaction in Triso-Coated LEU or MEU HTGR Fuel Particles*, ORNL/TM-6991, November 1980.

[12] R.L. Pearson, R.J. Lauf, T.B. Lindemer, *The Interaction of Palladium, the Rare Earths, and Silver with Silicon Carbide in HTGR Fuel Particles*, ORNL/TM-8059, April 1982.

[13] J.W. Ketterer, R.E. Bullock, *Capsule HRB-15B Postirradiation Examination Report*, GA-A15940, June 1981.

[14] J.W. Ketterer, M.J. Kania, R.E. Bullock, I.I. Siman-Tov, *Capsule HRB-15A Postirradiation Examination Report*, General Atomics, GA-A16758, July 1984.

3. Ion Implantation

3.1 INTRODUCTION

As discussed in Chapter 2, silver release has been observed from SiC-coated fuel particles during irradiation and out-of-pile testing. In most cases, however, silver release was reported only for batches of fuel particles or entire fuel elements, leaving uncertainties about individual particle performance. To date, silver concentration profiles, characteristic of diffusion in silicon carbide, have not been reported. To address this topic and to study silver transport mechanisms directly, ion implantation experiments were performed to observe silver diffusion within CVD SiC from a known initial concentration profile. These experiments were designed to obtain direct measurements of silver diffusion and to investigate the silver diffusion pathways.

In previous work, Nabielek et al. implanted low energy silver ions into SiC disk samples and measured the concentration profile before and after heating.[1] There was no change in the silver concentration profile after 30 min at 1180°C. Nabielek et al. attributed this result to silver ions trapped in silicon carbide grains during implantation not being able to diffuse along grain boundaries.

In this previous ion implantation experiment samples were heated at a fairly low temperature for a very short time. The goals of the current ion implantation experiment were to investigate silver behavior in SiC at higher temperatures, those more likely to facilitate silver diffusion, and to witness silver migration in silicon carbide starting with a known and measurable concentration. A lack of silver migration, however, in silicon carbide during heating, as described below, provides evidence that silver does not diffuse in silicon carbide via either a grain boundary or trans-granular mechanism.

3.2 EXPERIMENTAL SETUP

3.2.1 Materials

Flat plate SiC, 0.3 cm thick, was the starting material for the ion implantation experiments. Chemically vapor deposited (CVD) by Coorstek, the reported density was 3.21 g/cm^3 with grain sizes on the order of 3-10 μm, preferentially oriented in the direction perpendicular to the SiC surface.[2] XRD (X-ray diffraction) analysis on a polished SiC sample, shown in Figure 3-1, confirmed that the Coorstek CVD SiC contained crystalline β-SiC with a strong preferred orientation such that the (111) planes were parallel to the surface. Long, dendritic SiC grains, perpendicular to the surface, are evident in AEM analysis, show in the inset in Figure 3-1.

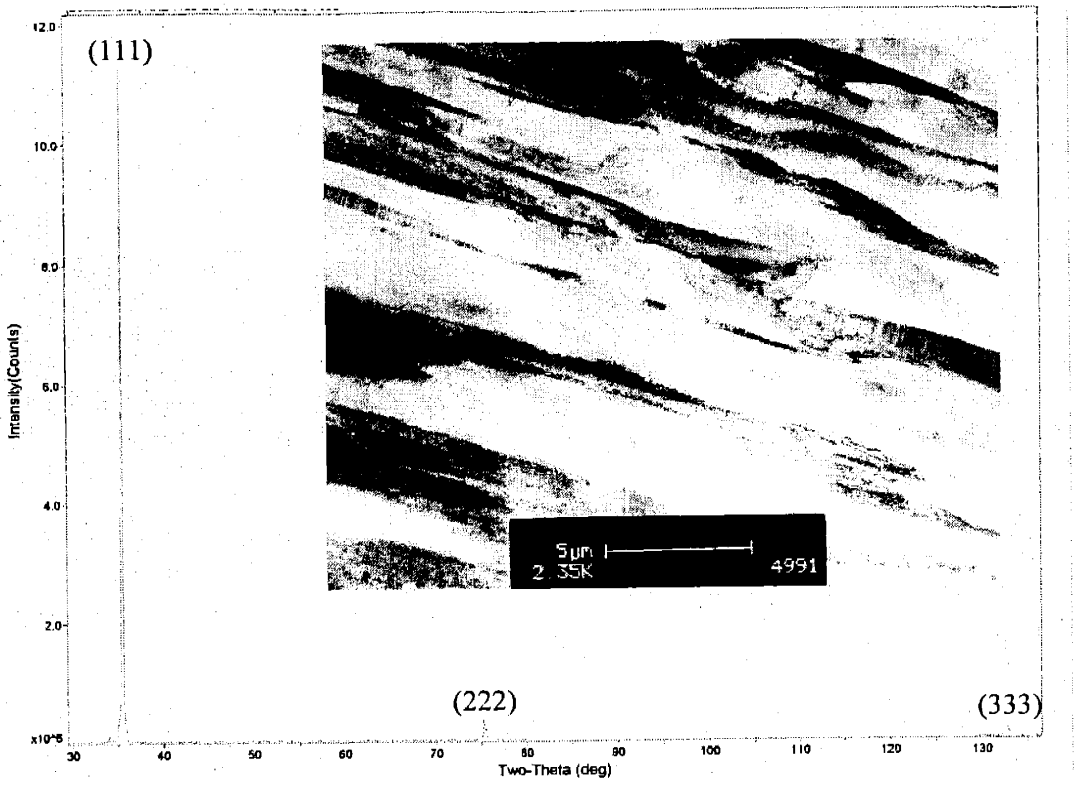

Figure 3-1. XRD analysis of an unexposed SiC sample shows β-SiC with a preferred orientation with (111) planes parallel to the surface. Long, dendritic grains are evident in AEM analysis (inset).

Each ion implantation sample was cut to 5 × 5 × 0.3 cm. One 5 × 5 cm face of each sample was polished to a mirror finish with a mean surface roughness, Ra, of 0.005 µm as measured by a Zygo interference microscope. A flat and uniform initial SiC surface ensured the best possible implanted silver profile. The silver ions began to slow down as soon as they hit the SiC surface during implantation. Excessive surface roughness across the implantation area would have caused variations in the silver implantation profile from the expected distribution which was predicted by the free-ware package SRIM (Stopping and Range of Ions in Matter).[3]

3.2.2 Ion Implantation

The goals of the ion implantation were to implant a measurable quantity of silver in silicon carbide and also to implant the silver deep enough that it would not migrate out of the sample during heating. Based on silver diffusion coefficients reported in the literature by Amian and Stöver, it was expected that the silver could diffuse greater than 10 µm in just 10 h at 1500°C with the peak concentration dropping to less than 1% of its original value.[4] To prevent possible silver loss during annealing and to avoid the region of surface anomalies resulting from the mechanical polishing process, the silver needed to be implanted approximately 9-15 µm into the silicon carbide. Calculations using the SRIM code indicated that ion beam energies on the order of 90-161 MeV were necessary to achieve implantation depths in the desired range.

The silver ions were implanted at the ATLAS facility at the Argonne National Laboratory using the positive-ion injector (PII) to create the silver beam. PII consists of three major subsystems: an electron cyclotron resonance (ECR) ion source and high-voltage platform, a 12-MHz beam bunching system, and a 12-MV super-conducting linac accelerator. The PII ECR source is a 10-

GHz electron cyclotron resonance ion source mounted on a high-voltage platform. The beam bunching system compresses the beam into narrow time packets, allowing the linac to accelerate the ion beam without introducing significant energy spread. The super-conducting resonators in the PII linac accelerate the ion beam from the low velocity provided by the PII ECR to the higher velocity required for injection into the remainder of ATLAS.[5] Figure 3-2 shows a floor plan of the ATLAS facility. All of the silver implantations were conducted upstream of the booster linac.

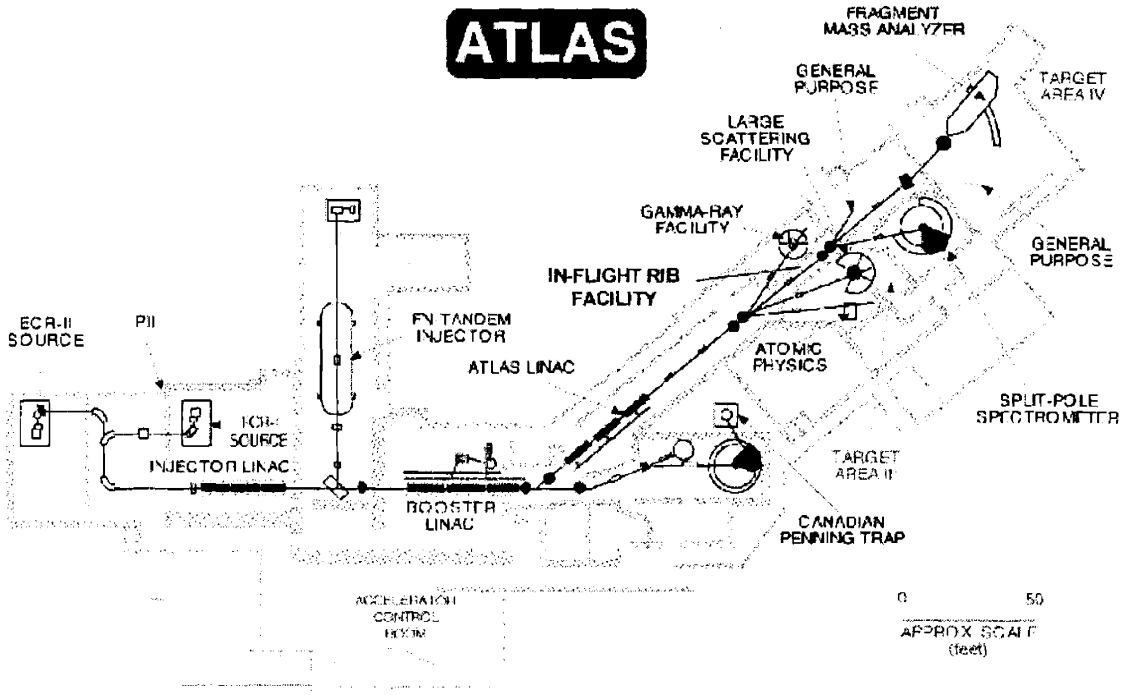

Figure 3-2. ATLAS floor plant (courtesy Argonne National Laboratory).

Two batches of samples were irradiated at ATLAS. The first batch contained samples designated 1, 2a, and 2b. Silver ions with a total energy of 161 MeV and charge state of +18 were implanted at a mean range of 12.8 μm with a peak at 13.0 μm. The second batch of samples (designated 4a-7b) were implanted with 93 MeV silver ions with charge state +19 at a mean range of 9.05 μm with a peak at 9.66 μm.

A copper braid connected from the back of the sample holder to a water-cooled copper block cooled the silicon carbide samples during implantation. Type K thermocouples were used to measure the temperature at the back of the SiC samples. Average temperatures during implantation varied from 120°C to 240°C.

The ion beam consisted of an irregular area approximately 10 mm in diameter with a 4 mm diameter central area where the ion concentration was the greatest and nearly uniform. The beam area can be seen on the surface of the SiC samples after implantation in Figure 3-3. The region outside the central beam area was much less uniform which resulted in variations in the as-implanted silver concentration profile. The entire ion beam was implanted directly in samples 1, 2a, and 2b. The depth profiles measured in sample 2b were taken from the center, high concentration area of the silver implantation. Silicon carbide plates with 4 mm diameter holes placed over samples 4a-7b provided masks, limiting silver implantation to only the high concentration, central beam area in the polished SiC samples. Figure 3-4*a* shows a SiC mask and Figure 3-4*b* shows a SiC sample after implantation with a mask.

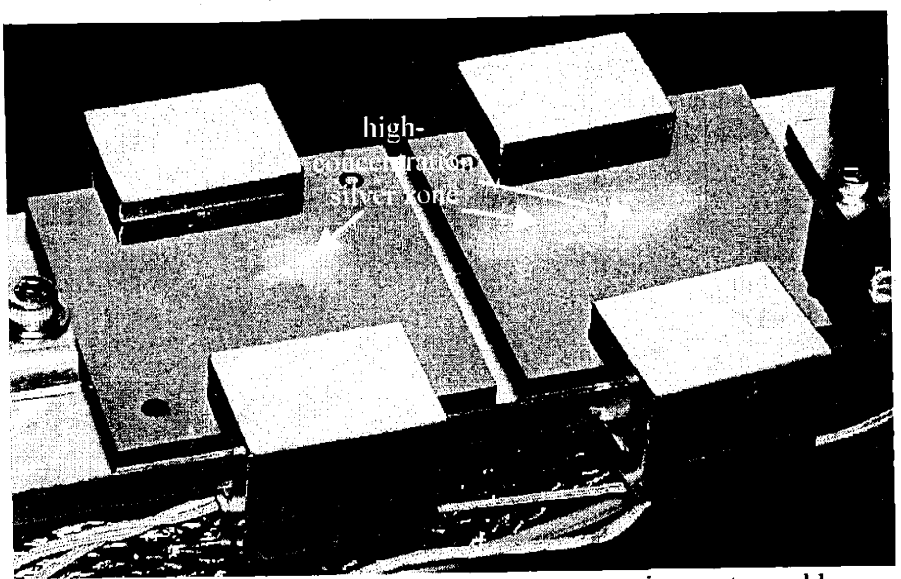

Figure 3-3. The silver implantation consists of a high-concentration center and low-concentration halo as seen on samples 1 (left) and 2 (right) after ion implantation.

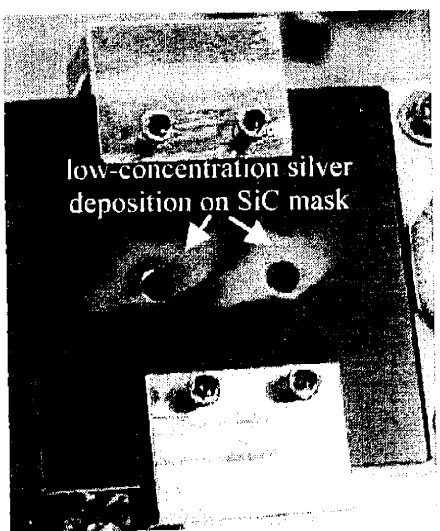

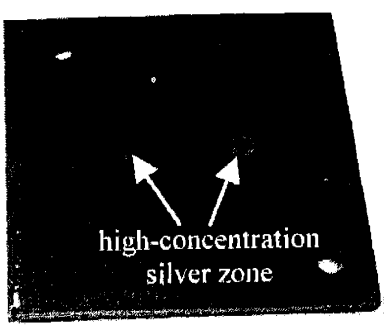

a) The mask on sample 5 after implantation shows low-concentration silver region.

b) The silver implantation zone is well defined beneath the mask on sample 6.

Figure 3-4. SiC masks in front of the SiC samples restrict silver implantation to well-defined areas.

Table 3-1 lists the silver ion implantation conditions for all of the implanted SiC samples. The total irradiation times were selected to achieve implanted doses on the order of 10^{16} to 10^{17} atoms given the actual current during each implantation run. The calculated cumulative doses in the high silver concentration volume (4 mm diameter × 1 μm depth) ranged from 2.4×10^{16} silver atoms to 1.4×10^{17} silver atoms.

Table 3-1. Silver ion implantation conditions for all of the SiC samples

Sample ID	Beam Energy (MeV)	Silver Charge State	Irradiation Time (h:min)	Time Averaged Current (eμA)	Minimum Current (eμA)	Maximum current (eμA)	Cumulative dose (atoms)
1	161	+18	11:43	1.7	1.4	2.2	2.5 E16
2a	161	+18	7:54	2.4	2.3	2.8	2.4 E16
2b	161	+18	22:17	3.2	1.5	4.8	9.3 E16
4a	93	+19	18:31	3.6	2.7	5.1	8.5 E16
4b	93	+19	20:09	5.1	4.1	8.2	1.3 E17
5a	93	+19	10:10	6.9	7.9	9.8	1.0 E17
5b	93	+19	9:21	7.6	7.0	9.0	8.7 E16
6a	93	+19	6:27	13.1	12.0	14.0	1.3 E17
6b	93	+19	6:33	12.4	12.0	13.5	1.2 E17
7a	93	+19	7:34	10.7	9.8	12.0	1.3 E17
7b	93	+19	13:21	8.7	7.2	9.8	1.4 E17

3.2.3 Expected Implantation Effects on SiC Microstructure

The silver implantation resulted in extensive radiation damage in the SiC due to the energy loss and displacement cascades associated with the slowing down of the silver ions. Questions related to the possible interaction between the SiC damage and silver transport processes are important and must be addressed. Slowing down of the high-energy silver ions produces radiation damage that can be grouped into two general categories: 1) electronic energy loss, and 2) displacement production. The slowing down process is, as a rule of thumb, dominated by coulombic interactions (electronic energy loss) until the energy of the ion is reduced to a value in keV approximately equal to its atomic weight. For silver ions, therefore, electronic energy loss will dominate until the energy has decreased to approximately 100 keV. Roughly 99% of the silver energy loss, therefore, will be in the form of heat which will be deposited, spatially, in front of the displacement damage. The remaining energy loss will result in the production of displacement cascades. The displacement cascades will produce damage in the form of displacements, dislocation loops, and, if the dose and dose rate are high enough, amorphization and/or recrystallization of the SiC.

For the implantation conditions in this work, SRIM calculations indicate that significant displacement damage begins at a depth of 5 μm and 7 μm for the 93 MeV and 161 MeV cases, respectively, with the peak in displacement damage occurring at about 9 μm and 13 μm, respectively. Figure 3-5 shows the results of the SRIM calculations for 93 MeV and 161 MeV silver ions in SiC. Although the SRIM code calculates damage using a simple Kinchen-Pease displacement model, the results are instructive on a relative basis when comparing the number of displacements and subsequent vacancy production and will be quite accurate when predicting the energy loss and spatial distribution of damage.

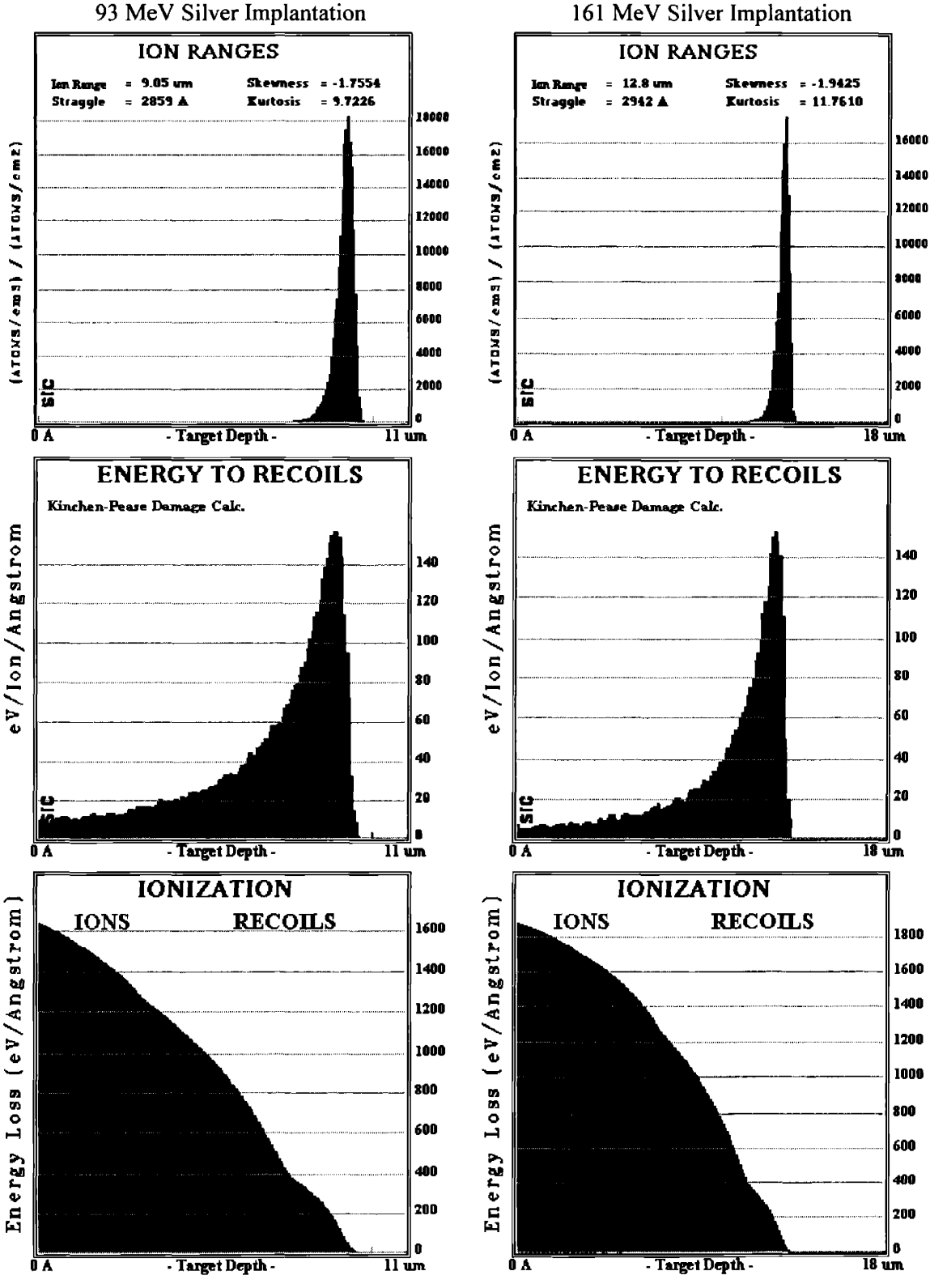

Figure 3-5. Results of SRIM calculations for silver implantation at 161 MeV and 93 MeV.

With respect to amorphization, Wendler et al. have shown that for high-energy ion damage, SiC amorphization becomes impossible at temperatures above approximately 250°C.[6] Heera et al. have discussed the dynamic relationship between the damage rate, ion characteristics, and the location of the ion-beam induced epitaxial/amorphized region boundary.[7] Also, Pacaud et al. have reported that the crystallization temperature for ion implanted SiC is approximately 950°C.[8]

Based on the above discussion, the implantation process was expected to result in a multi-zone damage region consisting of the following zones when proceeding from the beam entry point: 1) a region of unaltered SiC where, while the electronic loss energy deposition is very high, the displacement damage will be essentially zero; 2) a region where the displacement damage begins to accumulate and in which the SiC will be severely disrupted and probably dynamically recrystallized; 3) a region where amorphization has occurred since the irradiation temperature was not expected to exceed 250°C; and 4) a region of undamaged SiC beyond the which may have a diffuse boundary due to straggling of the ion slowing down process. The silver is expected to be in the rear of amorphous SiC region.

With respect to the effect of the radiation damage on the morphology of the silver, as it may affect migration during subsequent annealing, the damage process will result in complete mixing of the SiC and silver in the amorphous region. The silver, implanted at a peak concentration of approximately 20 atomic percent, is expected to precipitate, as elemental silver, within the damage zone since the solubility of silver in SiC is negligible. This arrangement should provide an almost ideal situation in which silver is in intimate contact, if not actually mixed, with the SiC matrix. Additionally, the recrystallized SiC region can be expected to provide grain boundary area for diffusion. Lastly, the annealing process will result in recrystallization of the damaged, amorphous region, producing grain boundaries in exactly the same location as the silver. Such conditions should be ideal for silver diffusion through the SiC as predicted in the literature.

3.2.4 Annealing Conditions

The goal of the ion implantation experiment was to observe silver migration in SiC from a known and measurable initial concentration. Implantation of a high silver concentration, on the order of 10 atomic percent averaged over the entire implantation volume, ensured that the silver concentration profile would be measurable, above the detection limits of the analysis techniques, both before and after annealing.

All of the heat treatments were conducted in a Webb graphite furnace at 1500°C ± 15°C. A heat treatment temperature higher than typical operating temperatures was selected in an effort to encourage diffusion. A review of the literature indicated that grain boundary diffusion was the dominant silver transport mechanism with a representative diffusion coefficient of 2×10^{-15} m^2/s. The heat treatment conditions were selected to observe measurable silver transport after the test, based on the literature values. At 1500°C, measurable silver transport was predicted, given representative diffusion coefficients, in fewer than 10 h. Heat treatments as long as 480 h were conducted to allow ample time for silver transport in the SiC samples.

The Webb furnace operates under low vacuum at 1500°C with typical vacuum readings in the range of 4-15 mTorr. Each sample was sandwiched between two blocks of silicon carbide, approximately 5 × 5 × 1.3 cm, to limit interaction between the surface of the implanted SiC and any contaminants in the furnace atmosphere.

The silver concentration profile was measured in sample 2b before and after annealing at 1500°C for 210 h. AEM (analytical electron microscopy) of sample 6a after implantation and sample 5a

after 480 h at 1500°C compared the effects of annealing on the silver distribution. Table 3-2 shows the heating data for the samples analyzed; details of the analyses are discussed below.

Table 3-2. Annealing conditions for selected samples.

Sample ID	Implanted Dose (atoms/cm^3)	Temperature (°C)	Time (h)	Analysis
2b	1.9 E+21	1500 ± 15	210 ± 0.25	XPS profiles
5a	2.1 E+21	1500 ± 15	480 ± 0.25	AEM
6a	2.6 E+21	n/a	n/a	AEM

3.3 RESULTS AND DISCUSSION

Before and after heating, the ion implantation samples were analyzed using XPS (X-ray photoelectron spectroscopy) to measure the silver concentration profile, and SEM (scanning electron microscopy) and AEM to examine the silver distribution within the SiC. XPS detected no measurable change in the bulk silver concentration profiles after heating. SEM and AEM analyses showed a change in the microscopic distribution of the silver, with a diffuse silver distribution after implantation transforming to discrete silver precipitates after heating. Additionally, the AEM analysis showed the diffuse silver residing in amorphous SiC after implantation and silver precipitates between recrystallized SiC grains after heating. Both the SEM and AEM analyses showed that the silver did not migrate out of its original deposition zone.

3.3.1 Silver Concentration Profiles

Measurements of the silver concentration profiles before and after heating were expected to show silver diffusion away from the initial implanted profile. Calculations based on previously reported diffusion coefficients predicted complete depletion of the silver concentration profile

after 210 h at 1500°C.

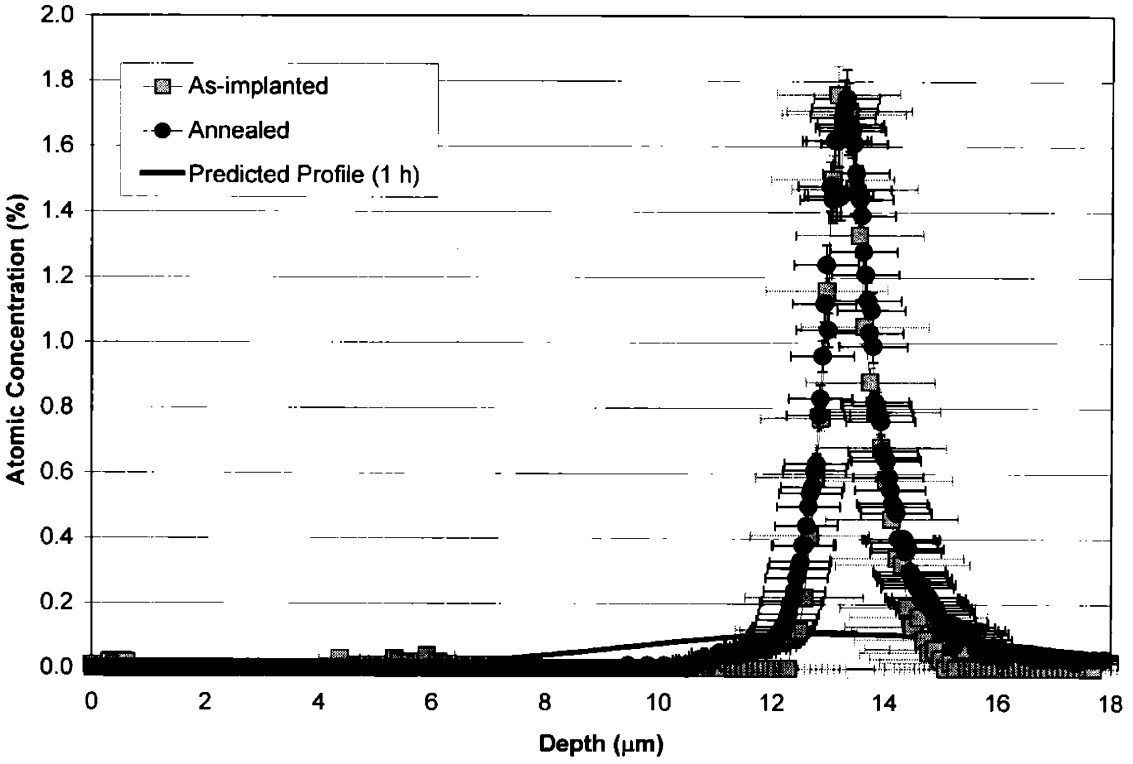

Figure 3-6, however, shows that there was no change in the silver concentration profile in sample 2b after heating at 1500°C for 210 h. The expected silver concentration profile, based on the diffusion coefficient reported by Amian et al., after just 1 h at 1500°C is also shown in Figure 3-6.[9] Diffusion of the magnitude previously reported clearly did not occur, if at all.

XPS, also known as ESCA (electron spectroscopy for chemical analysis), measures concentration profiles by alternating spectral data collection with sputter cycles. The spectral data collection includes the identification of the elements present along with bonding information while the sputter cycles remove material and expose successively deeper layers of the sample. One advantage of XPS analysis is the ability to distinguish not just the elements, but also the chemical bonds present; with this technique, for example, free silicon can be distinguished from silicon bound in silicon carbide. In the sample analyzed, XPS detected no free silicon above the detection limit of approximately 1 atomic percent.

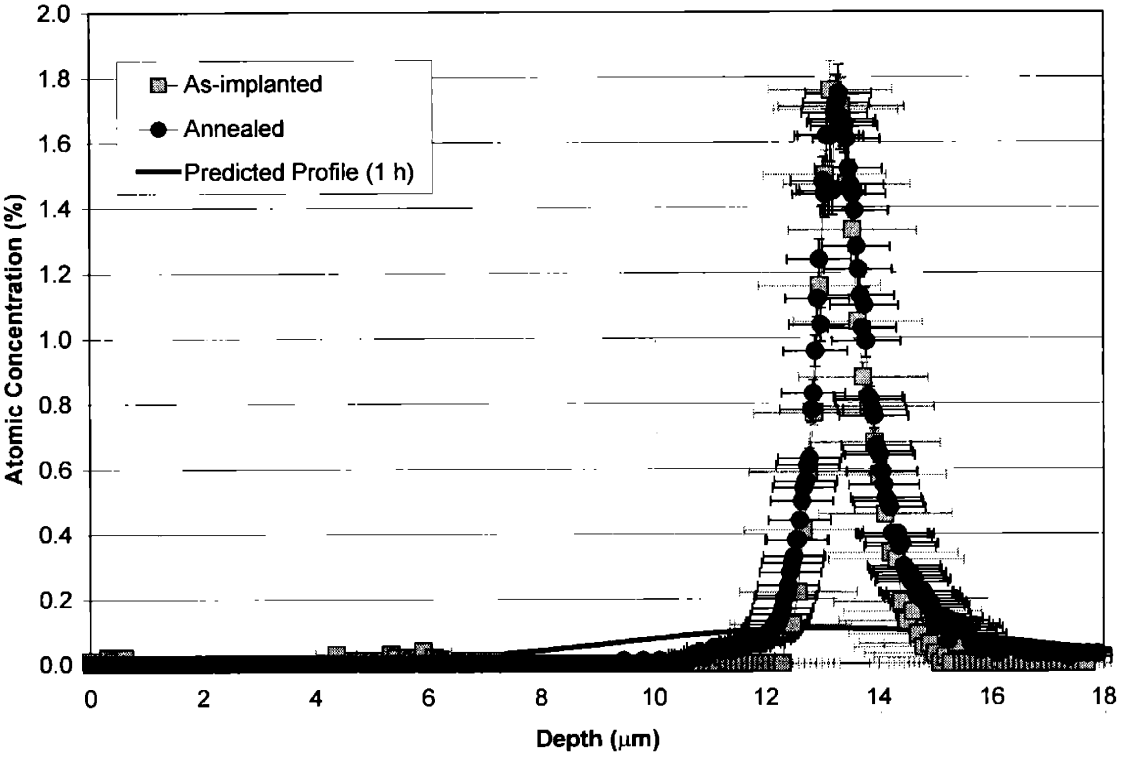

Figure 3-6. Silver concentration profiles before and after heating at 1500°C for 210 h are the same (sample 2b).

To achieve the best comparison between silver concentration profiles before and after heating, it was necessary to use the same sample. A 1.3 mm hole punched in a thin gold foil provided a mask over the 4 mm silver implantation area, preserving the small silver spot from the normally large XPS sputter area, usually a few millimeters in diameter. A schematic of the gold-foil mask over the SiC sample is shown in Figure 3-7. Use of the small gold mask increased uncertainties in the final XPS concentration profiles due to self-shielding during sputtering leading to edge rounding of the sputter crater. An uneven and sloped crater bottom also increased the uncertainty of the total depth of the crater.

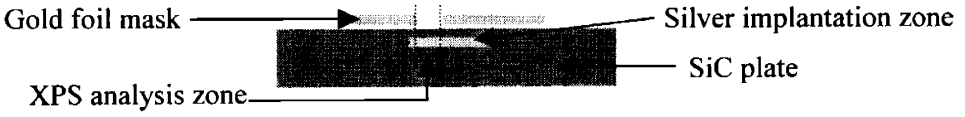

Figure 3-7. A gold-foil mask limited the XPS analysis area (schematic not to scale).

A tight fit between the size of the sputter area and the size of the XPS analysis beam increased uncertainty in the final concentration profile. The bottom of the sputter crater was about the same size as the analysis beam. When the analysis beam measured the concentration at a certain depth, up to 10% of the data signal actually came from the rounded edges of the sputter crater and even from the sides of the crater walls. At any depth, therefore, the detected signal was actually coming from a range of depths, not just the bottom of the crater. Although these uncertainties in the silver concentration profile tended to artificially widen the measured concentration profile, they were present in both analyses, still allowing for a direct comparison between the two profiles before and after heating.

A silicon carbide sputter standard was not available to determine the sputter rate during the XPS analysis. A Zygo interference microscope was used to measure the depth and shape of the sputter craters. Figure 3-8 shows the sputter crater after XPS analysis of the silver concentration profile after at 210 h, 1500°C heat treatment. The depth of the sputter craters was used to calculate the sputter rate during XPS analysis and generate a concentration depth profile from the spectral data. The sputter rate was assumed constant throughout the silicon carbide and equal to the total crater depth divided by the total sputter time. However, an uneven and sloped crater bottom created uncertainty in the total depth of the sputter crater and the sputter rate.

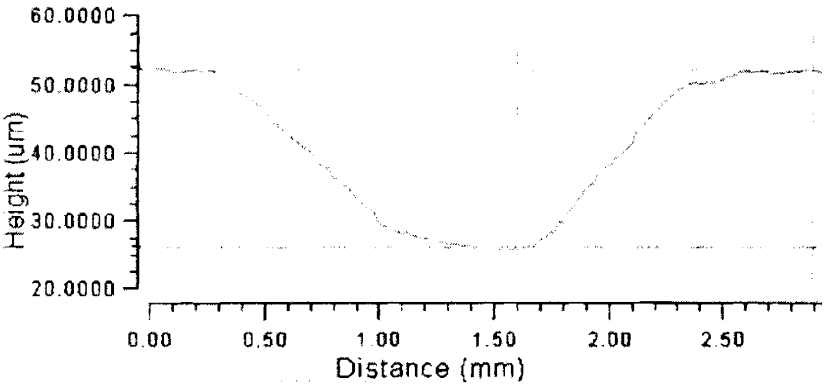

Figure 3-8. The sloped walls and narrow bottom of the XPS crater contribute to the measurement uncertainty.

These uncertainties are shown as error bars in

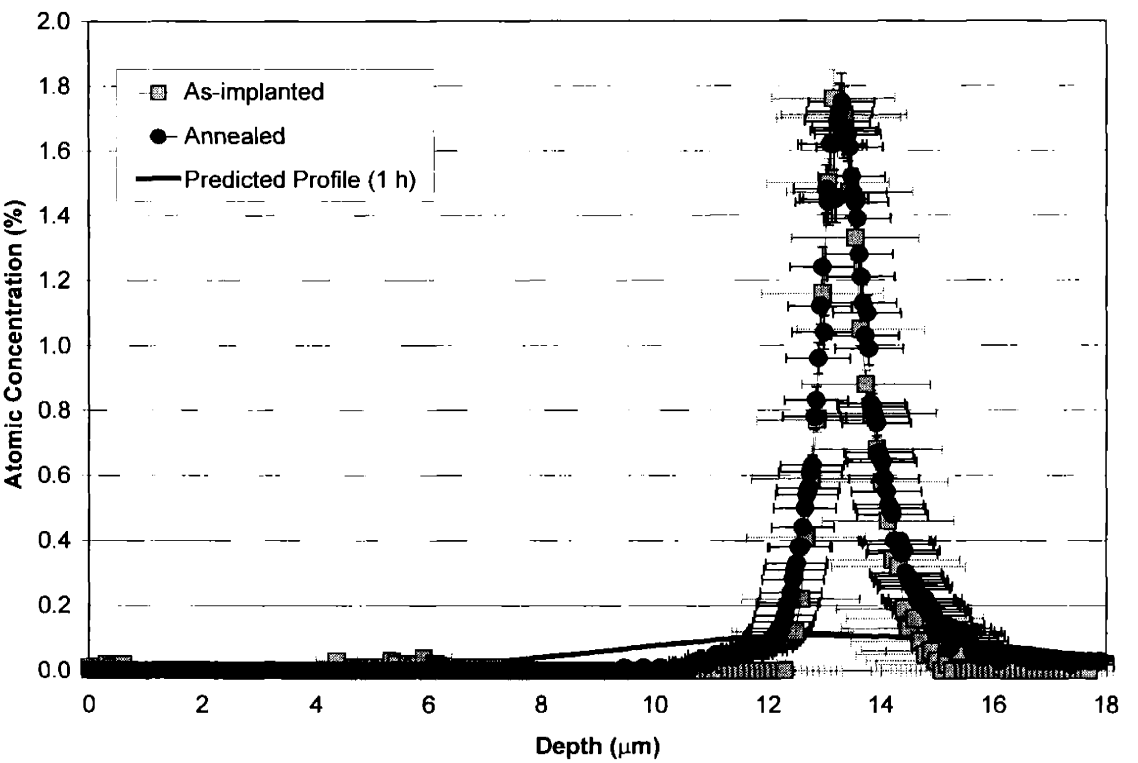

Figure 3-6, but it is still clear that, within the uncertainty of the XPS analysis, there was no silver migration during heating, a significant departure from the expected results. If silver migration were governed by typical diffusion coefficients reported in the literature, the silver concentration

after heating for 210 h at 1500°C would be completely depleted. However, there was no macroscopic silver concentration change during heating. Within the spatial resolution of XPS the silver concentration profiles before and after heating were the same and silver did not diffuse during the 210 h anneal at 1500°C. Based on the lack of change in the silver concentration profile after heating and the uncertainty of the measurement, the diffusion coefficient for silver in SiC must be less than 5×10^{-21} m^2/s at 1500°C.

XPS results average the spectral data collected over a fairly large area, approximately 800 μm × 800 μm. Techniques with finer spatial resolution, such as SEM and AEM, were needed to investigate the detailed silver behavior and the effects of ion implantation in silicon carbide.

3.3.2 Electron Microscopy

3.3.2.1 Background

Although it is significant that no macroscopic silver concentration changes occurred during heating for 210 h at 1500°C, the details of silver behavior in silicon carbide were of interest. Both SEM and AEM examinations of the SiC samples revealed details of the silver distribution and the SiC microstructure. The goals of the SEM analysis were to observe the distribution of the silver in the SiC samples and to compare the width, if possible, of the silver zone before and after heating. Higher magnification AEM analyses provide details of the SiC microstructure and the silver distribution and orientation with the SiC zones.

AEM was used to analyze thin cross-sectional slices of two ion implantation samples, one before annealing and one after. The goals of the AEM analysis of the ion implantation samples were to observe and identify the silver location in the implanted region, both before and after heating. An additional goal was to characterize the silicon carbide grain structure both within and outside the implantation region and also to characterize, if possible, the damage in the implanted region. The AEM analyses were performed on a Philips CM300 equipped with an EDAX X-ray detector for elemental analyses.

3.3.2.2 Scanning Electron Microscopy

SEM analysis of polished cross-sectional surfaces of the SiC ion implantation samples, both before and after annealing, highlights contrast in atomic number at the sample surface, with higher Z materials appearing brighter in the images (e.g., silver appears brighter than silicon). The SEM analysis was performed on a FEI/Philips XL30 FEG Environmental SEM with energy-dispersive X-ray capability. The SEM was operated under H_2O vacuum mode.

The silver distribution after implantation is seen in Figure 3-9*b* and *c* at low and high magnification, respectively. The implanted silver zone is approximately 9 μm below the front edge of the SiC sample and approximately 1 μm wide, in good agreement with the predicted silver profile calculated using SRIM and shown in Figure 3-9*a*. The silver location is also consistent with the calculated displacement damage morphology shown in Figure 3-5 (93 MeV). Chemical analysis by EDS (energy dispersive spectroscopy) indicates that silver is located only in the bright area. The EDS spectra associated with the locations identified in Figure 3-9*b* are shown in Figure 3-10; the locations identified as 1 and 3 are SiC and location 2, in the bright region, contains silver.

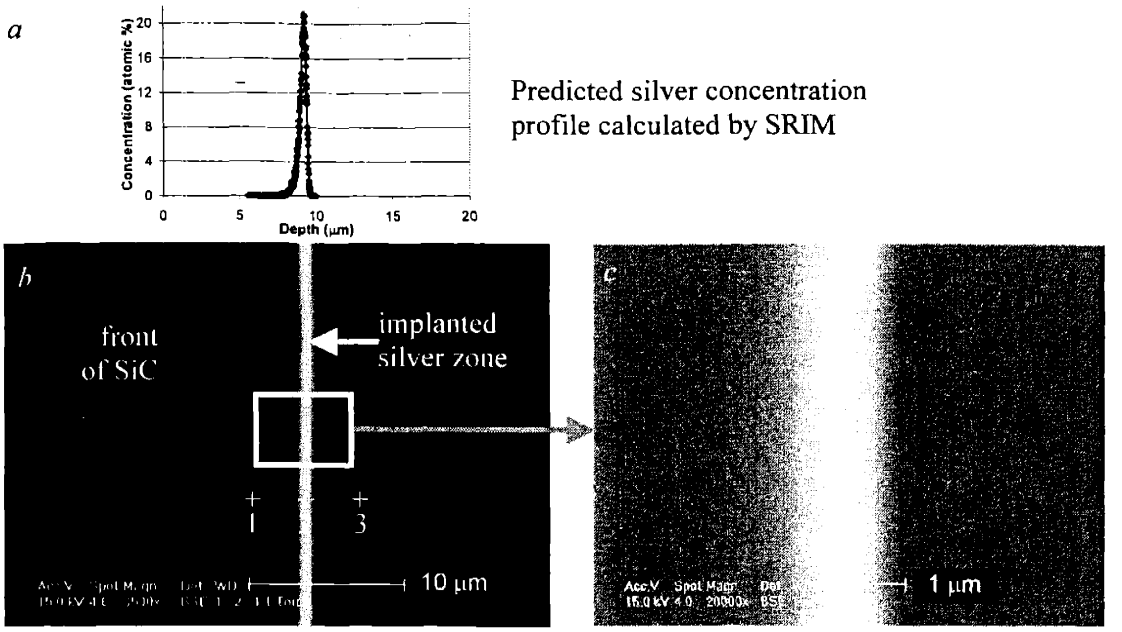

Figure 3-9. The as-implanted silver distribution matches the *a*) predicted profile from SRIM and appears bright in SEM backscatter imaging and is diffuse (homogeneous) in sample 6a at *b*) low magnification and *c*) high magnification.

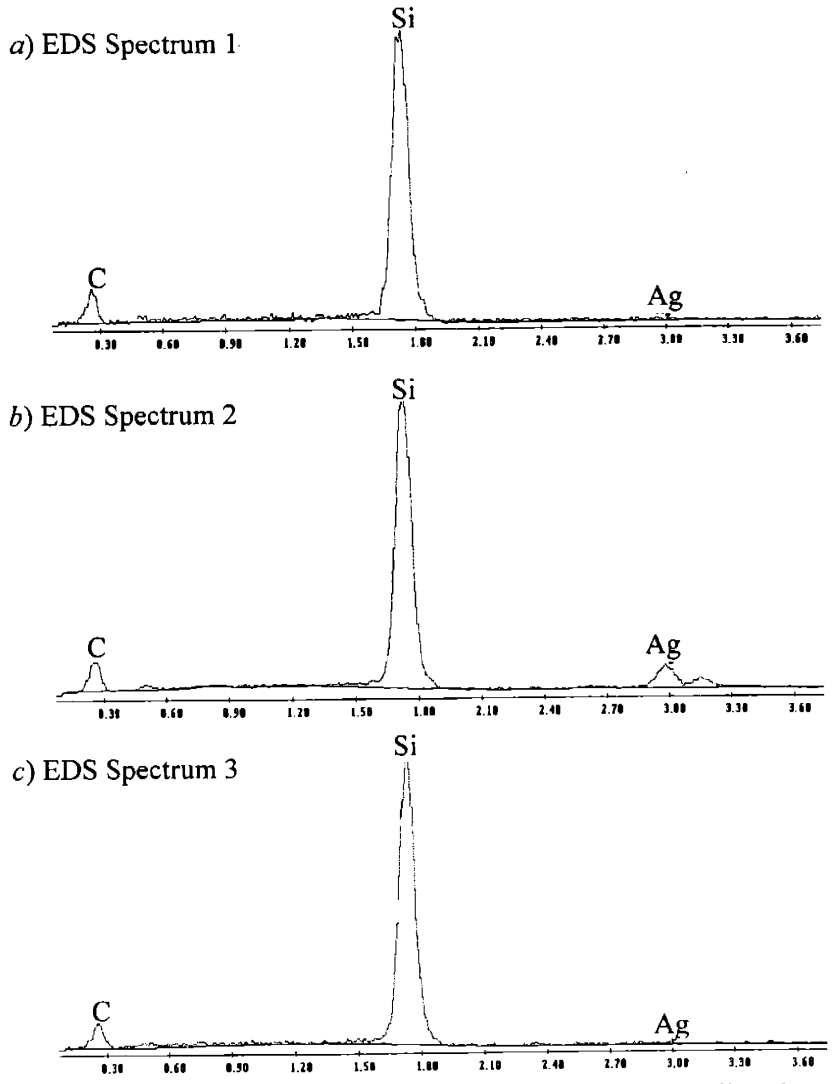

Figure 3-10. EDS spectra from points *a*) 1, *b*) 2, and *c*) 3 in Figure 3-9. Silver is only present in the bright area; no silver is detected on either side of the implantation zone.

After heating for 480 h at 1500°C, the silver appears discrete and individual silver particles are evident, as seen in Figure 3-11. While the arrangement of silver appears coarser after heating, the width of the silver zone is still approximately 1 μm, unchanged during heating.

As mentioned earlier, atomic number contrast in the SEM causes heavier elements to appear brighter in basckscatter images. Thus, silver appears as bright spots in contrast to the gray silicon carbide in the SEM images. Some bright spots appear in front of the implanted silver zone in Figure 3-11 (towards the left in the image). Although EDS confirmed that the composition of the bright spots in the implanted silver zone was silver, the bright spots in front of the main implanted silver zone were not analyzed. These spots are likely silver that has precipitated in a defect structure in the SiC.

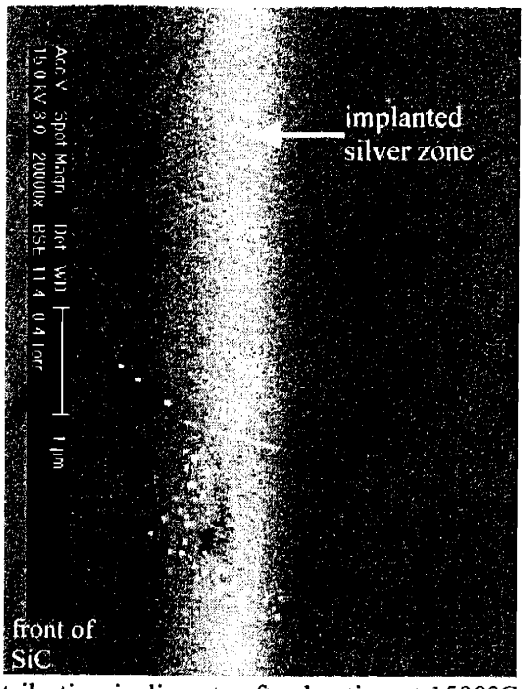

Figure 3-11. The silver distribution is discrete after heating at 1500°C for 480 h (sample 5a).

3.3.2.3 As-implanted SiC Microstructure

A recrystallized zone of silicon carbide defines the front of the silver implantation zone in sample 6a, before annealing, as seen in Figure 3-12. The original silicon carbide columnar grain structure is visible to the left and right of the implantation zone. The altered zone consists of three main regions. In the front-most region of the implantation zone, on the left in Figure 3-12, the SiC has already recrystallized. The middle of the altered zone contains amorphous SiC. Towards the back, the SiC is still mostly amorphous, but small SiC crystallites have nucleated.

While all of the SiC grains in the recrystallized zone at the front of the implantation zone are fine-grain equiaxed, there appears to be a further distinction between smaller, more equiaxed grains at the front and slightly larger, more elongated grains at the back. The smaller equiaxed grains are approximately 50-150 nm and the larger grains are about 100-200 nm wide by 250-400 nm long.

The back 1.1 μm of the altered zone is largely amorphous, but also contains some small equiaxed SiC crystallites ranging in size from less than 4 nm to about 30 nm. Silicon carbide grains have nucleated and started to grow in the back of the amorphous region during implantation, but have not been able to incorporate all of the SiC. A thin band of the original SiC behind the altered zone, about 80 nm wide, appears damaged with increased faulting, though the damage was not great enough to cause amorphization or recrystallization.

Predicted silver concentration profile from SRIM calculations

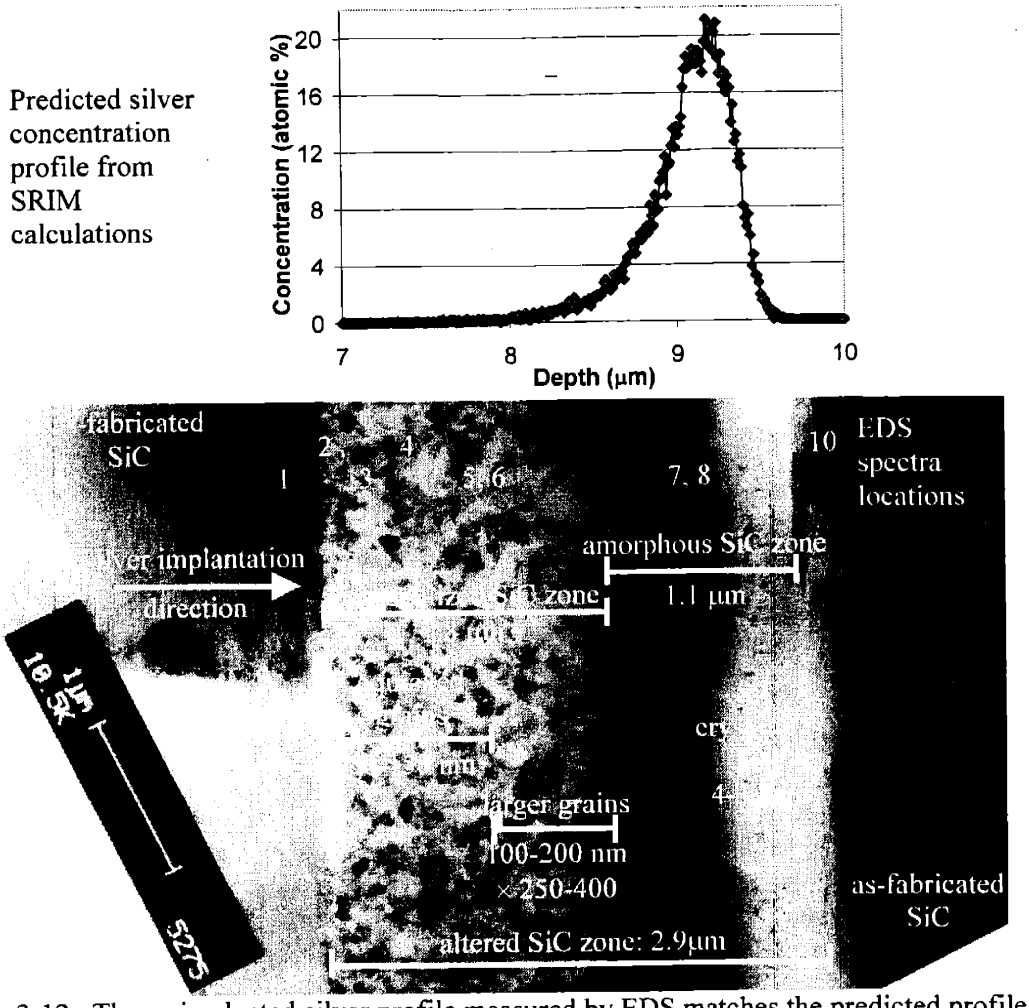

Figure 3-12. The as-implanted silver profile measured by EDS matches the predicted profile from SRIM calculations; numbers indicate EDS spectra locations.

EDS (energy dispersive spectrometry) measurements taken during the AEM analysis along the cross-section of the implanted sample provide a qualitative assessment of the silver concentration in the silicon carbide. The locations of EDS measurements are shown in Figure 3-12 and the silver concentrations are listed in Table 3-3. No silver was observed in the original SiC in front of the altered zone or in the front portion of the recrystallized zone. Silver just above the detection limit of approximately 1000 ppm (0.1 atomic percent) was measured in the recrystallized zone at the boundary between the equiaxed and slightly dendritic SiC grains. EDS detected peak silver concentrations in the amorphous SiC region. A small amount of silver was detected at the boundary between the amorphous region and the original SiC and just a trace of silver was measured in the damaged layer of the original SiC just behind the altered zone. The silver profile, measured by EDS, agrees with the predicted silver implantation profile, as seen in Figure 3-12, with the peak concentration occurring in the amorphous SiC.

Table 3-3. Most of the silver, detected by EDS, is located in the amorphous SiC region.

Spot #*	Location	Silver Concentration (%)
1	as-fabricated SiC, front -	none detected
2	interface between front SiC and recrystallized SiC	none detected
3	~0.2 μm into recrystallized SiC	none detected
4	in the middle of the recrystallized, equiaxed SiC	1.1 (trace)
5	between the equiaxed and dendritic recrystallized SiC	2.8
6		5.1
7	amorphous damaged region	26.3
8		25.1
9	interface between amorphous SiC and as-fabricated SiC	4.0
10	damage zone of as-fabricated SiC	1.2 (trace)

* EDS spot locations are shown in Figure 3-12.

Additional analysis using a VG HB603 STEM (scanning transmission electron microscopy) operated at an acceleration voltage of 250 kV highlights the presence of silver in the amorphous SiC zone and decorating the first row of grains in the recrystallized zone, as seen in Figure 3-13. The images displayed in Figure 3-13 correspond to the middle of Figure 3-12, the interface between the recrystallized and amorphous SiC zones. The small bright dots in the STEM images are silver-rich while the dark areas are silicon-rich. The spatial resolution of the chemical analysis in the STEM was on the order of the size of the bright features, so the quantitative composition of the bright features and dark areas cannot be determined. No silver was detected in the undecorated recrystallized SiC grains below about the first row next to the amorphous SiC zone, as seen in Figure 3-13*a*.

At this resolution it is clear that the silver morphology depends on the SiC region in question. In the amorphous region, seen in Figure 3-13*b*, the silver is separated into small, approximately 5 nm in diameter, regions. The distribution of these silver-rich regions is random, in keeping with the amorphous nature of the region. In the recrystallized SiC material, seen in Figure 3-13*c*, the silver regions are slightly larger, but the morphology now appears oriented within the SiC crystal structure. The β-SiC (3C-SiC) crystallizes in the zinc blende structure, which can be visualized as two interpenetrating (carbon and silicon) face-centered cubic lattices offset by ¼ cubic diagonal. The morphology of the silver suggests a preference for precipitation on the close packed planes in this structure, i.e., the (111) body diagonals.

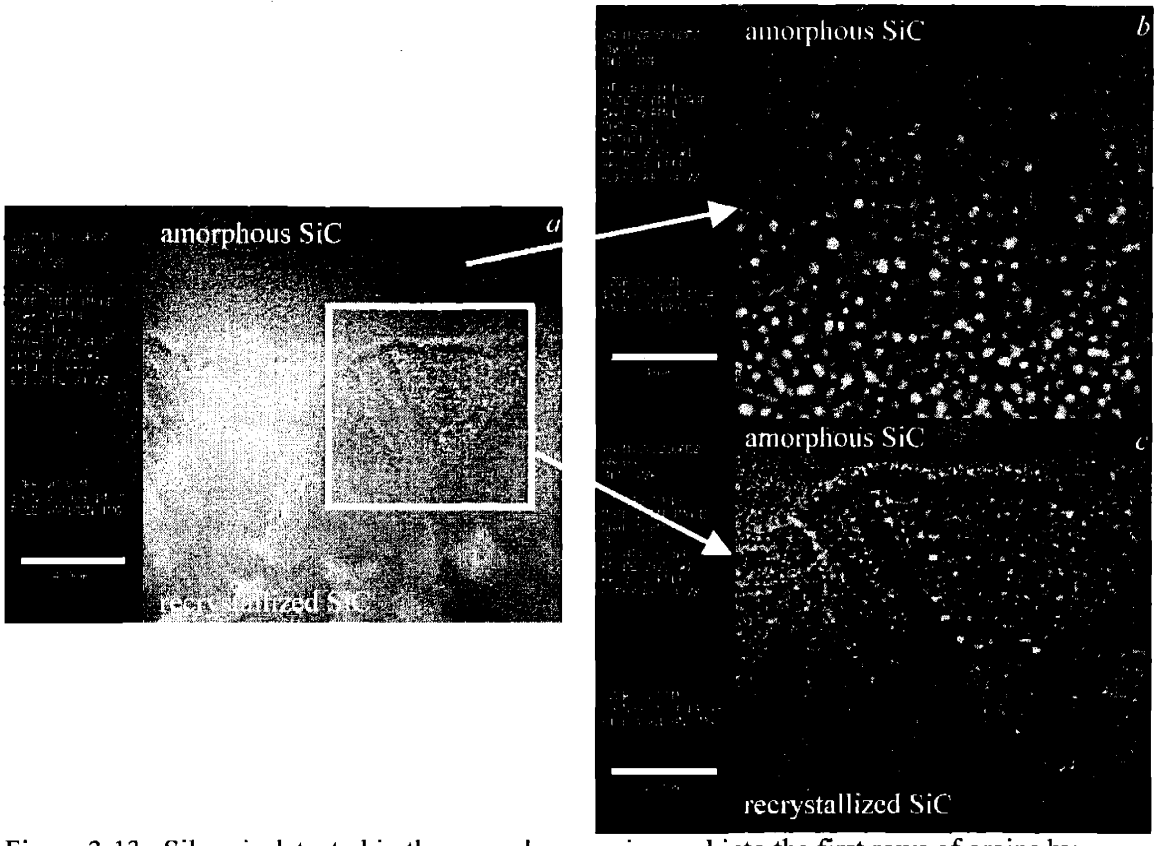

Figure 3-13. Silver is detected in the amorphous region and into the first rows of grains by STEM of the as-implanted sample 6a.

An elemental line scan collected during STEM analysis, shown in Figure 3-14, also confirms the implanted silver distribution as measured during AEM analysis and seen in Figure 3-12 and Table 3-3. The results, though qualitative, confirm that silver is located predominantly within the amorphous region and extends just into the recrystallized SiC zone.

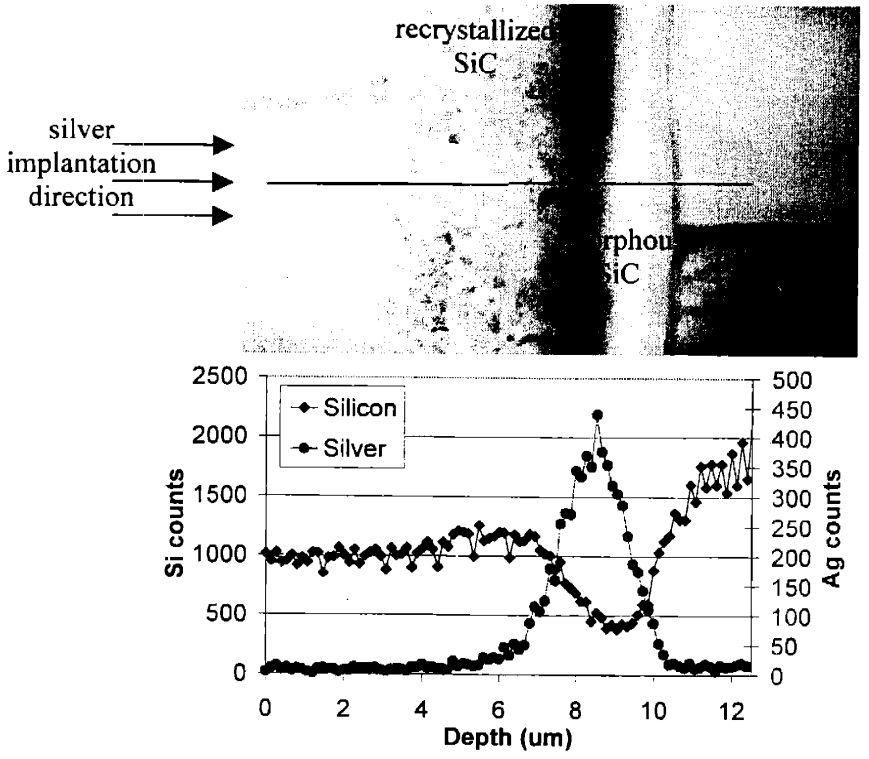

Figure 3-14. A line scan in STEM shows the silver concentration peak in the amorphous SiC zone of an as-implanted sample (6a).

3.3.2.4 *Annealed SiC Microstructure*

The amorphous implantation zone completely recrystallized, as expected, during a 480 h anneal at 1500°C (sample 5b), as seen in Figure 3-15. The amorphous SiC was completely eliminated from the altered zone during annealing. The recrystallized zone is approximately 2.1 μm wide and is characterized by two regions. The front region, which closely corresponds to the region that was dynamically recrystallized during implantation, has been transformed into an epitaxial, columnar region. The rear region, formally amorphous, has crystallized and is characterized by a fine, equiaxed structure. This region also contains precipitated silver, phase-separated from the SiC. Figure 3-16 shows a silver elemental map, taken during STEM analysis in the annealed material. The silver has clearly remained segregated within the implanted region. The crystallized SiC, after annealing, is shown in more detail in Figure 3-17. The silver appears darker than the SiC in the AEM images due to its higher atomic number. The silver is segregated from the SiC and has accumulated on grain boundaries.

While all of the recrystallized SiC grains are small and generally equiaxed, the front of the recrystallized zone features elongated grains, oriented along the implantation direction with widths approximately 30 nm to 100 nm and lengths ranging from 300 nm to 800 nm. The back half of the recrystallized zone contains smaller, more equiaxed SiC grains, on the order of 40 nm to 100 nm.

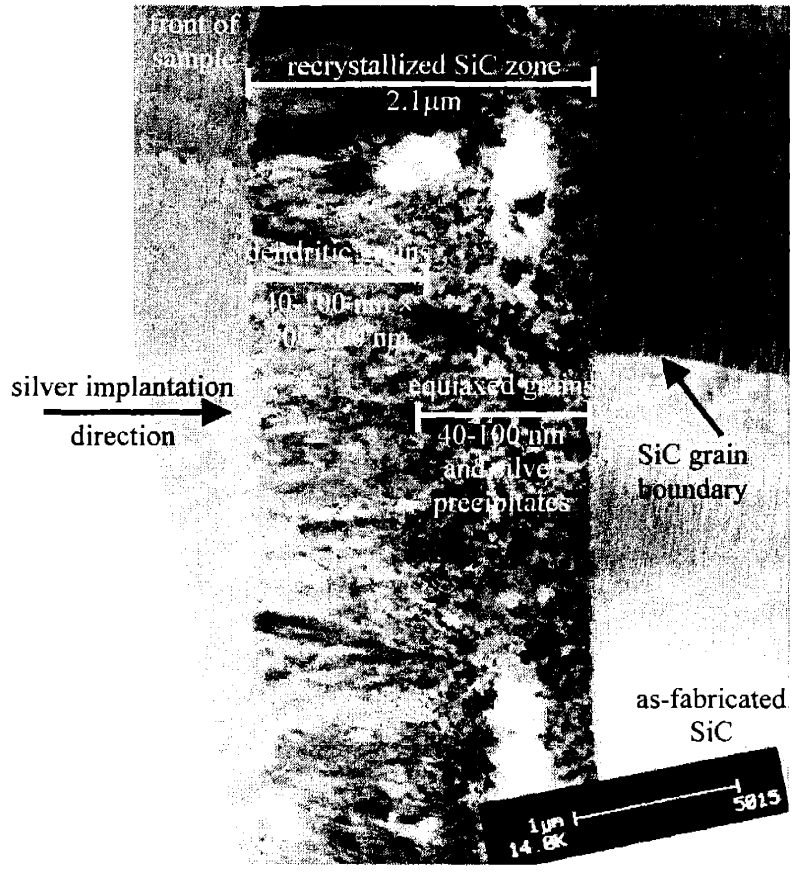

Figure 3-15. The SiC completely recrystallized in sample 5a after heating for 480 h at 1500°C.

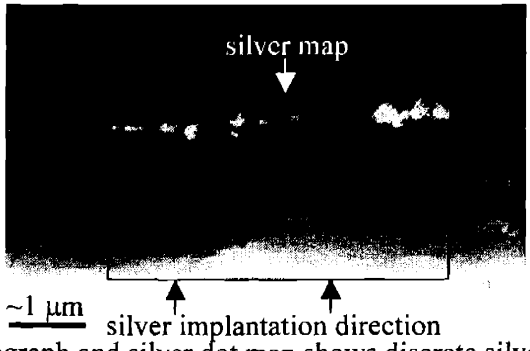

Figure 3-16. STEM micrograph and silver dot map shows discrete silver morphology in the SiC after heating for 480 h at 1500°C (sample 5a).

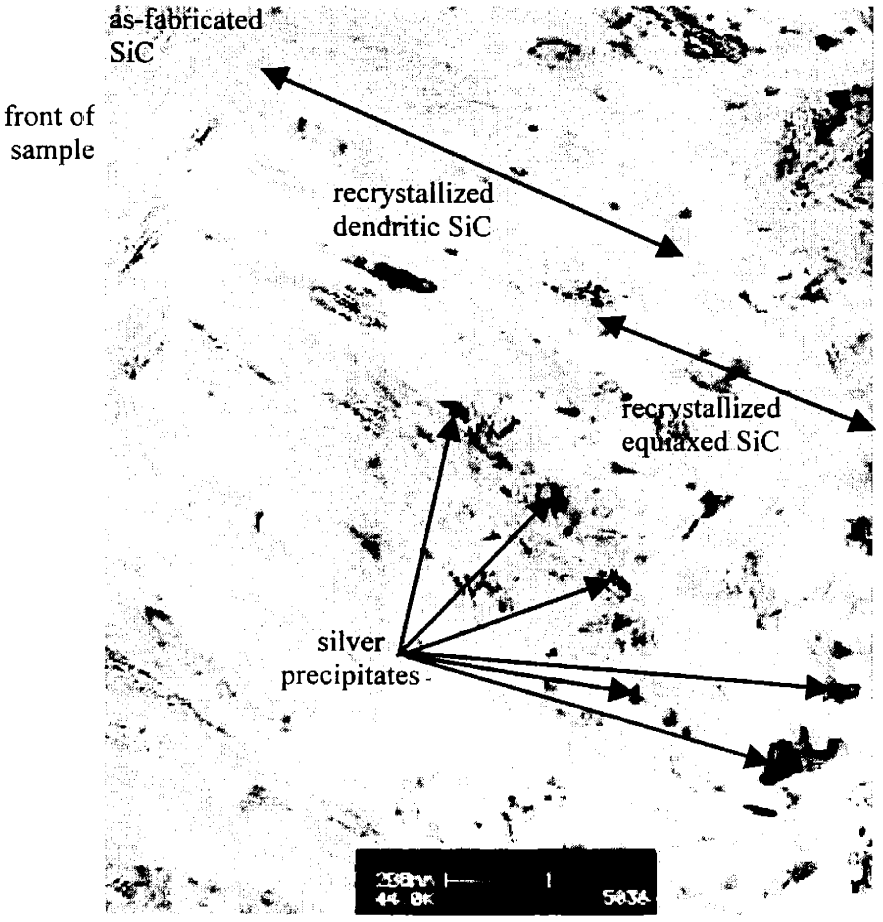

Figure 3-17. Detail of crystallized SiC after annealing for 480 h at 1500°C shows typical silver precipitates (sample 5a).

Just behind the recrystallized zone, there is a zone, approximately 0.5 μm wide, of heavily damaged, original silicon carbide, as seen in Figure 3-18*a*. In this region, the implantation damage was not sufficient to cause recrystallization or amorphization of the original SiC. The radiation damage calculations, however, indicate that a significant amount of displacement damage should have been present. Small precipitates of silver decorate the silicon carbide behind the recrystallized zone, shown in Figure 3-18*b*. These silver regions are approximately 4-20 nm in size. The damaged layer is approximately 300-400 nm wide. As seen by comparing Figure 3-18*a* and *b*, silver is only present in the heavily damaged SiC zone. The low concentration of silver in the damaged SiC just behind the recrystallized zone is consistent with the tails of the silver concentration profile predicted using the SRIM code and the EDS spectra collected during AEM, as shown in Figure 3-12 and Table 3-3. Silver has not migrated into the undamaged SiC regions.

Silver appears only in the rear portion of the altered SiC zone, the same region where it appeared in the as-implanted sample, as seen in Figure 3-12. After implantation, but before heating, silver was detected in the amorphous zone. This zone recrystallized during heating, forming equiaxed grains where the silver was detected. No silver was implanted in the front portion of the altered SiC, where the grains recrystallized during heating and grew slightly during annealing, and none is detected after heating.

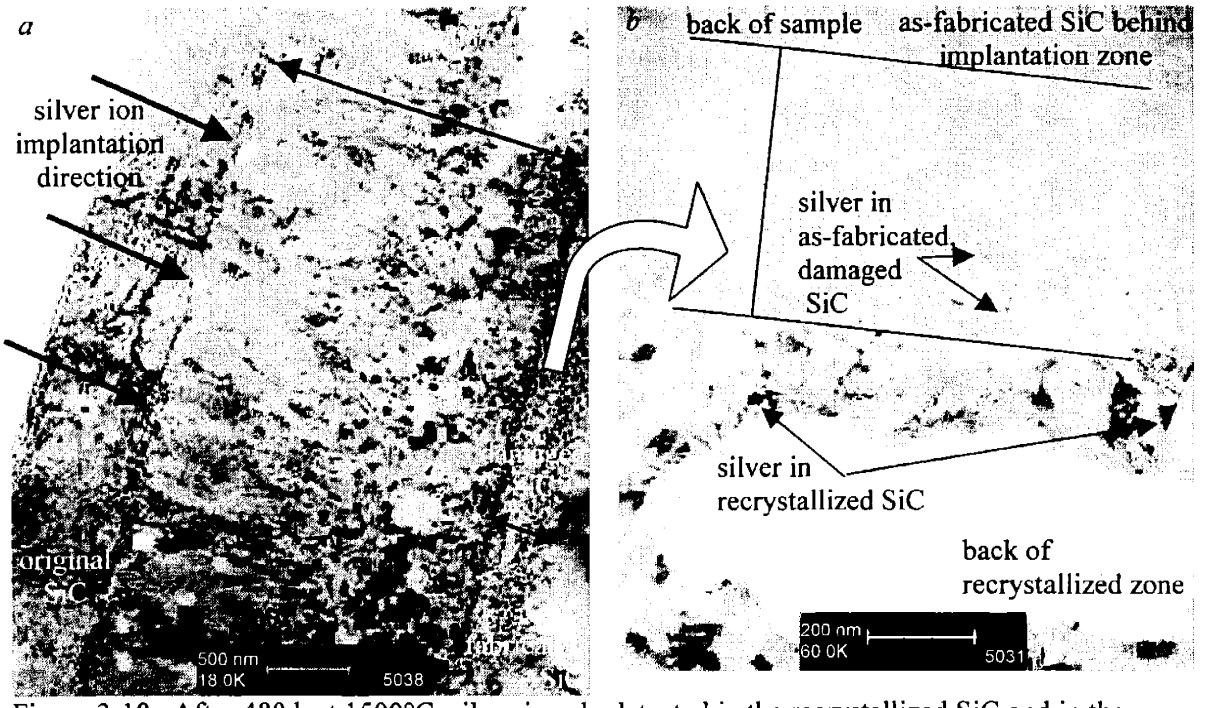

Figure 3-18. After 480 h at 1500°C, silver is only detected in the recrystallized SiC and in the heavily damaged SiC behind the recrystallized zone.

Figure 3-19 shows the details of a typical grain boundary region. Analysis of the grain boundaries in the region immediately behind the damaged region, where grain boundaries from the undamaged region intersect the damaged, silver-containing region, did not detect the presence of silver. Silver has not diffused into the undamaged SiC regions in spite of the fact that optimal conditions existed for migration to occur.

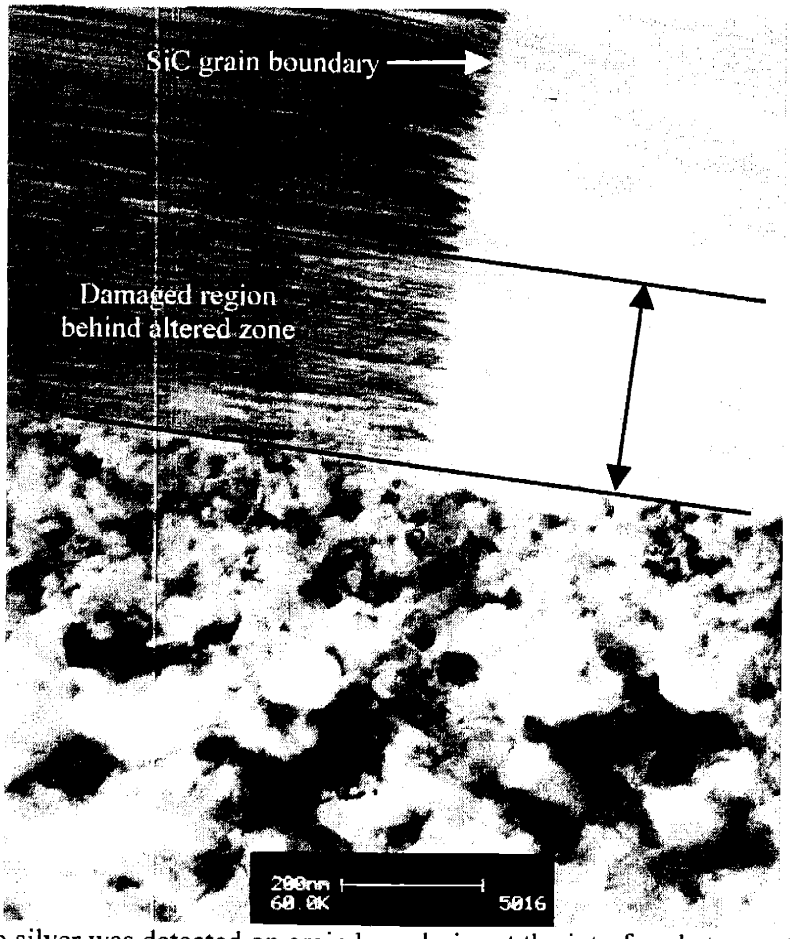

Figure 3-19. No silver was detected on grain boundaries at the interface between the damaged and undamaged regions after annealing for 480 h at 1500°C (sample 5a).

The recrystallization process created new grain boundaries as well as a significant increase in grain boundary area compared to the original CVD SiC microstructure. As the amorphous SiC crystallized and formed β-phase grains, impurity silver atoms were rejected due to their low solubility. The silver atoms, segregated from the recrystallized SiC grains, appear as phase separated precipitates in the SiC recrystallized zone, as seen in Figure 3-20. During annealing, silver was in intimate contact with SiC grain boundaries, but no silver migration was observed either by XPS or AEM analyses. A region of low concentration silver exists just behind the recrystallized SiC in the heavily faulted original SiC microstructure. There is no evidence, however, of silver migration along grain boundaries present in the original SiC, as shown in Figure 3-19 and in the lower right corner of Figure 3-20.

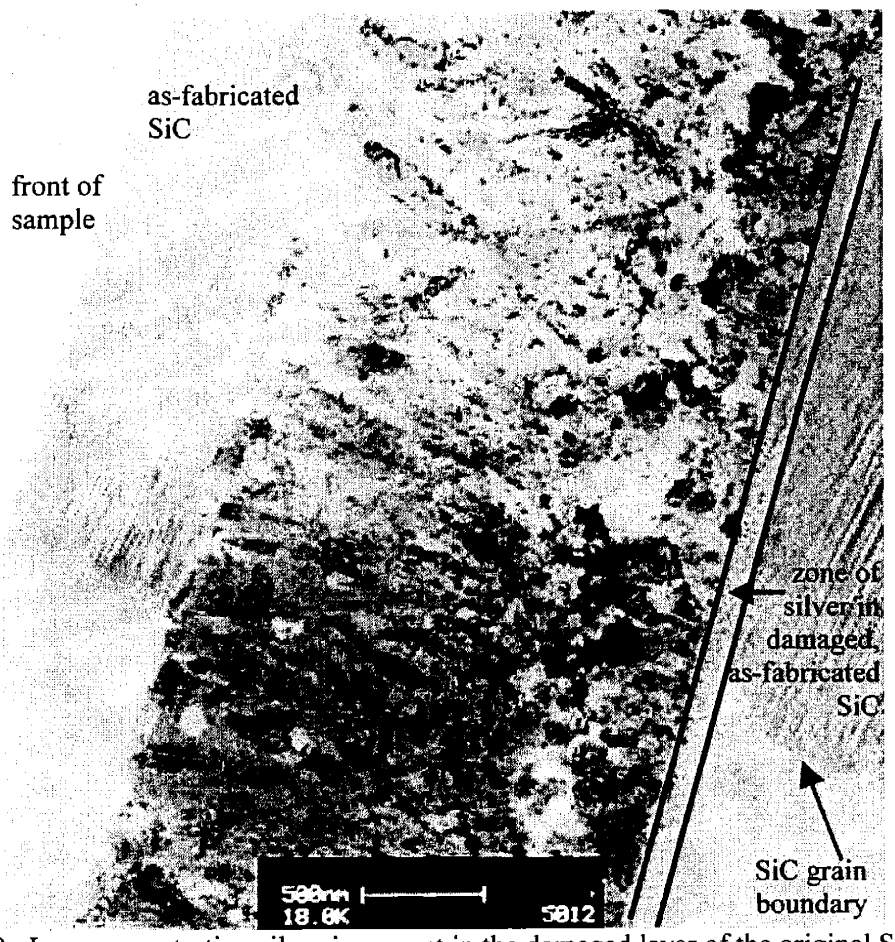

Figure 3-20. Low concentration silver is present in the damaged layer of the original SiC, but migration has not occurred along the grain boundaries.

The recrystallized zone in sample 5a after heating is narrower than the recrystallized plus amorphous zone in sample 6a before heating. Sample swelling measured after implantation is proportional to the implanted dose. Sample 6a had a higher implantation dose than 5a and, therefore, increased swelling, consistent with a wider implantation zone. The implantation zone in sample 5a is also narrower after heating due to the transition from the disordered and lower density amorphous SiC to the more compact β-SiC.

A comparison of the AEM analyses before and after annealing makes it clear that the amorphous SiC region observed before annealing has recrystallized during heating. After annealing, the altered zone contains all crystalline silicon carbide with phase-separated silver. The silver concentration profile after heating matches the profile before heating. EDS did not detect any silver in the front half of the recrystallized zone after heating. Discrete precipitates of silver lie between the SiC grains in the back half of the recrystallized zone. Lower concentrations of silver are present in the damaged layer of the original SiC, behind the recrystallized zone. The relative amounts and position of silver in the silicon carbide match before and after heating, showing that the silver did not move the distances expected based on previously published grain boundary diffusion coefficients.

The silver redistributed during heating as the amorphous silicon carbide recrystallized and the SiC grains grew. Silver, in intimate contact with SiC in the amorphous region before heating,

phase separated during heating as the SiC recrystallized. As the SiC grains grew they rejected the silver, which appears to have negligible solubility in SiC, to the grain boundaries.

Recrystallization created new grains and new grain boundaries, which advanced as SiC grains grew. Yet, no large-scale silver migration occurred. Silver rejected from SiC during recrystallization and grain growth had access to SiC grain boundaries, but no grain boundary diffusion was observed. Even silver at grain boundaries in the heavily faulted region of the original SiC just behind the recrystallized zone did not migrate, an observation in contradiction with the assumptions found in the previous literature.

3.3.2.5 Summary of Electron Microscopy Observations

The silver implantation resulted in a region of dynamically recrystallized SiC and a region of amorphous SiC. The amorphous SiC zone contained most of the deposited silver along with the peak of the silver concentration profile. The amorphous SiC recrystallized during heating and the grains that recrystallized during implantation also grew slightly during heating.

There was no macroscopic change in the silver distribution in the SiC after heating for 480 h at 1500°C. The implanted silver appeared as randomly distributed, small, discrete regions in the amorphous SiC zone after implantation and as larger precipitates between crystalline SiC grains after heating. No silver migration was observed into the dynamically recrystallized SiC zone, in front of the amorphous zone, or into the original SiC behind the implantation zone either during implantation or heating. Additionally, no silver was detected along the grain boundaries, either in the recrystallized SiC or in the original SiC. These results are not consistent with the expected diffusive behavior. Had the silver diffused according to the values reported in the literature, the silver should have diffused many microns away from the initial concentration profile and dropped to undetectable levels in the peak implantation zone.

3.3.3 SiC and Silver Behavior

In order to evaluate the possible effect of radiation damage on potential introduction of "artifacts" in the diffusion process, consider the shape of the silver concentration profiles before and after annealing. An extremely high concentration of vacancies existed in the SiC as a result of the implantation process and should have enhanced diffusion in the damaged SiC region, but not in the undamaged region. Rough calculations indicate that the vacancy production rate in the peak damage region was on the order of 10^{21} vacancies/s/cm^3. The vacancy production rate decreased toward the front of the SiC (the beam entry side), but was still significant. Beyond the peak damage region, however, the vacancy production rate decreased much more abruptly and was zero in the region behind the damaged zone. Since the implantation temperature was far below the temperature for which vacancy migration is significant, the vacancy concentration should have been very high prior to annealing. This should have greatly enhanced the silver diffusion. Inspection of the silver concentration profile, however, shows that there is little, if any, change in the shape resulting from the heat treatment.

3.4 COMPARISON TO LITERATURE

No silver diffusion was measured in a previously reported ion implantation experiment. Nabielek et al. implanted lower energy silver ions into silicon carbide, just below the surface, and annealed the sample for only 30 min at 1180°C.[1] Rutherford backscattering measurements before and after heating showed no change in the silver concentration profile. The authors concluded that silver

had most likely been trapped in SiC grains and, therefore, silver diffusion was not observed because matrix diffusion of silver in SiC is much, much slower than grain boundary diffusion.

The current experiments show that massive SiC recrystallization occurred during both implantation and heating. The solubility of silver in silicon carbide is extremely low and silver was swept out of SiC grains during SiC recrystallization. This evidence shows that silver is not trapped in SiC grains during heating and that trapping, therefore, does not prevent silver migration in ion implantation experiments. Silver, however, is immobilized at SiC grain boundaries; silver, in intimate contact with SiC grain boundaries, did not migrate.

The silver concentration in this work was far above that which would be expected to exist in typical TRISO-coated particle fuel. The annealing temperature, however, was in the same range as the post-irradiation annealing studies used to derive diffusion coefficients for coated particle fuel. Also important to note is that the final recrystallized SiC grain structure is similar to that fabricated in typical SiC layers in tested TRISO-coated particle fuel. While there are variations in some of the coating parameters, the SiC used in the current experiments and the SiC from previous fuel tests were coated using a high temperature CVD process resulting in high-density β-SiC with a fine-grain structure. The results from this experiment are, therefore, applicable to silver migration in CVD SiC in typical TRISO-coated particle fuel.

A comparison of the recrystallized SiC from the current experiments and a typical CVD SiC coating is shown in Figure 3-21. This similarity suggests that it is possible to manufacture CVD SiC that prevents the migration of silver. This would increase silver retention in coated particle fuel, reducing the activity levels in high temperature gas reactors.

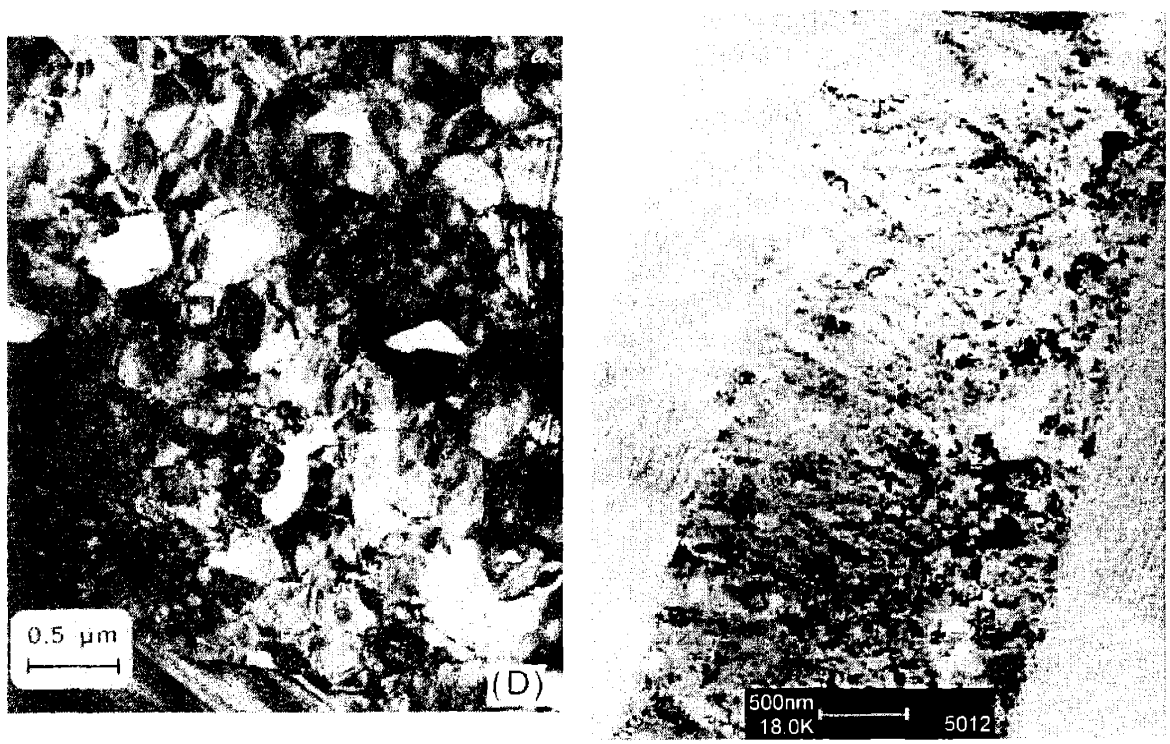

Figure 3-21. Comparison of typical SiC microstructures from *a*) a typical SiC coating and *b*) the current ion implantation experiments.[10]

3.5 CONCLUSIONS

The results of this work clearly show that silver does not move by diffusion, either in the matrix or along the grain boundaries, in CVD SiC for the conditions studied. Even silver near grain boundaries in the original SiC material, observed just behind the recrystallized zone in Figure 3-18*a* and Figure 3-20, did not migrate. There is considerable grain boundary area in the recrystallized portion of the SiC, but no silver was detected outside of its original deposition area. Recrystallization of the silicon carbide grains during annealing and the high vacancy concentration resulting from implantation damage could have provided many pathways for silver diffusion and migration during annealing, but no silver movement was measured.

Typical SiC coatings for fission product barriers in TRISO fuel consist of fine-grained SiC, usually slightly columnar, with grain sizes on the order of a few microns. The desired grain length is small enough such that the total width of the SiC layer consists of many grains and the probability of one grain extending through the total thickness is very small. The SiC grains in the recrystallized portion of the silicon carbide, where most of the silver remains, are fine grained, slightly columnar, and have grains sizes less than 1 μm. This silicon carbide exhibits characteristics very similar to the desired characteristics of silicon carbide coatings in typical TRISO fuel for high-temperature gas reactors and silver diffusion did not occur.

If silver does not diffuse in silicon carbide, then silver release from high-temperature coated particle fuel must be controlled by transport along another path. Additional work is required to identify the exact release path for silver in silicon carbide and to understand its cause and how to mitigate its effects. The results of this ion implantation experiment suggest that silver migration is not intrinsic to SiC but rather, that SiC can be an effective barrier to silver.

3.6 REFERENCES

[1] H. Nabielek, P.E. Brown, P. Offermann, "Silver Release from Coated Particle Fuel," *Nucl. Tech.* **35** (1977) 483-493.

[2] CoorsTek Advanced Silicon Carbides, 2003, C0301 8510-1024 Rev.B. (personal communication with Tom Sibley) www.coorstek.com.

[3] J.F. Ziegler, J.P. Biersack, The Stopping and Range of Ions in Matter (SRIM), www.SRIM.org, Copyright 2003.

[4] W. Amian, D. Stöver, "Diffusion of Silver and Cesium in Silicon-Carbide Coatings of Fuel Particles for High-Temperature Gas-Cooled Reactors," *Nucl Tech.* **61** (1983) 475-486.

[5] ATLAS Facility, Argonne National Laboratory, http://www.phy.anl.gov/atlas/fac-acc.html.

[6] E. Wendler, A. Heft, W. Wesch, "Ion-Induced Damage and Annealing Behavior in SiC," *Nucl. Instr. Meth. B* **141** (1998) 105-117.

[7] V. Heera, T. Henkel, R. Kogel, W. Skoroupa, "Evidence for Diffusion-Limited Kinetics of Ion-Beam-Induced Epitaxial Crystallization in Silicon," *Phys. Rev. B* **52** (1995) 776.

[8] Y. Pacaud, et al., "Radiation damage and annealing behvaiour of Ge+-implanted SiC," *Nucl. Instr. Meth. B* **120** (1996) 177-180.

[9] W. Amian, D. Stöver, "Diffusion of Silver and Cesium in Silicon-Carbide Coatings of Fuel Particles for High-Temperature Gas-Cooled Reactors," *Nucl. Tech.* **61** (1983) 475.

[10] C.H. Carter, Jr., R.F. Davis, J. Bentley, "Kinetics and Mechanisms of High-Temperature Creep in Silicon Carbide: II, Chemically Vapor Deposited," *J. Am. Ceram. Soc.* **67** (1984) 732-740.

4. Spherical Diffusion Couples

4.1 GOALS AND BACKGROUND

The goals of the experimental program were to directly witness silver diffusion and measure silver concentration profiles in silicon carbide. Two types of experiments attempted to directly measure silver concentration profiles in silicon carbide as a result of diffusion. Chapter 3 discussed the ion implantation results and this chapter reviews the results of spherical diffusion couple tests.

The aim of the spherical diffusion couple tests was to observe silver diffusion in silicon carbide by measuring silver concentration profiles in either a thin SiC coating over a hollow graphite shell or in a thick SiC shell. A lack of evidence, however, of silver migration in the silicon carbide layer resulted in a proposed change in the assumed mechanisms and a change in the goals of the experimental program. The new goals were to understand the causes of silver migration in silicon carbide and to determine what mechanisms govern silver release from silicon carbide.

As discussed in detail in this chapter, silver, although released in measurable quantities, did not diffuse through silicon carbide. Vapor migration is proposed as an alternative mechanism to solid-state diffusion to explain silver release in the current diffusion couples and in typical coated fuel particles.

4.2 EXPERIMENTAL SETUP AND FABRICATION

A standard diffusion couple consisting of a diffusing substance plated on a substrate is not sufficient for silver experiments because of silver's low melting temperature and high vapor pressure. Silver plated on silicon carbide will evaporate from the surface or escape through any open edges rather than diffuse into the substrate material at temperatures near or above 960°C, silver's melting temperature.[1] A novel diffusion couple design attempted to resolve this problem by enclosing silver within a silicon carbide coated sphere.

4.2.1 Novel Diffusion Couple Design

Hollow shells, fabricated from either graphite or silicon carbide, formed the basis of the novel spherical diffusion couple. Two half shells, fabricated with an overlapping seam, mated together to form a 1.9 cm hollow sphere with 0.076 cm thick walls. Silver powder (99.9995% purity, -22 mesh) placed inside one half shell was completely enclosed inside the diffusion couple after a silicon carbide coating was deposited on the outside of two joined half shells. Figure 4-1 shows two open half shells, Figure 4-2*a* shows one half shell with silver powder, and Figure 4-2*b* displays a complete diffusion couple with a silicon carbide outer coating.

Graphite shells, selected for the best coefficient of thermal expansion matching to silicon carbide, were used in the first and second sets of diffusion couples, types SiC-1 and SiC-2. The graphite shells were fabricated from machined graphite with approximately 13%-15% porosity. A third set of diffusion couples, type SiC-3, were fabricated with chemical vapor deposited silicon carbide as the substrate shell. An outer coating of CVD SiC sealed the silver inside all of the substrate shells.

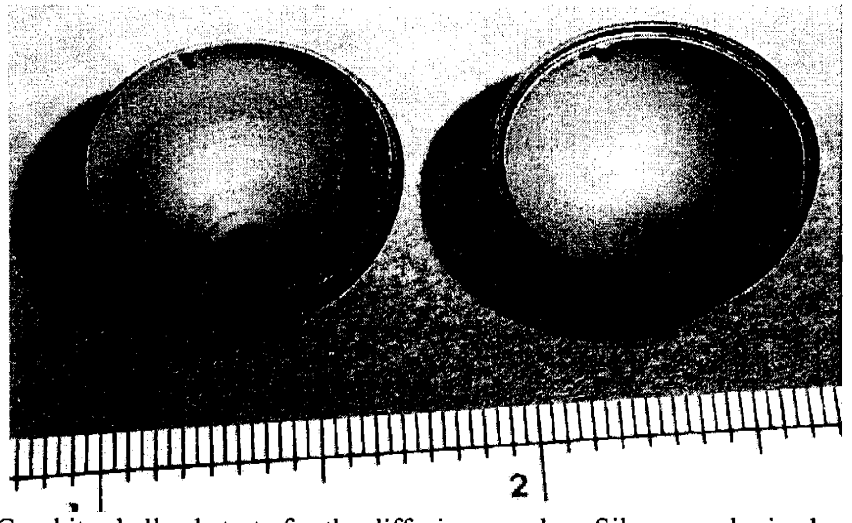

Figure 4-1. Graphite shell substrate for the diffusion couples. Silver powder is placed inside the shell then SiC is coated on the outside.

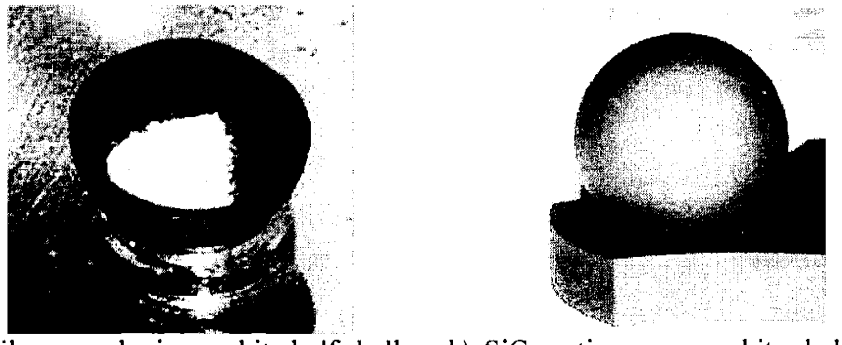

a) Silver powder in graphite half shell *b)* SiC coating over graphite shell

Figure 4-2. Diffusion couple fabrication steps including *a)* loading with silver powder and *b)* coating with SiC.

The graphite shell of the diffusion couple types SiC-1 and SiC-2 created some challenges for silver migration analysis but also added some potential benefits. Among the challenges were the numerous literature summaries which indicate that there is no holdup of silver in PyC or any graphite material.[2] Over a long heating period a range of fast silver diffusion coefficients in graphite adds only minimal uncertainty, but for short heat treatments, the finite silver diffusion rate in the graphite shell needs to be considered. A more significant challenge, however, appeared to be the lack of silver wetting on graphite. If silver doesn't wet graphite then molten silver at the bottom of the diffusion couple during heating will not be able to penetrate the graphite surface and, hence, will not come into contact with the SiC layer.

A major difference between the diffusion couples and typical coated particle fuel is the size of the diffusion couples. Typical diameters are on the order of 1 mm for coated fuel particles and 2 cm for the diffusion couples. In addition, the thickness of the SiC layer is greater on the diffusion couples (60-150 μm) than in typical coated fuel particles (35-40 μm). This significant difference in size affects the stress state of the silicon carbide layer and is also important when calculating the probability of a critical flaw occurring in a given volume of SiC.

Even though the uncertainties of silver transport through the graphite layer introduce challenges for analysis of these diffusion couples, advantages of this design include eliminating edge effects

by trapping the silver inside the diffusion couple and a chemical similarity to fuel particles. Coated fuel particles generally contain a porous graphite buffer layer around the kernel and a high-density pyrocarbon layer surrounding the buffer, before the SiC layer. Although the diffusion couple shells consist of machined graphite and not pyrocarbon, the environment is chemically similar to that existing for silver in coated particles. Even though the exact diffusion rate of silver in graphite materials is not known, the porosity in the graphite shells is within the range of connected porosity, suggesting that silver in the graphite layer can move quickly through the connected porosity by vapor transport and be transported to the SiC inner surface rather easily.

Replacing the graphite shell in favor of a silicon carbide shell provided a more direct investigation of silver migration in SiC and eliminated the uncertainties associated with silver migration through the graphite layer. In the SiC-3 type diffusion couples, silver was in direct contact with the silicon carbide, providing access to direct measurements on the SiC shell.

4.2.2 SiC Fabrication

The silicon carbide outer coating on the diffusion couples was formed by chemical vapor deposition using MTS (methyltrichlorosilane, CH_3SiCl_3) as the feed gas with a hydrogen carrier gas. The standard SiC coating used on diffusion couple types SiC-1 and SiC-3 was deposited at 1200°C and 75 torr with a total flow rate of 75 cm^3/min and an H_2/MTS ratio of 7.5. The standard coating run lasted 6 h. Raising the deposition temperature to 1300°C and increasing the H_2/MTS ratio to 12.5 created a modified SiC coating deposited on diffusion couple type SiC-2. Each coating run for the SiC-2 samples lasted 9.25 h.

All of the diffusion couples consist of two hemispheres, both either graphite or silicon carbide, loaded with silver and coated with silicon carbide. The three types of diffusion couples are referred to as SiC-1, SiC-2, and SiC-3 and are briefly summarized in Table 4-1. A modified SiC coated was deposited on some of the graphite-shell diffusion couples to permit a comparison of silver diffusion in SiC with different grain structures, one of the original objectives of the experimental program.

Table 4-1. Summary of diffusion couple set parameters.

	SiC-1	SiC-2	SiC-3
Shell Substrate	graphite	graphite	SiC
SiC Coating	standard	modified	standard
Microstructure	β-SiC	β- with α-SiC	β-SiC

The silicon carbide coating on diffusion couple types SiC-1 and SiC-3 consisted of columnar grains radially oriented, growing from the inner surface towards the outer. The grain sizes, as estimated from optical and transmission electron micrographs seen in Figure 4-3, range from small equiaxed grains near the inner surface, on the order of 0.5 μm to 1 μm, to long columnar grains on the order of a couple microns wide by tens of microns long.

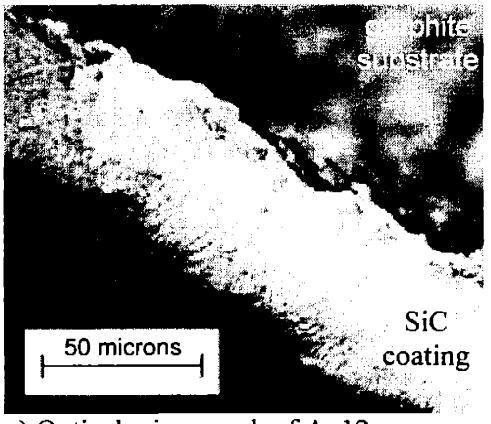

a) Optical micrograph of Ag12, unheated

b) AEM of Ag21 after heating at 1400°C for 240 h

Figure 4-3. SiC coatings consist of columnar grains with some small equiaxed grains near the substrate interface; a) an optical micrograph of unheated sample Ag12 shows typical fan patterns and b) a transmission electron micrograph of sample Ag21 after heating shows small equiaxed grains near the inner surface.

4.2.3 Heat Treatments

The heat treatment temperatures were selected to cover the higher range of typical fuel operating temperatures, between 1050°C and 1600°C, a temperature range also applicable to some accident analyses. Many of the heat treatments focused on the higher end of the temperature range, around 1500°C, to accelerate silver migration. Based on silver diffusion coefficients reported in the literature, the heat treatments conducted around 1500°C should have produced measurable silver concentration profiles.

Two high-temperature graphite-based furnaces were used for the diffusion couple heat treatments. Each was a Red Devil™ vacuum furnace, seen in Figure 4-4*a*, from the R.D. Webb company, heated by a carbon-carbon heating element inside fibrous graphite insulation block. A solid graphite retort, shown in Figure 4-4*b*, sits above the heating element and defines a work zone 9 cm in diameter and 5 cm tall.[3] A solid graphite lid covers the retort during operation. The furnaces were maintained under medium vacuum (on the order of millitorr) during the diffusion couple heat treatments.

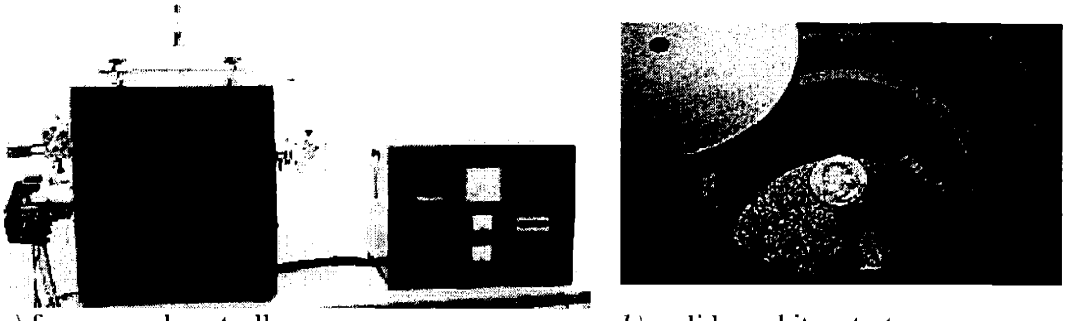

a) furnace and controller *b)* solid graphite retort

Figure 4-4. R.D. Webb Company Red Devil™ furnace used for the diffusion couple heat treatments: *a)* furnace and controller, *b)* solid graphite retort.

In the Webb furnace, the heating element is situated beneath the solid graphite retort. This arrangement results in a thermal gradient inside the working zone during heating with the bottom of the graphite cup hotter than the top. During the heat treatments, 0.6 cm thick graphite plates with approximately 0.6 cm holes held the spherical diffusion couples in a secure position and also provided adequate physical contact between the retort and the sample, likely ensuring good heat transfer from the retort to the bottom of the diffusion couple. In this arrangement, the top of the diffusion couple was not in contact with any surface of the furnace and radiated heat from the diffusion couple to the cooler graphite lid on the retort, leading to an approximately 10°C-15°C temperature drop from the bottom to the top of the diffusion couple.[4]

Heat treatments covered temperatures from 1050°C to 1700°C for cumulative times ranging between 2 h and 1760 h. Twenty-seven samples were annealed in all and seven of those samples were heated twice to obtain intermediate, nondestructive data, such as mass measurements, leak rates, and X-ray images, while accumulating longer anneal times. The uncertainty in heating temperature is ±15°C due to the hot zone geometry and thermocouple location and the uncertainty in heating duration is ±5 min. Heating rates varied from 4°C/min to 25°C/min with most of the diffusion couples heated at rates between 4°C/min and 10°C/min. Cooling rates were controlled by the natural cooling of the furnaces, typically about 5°C/min.

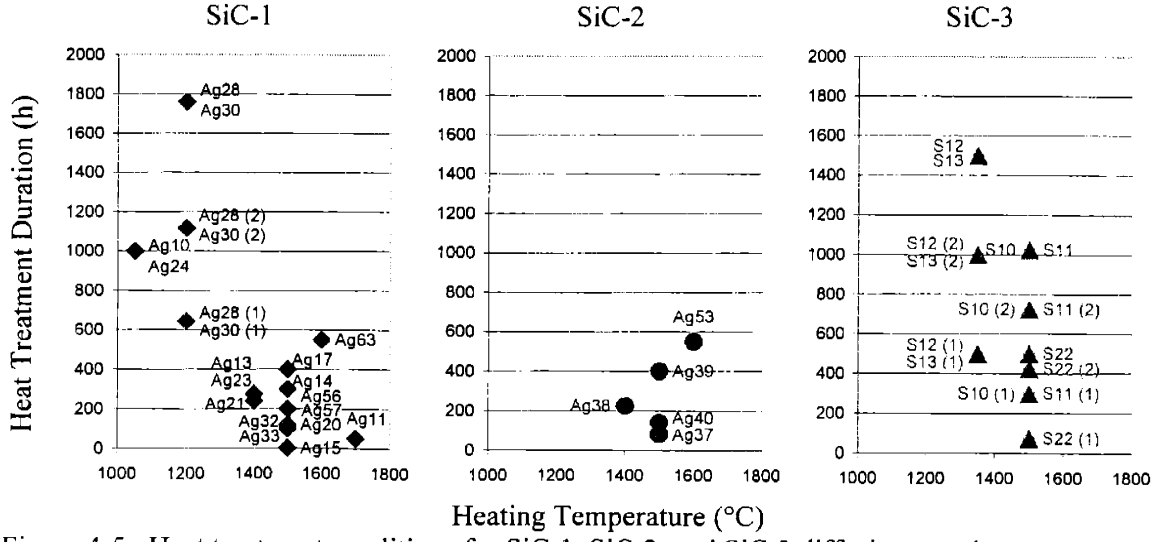

Figure 4-5. Heat treatment conditions for SiC-1, SiC-2, and SiC-3 diffusion couples.

4.3 RESULTS AND DISCUSSION

4.3.1 Silver Distribution in Silicon Carbide

Various techniques aimed at detecting and analyzing the silver distribution in the diffusion couples were employed. None of the techniques used detected any silver in the silicon carbide layer below a detection limit of approximately 100 ppm.

4.3.1.1 X-ray Analysis

X-ray analysis and CT-scanning provide images highlighting atomic number contrast in the diffusion couples. Since silver has a much higher atomic number (Z=47) than either silicon (Z=14) or carbon (Z=6), these techniques provide a qualitative picture of the silver location in the diffusion couple. Both X-ray and CT imaging show solid, excess silver in the bottom of the SiC-1 diffusion couples and dispersed silver in the upper portion of the couples.

Both X-ray radiography and CT-scanning are non-destructive techniques that take advantage of atomic number differences to distinguish between silver and silicon carbide in the diffusion couples. Additionally, CT-scanning is capable of rendering digital cross-sections of a sample. Unfortunately, due to the limited resolution of X-ray radiography and CT-scanning and the thin SiC layer (relative to the overall size of the diffusion couple), the SiC coating could barely be distinguished using these techniques. The images and digital reconstruction of cross-sectional slices do, however, clearly show that silver has penetrated the graphite shell in the upper portion of the SiC-1 diffusion couples where the vapor existed (and was coolest), but not in the bottom underneath the molten silver pool.

Figure 4-6 shows an X-ray image from the CT-scan of sample Ag32 after heating for 100 h at 1500°C. Excess solid silver remains in the bottom of the diffusion couple after heating, a clear indication that sufficient silver was present during heating to maintain equilibrium between the liquid and vapor phases. A halo of silver exists in the upper portion of the couple, but silver is only detected in the graphite shell, not in the SiC coating, as seen in an optical micrograph cross-section of the upper portion of a typical diffusion couple in Figure 4-7.

Silver particles can be seen at the seam location using X-ray techniques. Further investigation of the inner surface of the diffusion couple near the seam area using optical stereo microscopy shows discrete silver particles in the open spaces of the seam, between the overlapping lips of the two half shells.

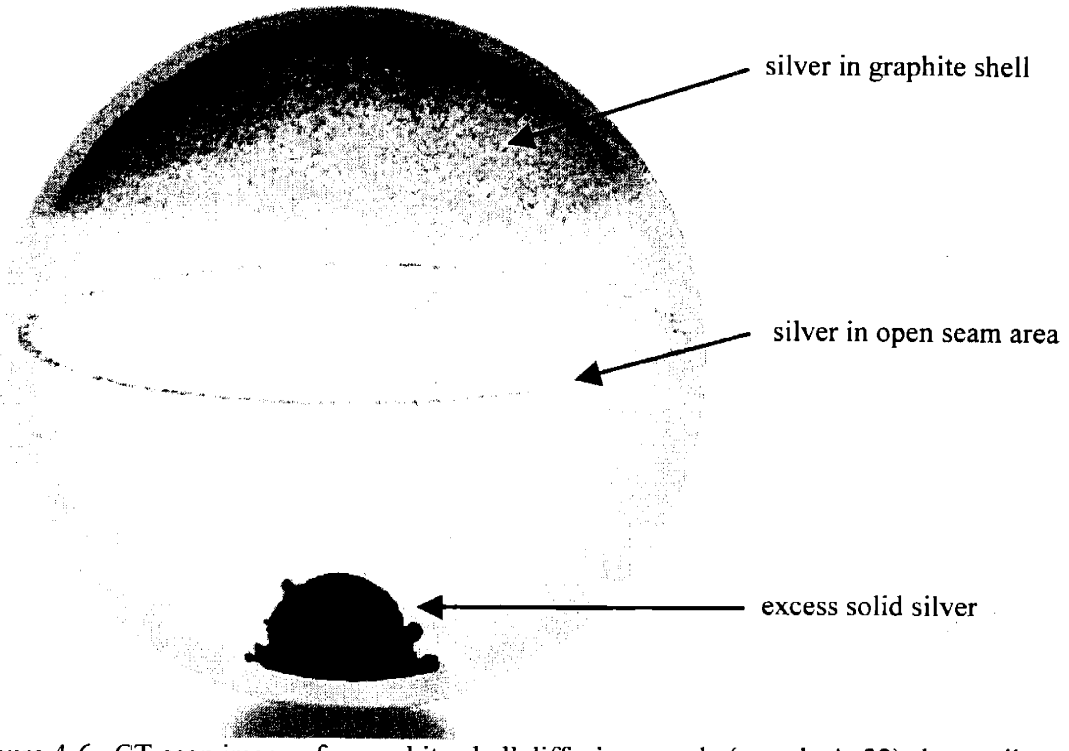

Figure 4-6. CT-scan image of a graphite-shell diffusion couple (sample Ag32) shows silver dispersed in the graphite in the upper region, silver particles in the seam, and excess silver at the bottom of the couple.

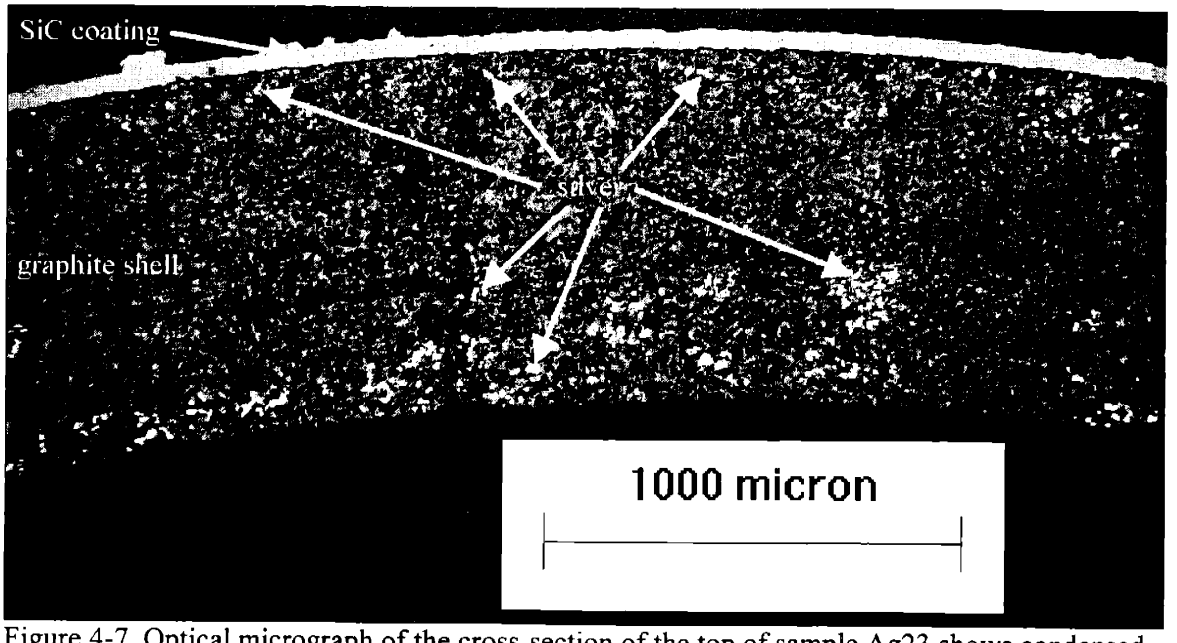

Figure 4-7. Optical micrograph of the cross-section of the top of sample Ag23 shows condensed silver in graphite pores but not in the SiC coating.

X-ray analysis and CT-scans of the SiC-3 diffusion couples with SiC substrate shells show a spattering of silver at the inner surface of the half shell, but no silver penetration into the SiC

shell or outer coating. There was no evidence of silver diffusion into the SiC substrate shell either below the high-concentration molten pool or above the low-concentration vapor phase.

X-ray images and CT-scans show silver in the upper potions of the SiC-1 and SiC-2 diffusion couples after heating. This silver appears finely distributed around the upper third of the diffusion couples, but no silver was identified in the SiC coatings during digital reconstructions of the cross-section planes. No silver was identified in the SiC substrate shell or SiC coating in the SiC-3 diffusion couples. Discrete silver precipitates were identified in the free space of the seams of the diffusion couples. The excess silver remaining after heating is clearly visible in X-ray images and CT-scans, but there is no evidence of silver transport into the graphite or SiC substrate shells at the bottom of the diffusion couples.

Although the X-ray and CT techniques provide good qualitative, non-destructive images of the silver location in the diffusion couples, they require a fairly high concentration of silver in SiC to be detectable and are not readily applicable for quantitative analysis. Additional techniques were required to look for lower silver concentrations in the SiC shells and coatings.

4.3.1.2 XPS Depth Profiles

To achieve the goal of observing silver diffusion by measuring characteristic concentration profiles after heating, XPS (X-ray photoelectron spectroscopy) was employed. XPS measures not only elemental components of a sample, but also determines bonding information, distinguishing, for example, between free silicon and silicon bound as silicon carbide. XPS measures concentrations at the surface of a sample and by alternating measurements with sputtering to remove material obtains a depth profile. XPS profiling through the diffusion couples attempted to measure the concentration profile due to diffusion and observe signs of silver migration through silicon carbide.

The detection limit for silver in the XPS analyses was approximately 100 ppm (atoms silver per total atoms measured). Silver may have been present in the SiC layers in concentrations less than 100 ppm, but anything greater than 100 ppm would have been detected during XPS concentration depth profiles. The highest silver concentrations existed in the bottom of the diffusion couples where solid silver formed a molten pool during heating.

The graphite substrate shell was removed by oxidation to reveal the inner surface of the SiC coating for XPS analysis in the SiC-1 and SiC-2 diffusion couples. For the SiC-3 diffusion couples, XPS measurements were obtained starting at the inner surface of the SiC substrate shell. Sample areas from both the top and bottom of selected diffusion couples were analyzed using XPS. No silver was detected, above the detection limit of 100 ppm (atoms of silver per total atoms measured) in the silicon carbide coating of and of the samples and no silver was detected in the SiC shell of the SiC-3 samples.

The density of the molten silver at the bottom of the diffusion couples is given by Equation (4-1).[1] At 1500°C, the density of molten silver in contact with the SiC shell in the SiC-3 diffusion couples was 8.8 g/cm^3. The expected concentration profile through the SiC shell using the diffusion coefficient recommended by Amian and Stöver is shown in Figure 4-8. Concentrations of this magnitude are easily detectable by XPS.

$$\rho_{liq} = \left(9.320 - 9 \cdot 10^{-4} \frac{1}{K}\left(T - T_m\right)\right)\frac{gm}{cm^3} \qquad (4\text{-}1)$$

where ρ_{liq} = density of liquid silver at temperature T (gm/cm^3),
T = Temperature (K), and
T_m = melting temperature (962°C, 1235 K).

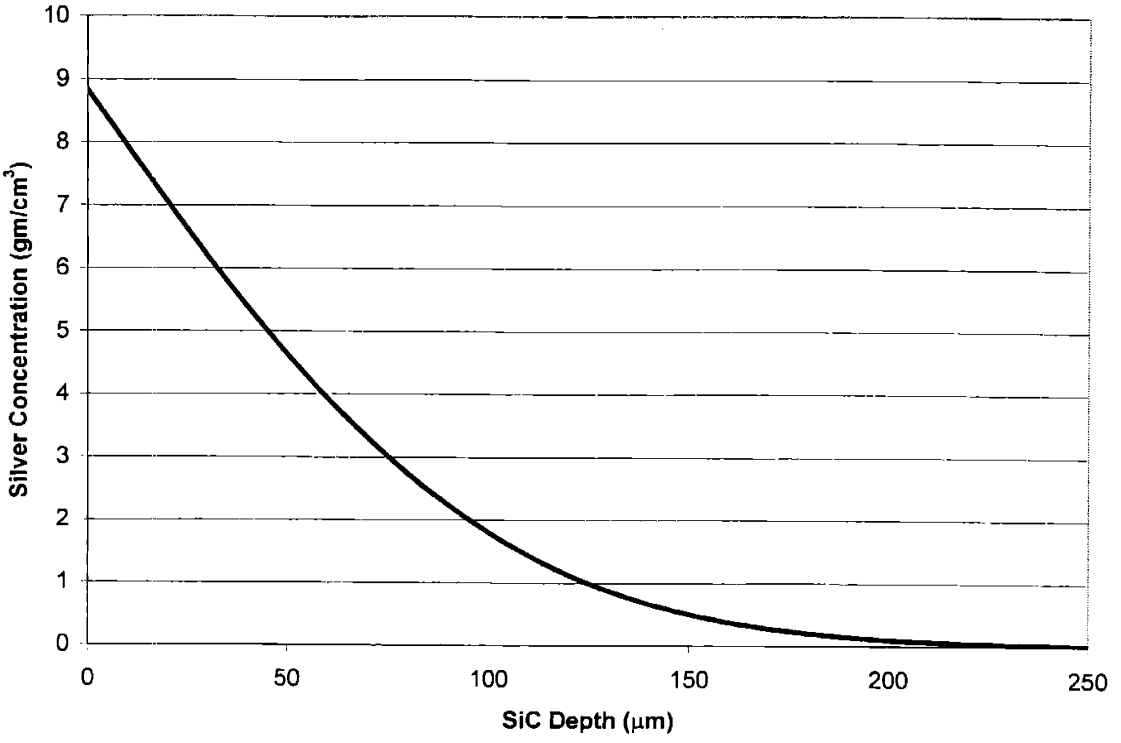

Figure 4-8. The expected silver concentration profile in the SiC shell after 500 h at 1500°C should have been easily detectable.

Incompatibility of the molten silver with the graphite shell may have prevented silver access to the SiC coating in the SiC-1 diffusion couples, but this should not have been a problem in the SiC-3 couples with SiC shells. Even after heating for 500 h at 1500°C, no silver was detected in the silicon carbide shell, at concentrations greater than 100 ppm, at the top or bottom of the diffusion couple. If silver diffused at rates in the range reported in the literature, XPS should have been able to measure characteristic concentration profiles. The lack of any silver detection in the SiC coatings or shells was an unexpected result and runs counter to the presumed diffusive mechanism.

XPS analysis provides quantitative chemical analysis over a fairly large area of the diffusion couple. The analysis area used for the XPS analysis measured approximately 800 μm in diameter. The concentration profiles collected during XPS analysis average the constituents in an area very large compared to the typical SiC grain size. To investigate these couples on a finer scale, higher magnification techniques were required.

4.3.1.3 Electron Microscopy Analysis

SEM (scanning electron microscopy) and EMPA (electron microprobe analysis) both clearly show silver penetration in the upper portions only of the SiC-1 and SiC-2 diffusion couple graphite shells. Neither analysis tool detected any silver in the SiC coating. Silver was observed near the graphite-SiC interface, as seen in Figure 4-9, but no penetration into the SiC coating was found.

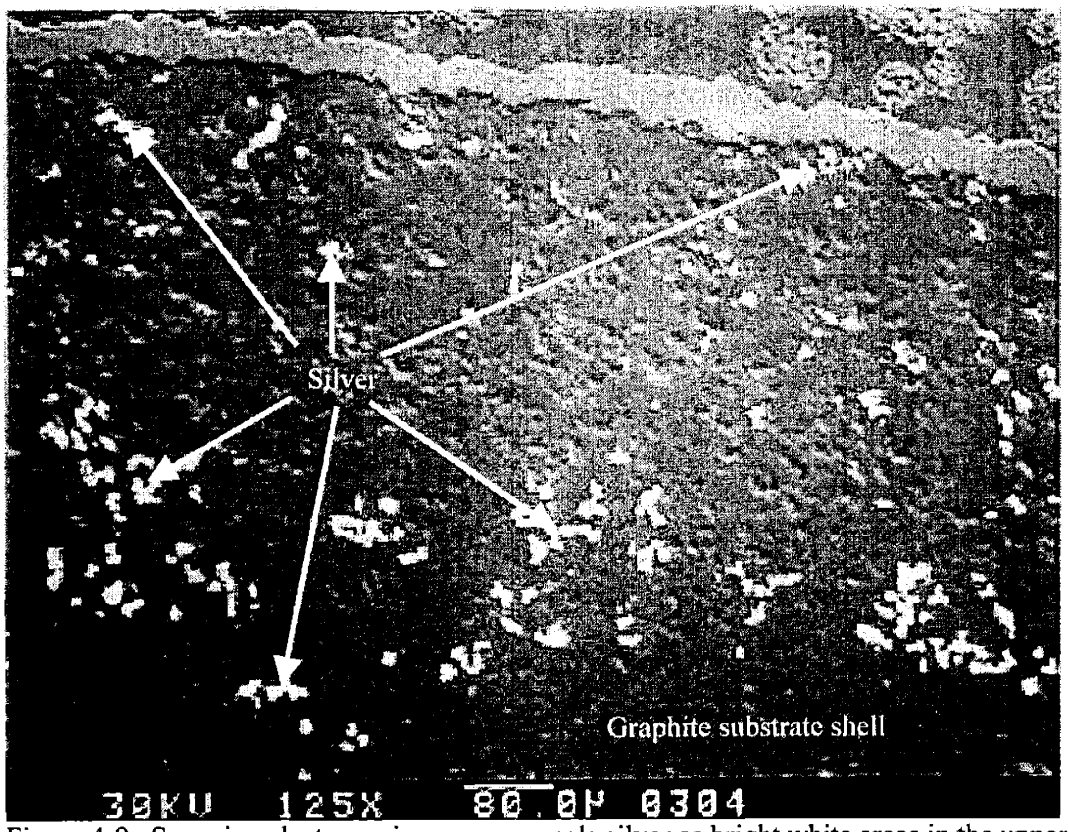

Figure 4-9. Scanning electron microscopy reveals silver as bright white areas in the upper portion of sample Ag20 after 120 h at 1500°C.

Silver was easily detected in AEM (analytical electron microscopy) analysis of the graphite shells of SiC-1 sample Ag21after 240 h at 1400°C and SiC-2 sample Ag39 after 400 h at 1500°C. The AEM analyses were performed on a Philips CM300 equipped with an EDAX X-ray detector for elemental analyses. Silver fills many of the graphite pores near the graphite-SiC interface. In sample Ag21 (SiC-1 diffusion couple), AEM clearly reveals silver at the graphite-SiC interface, as seen in Figure 4-10*a*, but not in the SiC coating. AEM provides high magnification images of the SiC grains and shows details of the fine-grained β-SiC structure, as seen in Figure 4-10*b*.

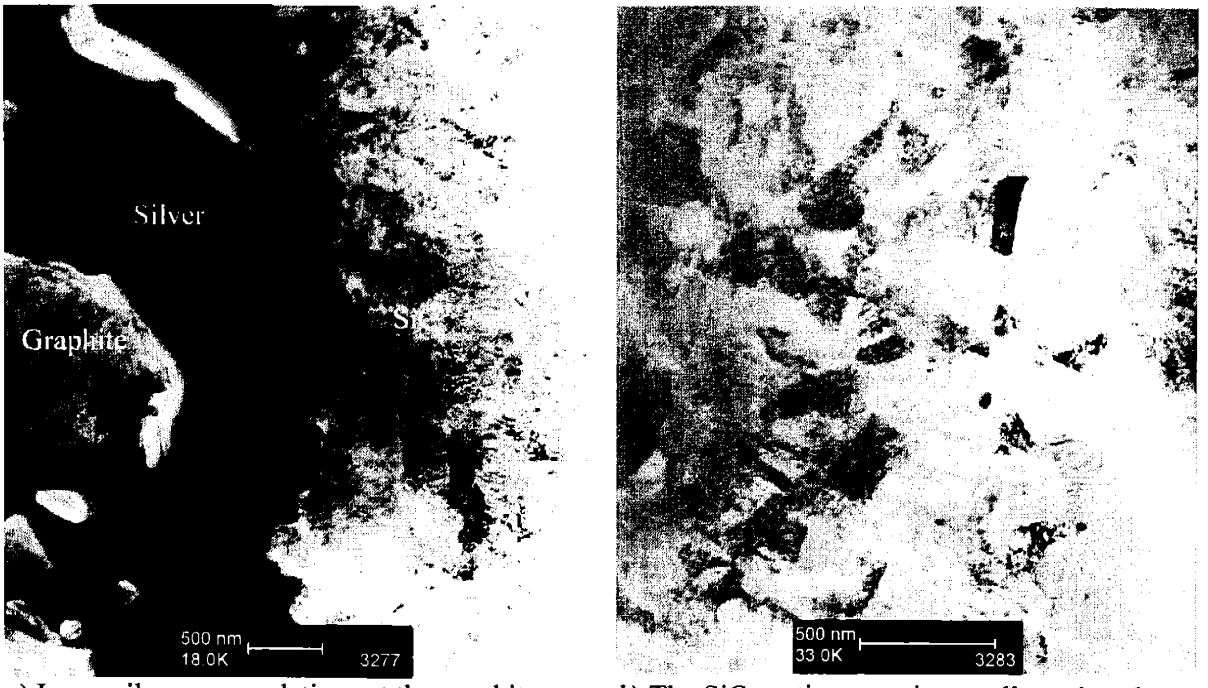

a) Large silver accumulations at the graphite-SiC interface

b) The SiC coating contains small, equiaxed grains, but no silver

Figure 4-10. AEM of SiC-1 sample Ag21after 240 h at 1400°C shows *a)* silver at the graphite-SiC interface and *b)* small SiC grains.

Sample Ag39, a SiC-2 diffusion couple fabricated according to the modified CVD conditions discussed in Section 4.2.2, consisted of large, blocky SiC grains near the graphite-SiC interface and thin dendritic grains further out into the SiC coating, oriented in the radial direction. AEM analysis detected silver decorating and bracketing the large SiC grains, as seen in Figure 4-11 and Figure 4-12, but there was no silver in the dendritic SiC grains. The diffraction patterns for both the large, single crystals and the polycrystalline dendritic regions index to β-SiC, as seen in the diffraction patterns in Figure 4-11.

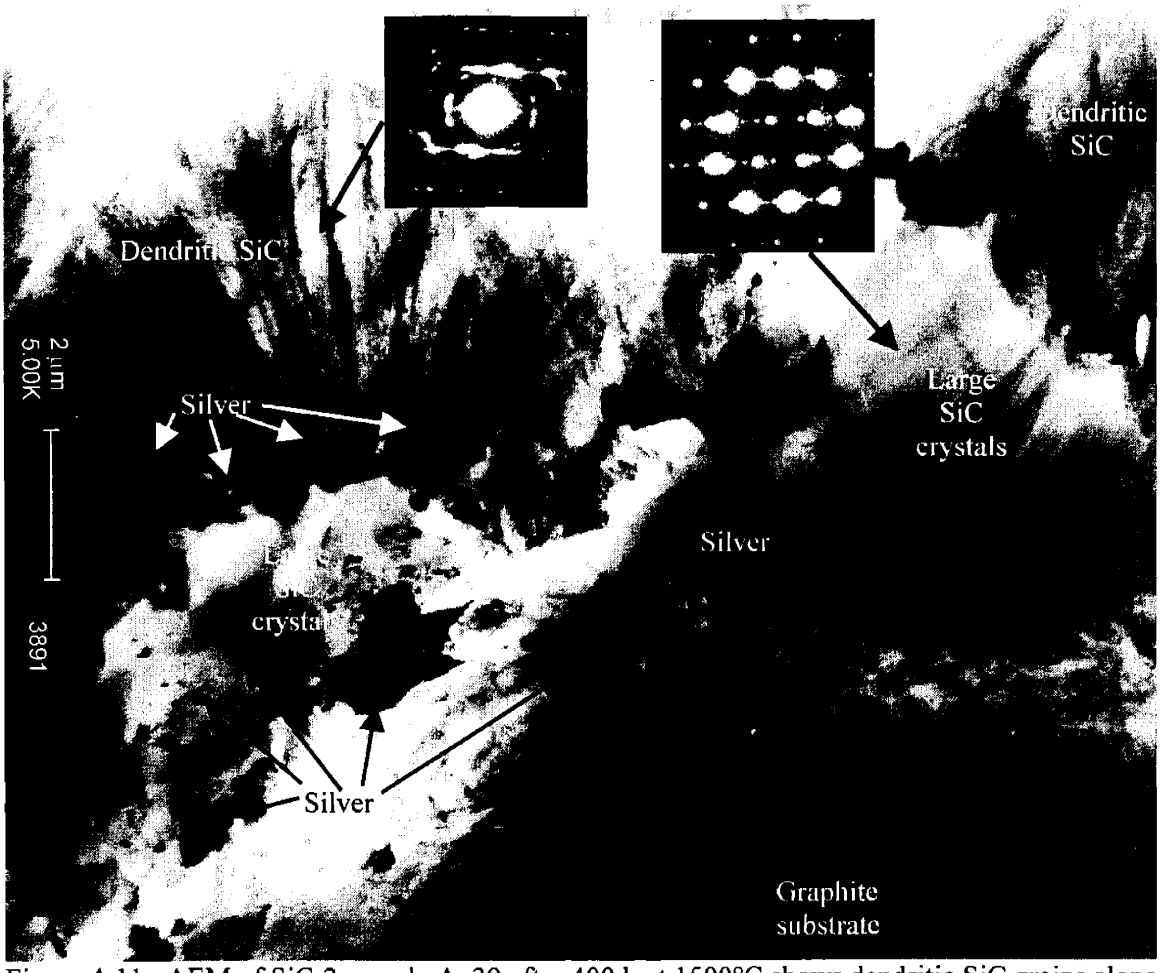

Figure 4-11. AEM of SiC-2 sample Ag39 after 400 h at 1500°C shows dendritic SiC grains along with large SiC crystals.

The large SiC crystals appear somewhat misaligned with each other, the surrounding graphite, and the dendritic SiC grains, providing room for silver migration around the large, blocky SiC grains. No silver, however, was observed in the dendritic SiC grains beyond the interface between the large, blocky crystals and the dendritic grains, as seen in Figure 4-11 and Figure 4-12*a*. These observations suggest that large SiC grains, present in the modified SiC-2 coating, and the mismatch between the different types of SiC grains provide pathways for silver transport not observed in fine-grain equiaxed or dendritic structures in the standard SiC coating used in these experiments and seen in the AEM of sample Ag21 in Figure 4-10.

The mismatch between poorly aligned SiC crystals likely increases residual stresses and may lead to localized cracking within the SiC coating which could provide open, direct pathways for silver escape. Although the SiC microstructure observed in the AEM analysis of SiC-2 sample Ag39 is not likely to be present in typical coated fuel particle SiC coatings, the ability of silver to migrate around poorly aligned crystals emphasizes the importance of silver transport along short-circuit paths through SiC. Typical SiC coatings in coated fuel particles consist of many individual grains and how well those grains fit and grow together during deposition may be important for silver retention. The PyC and SiC coatings for typical TRISO fuel particles are fabricated in fluidized beds and, although the overall deposition parameters are closely controlled, a range of conditions exists within the fluidized bed. These variations could lead to variations in the microstructure of

the SiC coating within individual particles, possibly creating regions or poorly aligned grains. Although the SiC microstructure seen in sample Ag39 is not desired for typical SiC coatings, the apparent ease of silver transport around ill-fitted SiC grains emphasizes the importance of localized SiC microstructure.

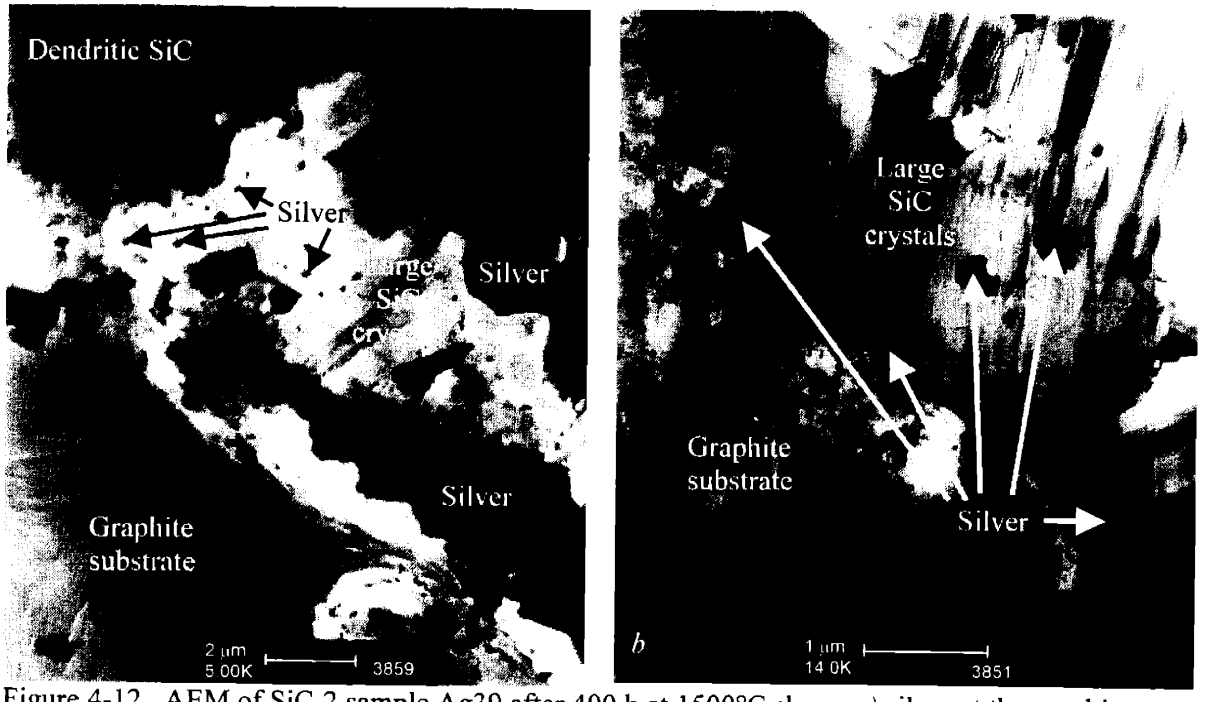

Figure 4-12. AEM of SiC-2 sample Ag39 after 400 h at 1500°C shows *a)* silver at the graphite-SiC interface and at the interface between large SiC crystals and dendritic SiC and *b)* silver bracketing and decorating the large SiC crystals.

4.3.2 Leak Testing

Standard helium leak testing of the diffusion couples showed an increase in leak rates for all samples after heating. These leak rates indicate a change in the diffusion couples during heating, possibly providing a silver escape route other than grain boundary diffusion, as previously assumed. Silver release due to grain boundary diffusion would not show an increase in leak rate, however a leak rate does indicate an open mechanical path.

In direct-read leak testing, the diffusion couple was soaked in a pressure chamber under 75 psi of helium for 20 min. During the soak period, helium entered the diffusion couple through any open mechanical paths. After 20 min, the sample was quickly transferred to a leak detector. This chamber was held under vacuum and a spectrometer was tuned to detect helium in the sample chamber. Any helium that leaked into the diffusion couple leaked out in the vacuum chamber and was detected by the spectrometer. The measured leak rate was recorded at 60 s and 120 s. An analytical fit, shown in Equation (4-2), was used to determine the predicted actual leak rate of the samples.[5]

$$Q_{meas} = Q_{eq} \cdot \frac{P_{over}}{P_{ref}} \cdot \left(1 - \exp\left(-\frac{Q_{eq}\, t_{soak}}{V_{sp}\, P_{ref}} \sqrt{\frac{M_{air}}{M_{He}}}\right)\right) \cdot \exp\left(-\frac{Q_{eq}\, t_{dwell}}{V_{sp}\, P_{ref}} \sqrt{\frac{M_{air}}{M_{He}}}\right) \qquad (4\text{-}2)$$

where Q_{meas} = measured leak rate of the tracer gas (He) (atm·cm^3/s),
Q_{eq} = equivalent leak rate in air (atm·cm^3/s),
P_{over} = over pressure applied to sample (5.1 atm = 80 psi),
P_{ref} = reference pressure (1 atm),
t_{soak} = soak time at pressure (1200 s),
t_{dwell} = dwell time between pressure release and spectrometer inspection (measurements recorded at 60 s and 120 s),
M_{air} = molecular mass of air (29 g/mol),
M_{He} = molecular mass of helium (4 g/mol), and
V_{sp} = volume of the specimen (cm^3).

The results of helium leak testing, shown in Figure 4-13, show that the leak rates for all types of samples were greater after heating than before. In general, the SiC-1 samples had low leak rates before heating, but high measured leak rates after heating. The SiC-2 samples had high leak rates before heating and even higher leak rates after. The SiC-3 samples received at least two coatings of SiC to achieve low leak rates in the as-fabricated samples. The leak rates for the SiC-3 samples increased after heating, but not as much as the increase for the SiC-1 samples. These qualitative results are listed in Table 4-2.

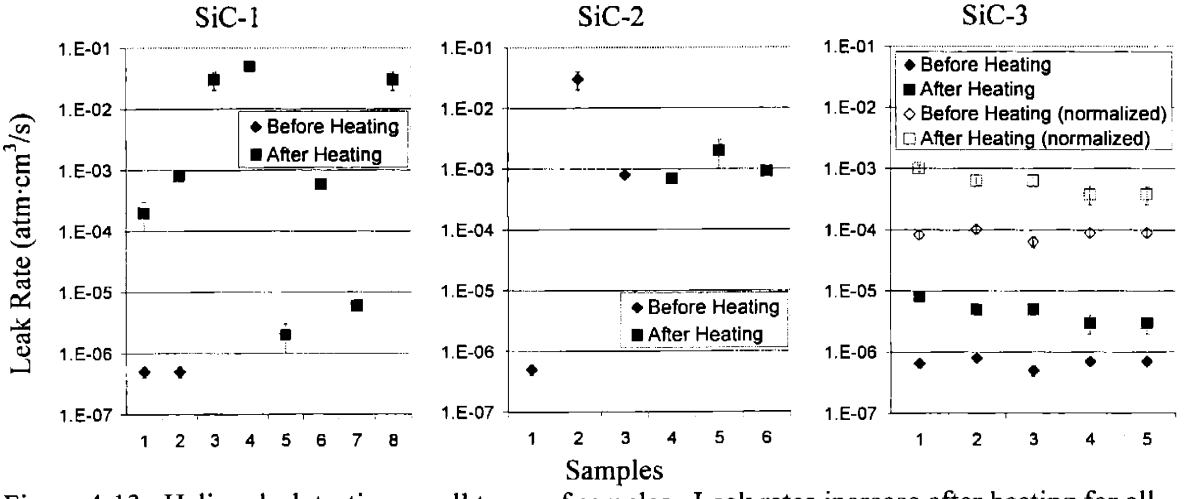

Figure 4-13. Helium leak testing on all types of samples. Leak rates increase after heating for all samples, with SiC-3 samples having the lowest increase.

Table 4-2. Qualitative assessment of leak rates. All samples measured higher leak rates after heating.

Sample Type	Substrate Shell	SiC Coating	Measured Leak Rates[1]	
			Before Anneal	After Anneal
SiC-1	graphite	standard	low[2]	high[3]
SiC-2	graphite	modified	high	higher
SiC-3	SiC	standard	low	medium

[1] low = 1 E-7 to 1 E-6 atm·cc / s
medium = 2 E-6 to 1 E-4 atm·cc / s
high = 2 E-4 to 8 E-2 atm·cc / s

[2] exception: sample Ag62 had a medium leak rate

[3] exception: sample Ag30 had a medium leak rate

Since helium can only leak through mechanical paths (helium does not diffuse through SiC) the leak testing results indicate increases in crack paths after heating compared to before heating. A review of the results for the three types of samples shows that the SiC-1 diffusion couples had mostly low leak rates before heating with generally large increases after heating. The SiC-2 samples had mostly large leak rates before heating, indicating poor quality of the modified SiC coating. The SiC-3 diffusion couples started with low leak rates and experienced modest increases after heating. Overall, the SiC-1 and SiC-3 couples had the best leak rates before heating while the SiC-3 samples had the lowest leak rates after heating.

Leak testing measures the infiltration of helium into the sample under pressure and helium leaking out of the sample under vacuum. In the SiC-1 and SiC-2 diffusion couples, the SiC coating surrounds a porous graphite substrate shell; in the SiC-3 couples the SiC coating surrounds a fully dense SiC substrate shell. A crack anywhere in the SiC coating in SiC-1 and SiC-2 diffusion couples would allow helium infiltration into the interior of the diffusion couple. Helium is impermeable through solid, intact SiC, so in the SiC-3 diffusion couples, only cracks in the SiC coating near the seam between the two SiC half shells would give helium access to the couple's interior volume.

Leak testing after heat treatment does not identify when leaks become active. There is no information on the time dependence for this data. No correlation between the duration of the heat treatment and leak rate appears. When a leak path opened during the heating and cooldown process cannot be determined from leak testing. Leak paths created near the end of a heat treatment or during the cooldown process would result in large measured leak rates after heating but may result in very little mass loss.

4.3.3 Mass Loss

Mass measurements of the samples before and after heat treatment on a Mettler AG245 scale with 0.0001 g resolution show that the diffusion couples lost weight during annealing. Contributors to mass change may include silver loss, oxidation of silicon carbide from the diffusion couple's surface, interactions between SiC and other contaminants in the furnace, and evaporation of water vapor adsorbed to the diffusion couple.

Since the furnace operated under medium vacuum, there should have been little oxygen available to oxidize the surface SiC. Any oxidation, however, of SiC to the volatile SiO would result in a net mass loss. A control sample without any silver was heated to estimate this effect along with any other mass effects.

Reporting mass loss as a fraction of the initial silver inventory attempts to normalize all of the diffusion couple test results since varying amounts of silver were loaded into the samples. Even though the total amount of silver varied among the diffusion couples, in all but two cases (samples Ag53 and Ag63) there was excess silver available during the entire heat treatment to maintain equilibrium between the molten silver pool and the silver vapor.

4.3.3.1 Graphite-Shell Diffusion Couples

Sample Ag56, an SiC-1 type diffusion couple, was fabricated as a control sample with no silver to estimate any contribution to mass change from surface effects, contamination in the furnace, or oxidation of the silicon carbide. After heating for 200 h at 1500°C, control sample Ag56 exhibited a mass loss of 0.0061 g. Cutting a slice off sample Ag17, another SiC-1 type diffusion couple, created a second control sample. Sample Ag17 recorded a mass loss of 0.0071 g after heating for 400 h at 1500°C. With one end of the diffusion couple removed, the inner graphite surface of sample Ag17 was exposed. This additional exposed surface area could influence the total amount of mass change based on any oxidation of the graphite layer during heating. Based on the mass loss of the two SiC-1 control samples, a possible threshold appears around 0.006 g; any mass loss below this level is most likely due to surface effects, not silver loss.

In the population of SiC-1 diffusion couples, mass loss ranged from 0.0013 g to 0.3297 g, equivalent to a range of 0.5% to 101% fractional release. The SiC-2 diffusion couples suffered mass loss between 0.0110 g and 0.3009 g, equivalent to fractional releases between 43% and 115%. Reported fractional release values greater than 100% are due to uncertainties in the measurement and from other possible interactions, such as oxidation at the surface, resulting in additional mass loss beyond silver escape. As can be seen in Figure 4-17*a* and *b*, the different diffusion couples cover a wide range of fractional loss values with some samples retaining nearly all of their silver inventory while others suffer complete loss.

This range of results does not support the assumption of diffusion as the controlling mechanism for silver release. The diffusion couples were all fabricated using the same silicon carbide deposition method. Some variation occurs between coating batches when making these diffusion couples, but this is probably on the same order as variations within a single coating batch due to fluctuations between the top and bottom and between the center and outside edges in the fluidized bed. For similar diffusion couples with high-density SiC with similar microstructure, a diffusion mechanism does not explain the 0 to 100% range of fractional release. As discussed in Chapter 2, variations in grain structure could account for roughly a factor of 2 variation in the diffusion coefficient, but cannot account for the difference of 1-2 orders of magnitude or for the variation between 0% and 100% release.

4.3.3.2 SiC-Shell Diffusion Couples

SiC-shell diffusion couples (SiC-3) all had small mass losses recorded after heating. The mass loss ranged from 0.0007 g to 0.0037 g for heat treatments at 1350°C and 1500°C for 200 h to 1500 h. These values for mass loss are measurable, but may be within the limits of uncertainty for both the measurement and due to other mass loss phenomena in the furnace including water vapor loss from the couple surface and oxidation of SiC from any oxygen in the furnace.

The SiC outer coating on the SiC-3 couples was deposited using the same procedure under the same conditions as the SiC coating on the SiC-1couples so changes in the diffusion couple performance are not due to drastic variations in the SiC coating. The SiC-1 and SiC-3 diffusion couples, however, differ in the substrate material used as the basis of the diffusion couple. The SiC-1 and SiC-2 diffusion couples consist of a porous graphite shell and the SiC-3 couples

contain fully dense SiC as the substrate shell. Silver vapor can migrate through the porous graphite shell and, therefore, has access to the entire inner surface of the SiC outer coating in the SiC-1 and SiC-2 diffusion couples, but in the SiC-3 diffusion couples silver has access only to the outer SiC coating in the vicinity of the gap at the SiC shell seam. This difference in silver access in shown schematically in Figure 4-14.

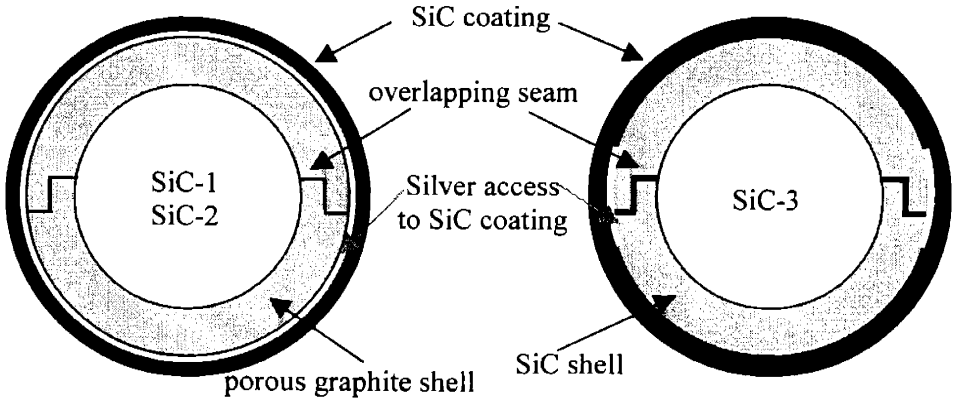

a) Silver has access to entire SiC inner surface in SiC-1 and SiC-2 couples with porous graphite shells

b) Silver only has access to SiC near the seam in SiC-3 couples with dense SiC shells

Figure 4-14. Schematic of diffusion couple cross-section showing the silver access to the SiC inner surface as white bands (not to scale).

The gap between the overlapping rim of the two SiC half shells forms the basis of the area normalization for the SiC-3 diffusion couples. This gap, shown in Figure 4-15, provides a direct pathway for silver vapor to reach the SiC outer coating. Any flaws in the SiC coating in the region near the seam in the SiC-3 diffusion couples will allow silver release during heating. Based on the gap observed in Figure 4-15 a band of SiC coating with a 150 μm width around the entire diameter of the diffusion couple is assumed to be accessible to the silver vapor during heating. The ratio of the area of the band surrounding the seam in the SiC-3 couples to the total SiC coating area in the SiC-1 couples provides the area normalization factor of 0.0079. The gap at the seam in a graphite-substrate diffusion couple is shown in Figure 4-16. The gap at the seam is not considered in the graphite-substrate diffusion couples because the graphite shell itself is porous, allowing silver access to the SiC coating.

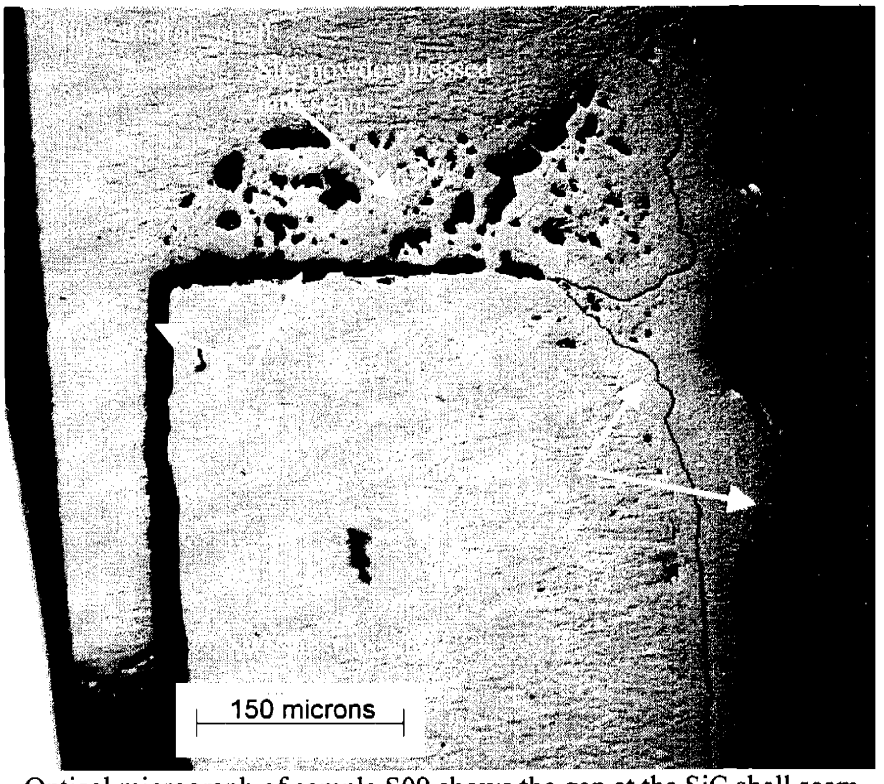

Figure 4-15. Optical micrograph of sample S09 shows the gap at the SiC shell seam.

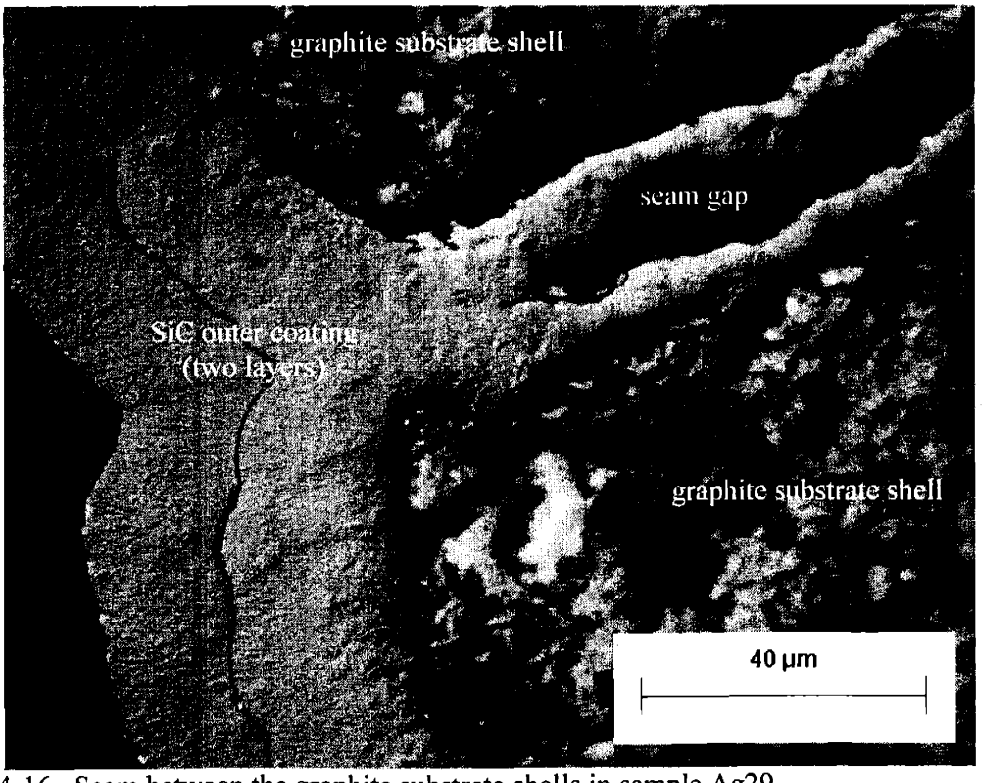

Figure 4-16. Seam between the graphite substrate shells in sample Ag29.

Initially, it appears that the SiC-3 diffusion couples have much lower mass losses than the SiC-1 and SiC-2 type diffusion couples. Adjusting the SiC-3 mass loss results for the fraction of the SiC area actually accessible to the silver, however, produces values in the same range as the SiC-1 and SiC-2 diffusion couples as seen in Figure 4-17.

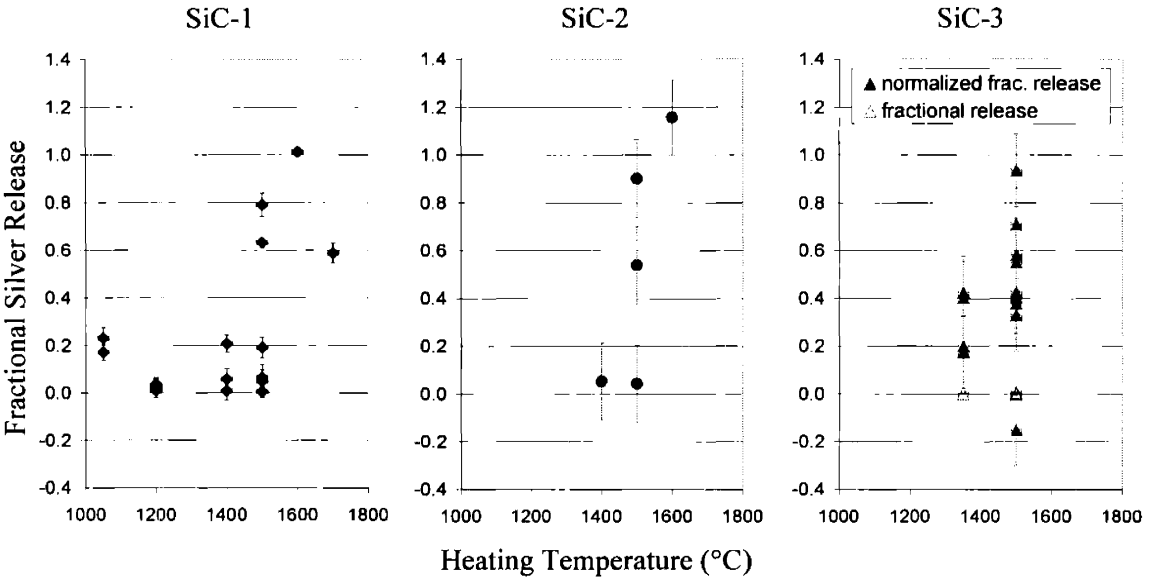

Figure 4-17. Fractional silver loss spans the range from 0% to 100% in the diffusion couples with large variations in each type of diffusion couple design.

No direct correlation between the mass loss and leak testing results is evident, as shown in shown in Figure 4-18. In general, the leak rates associated with the samples with high fractional release are very high, but all the leak rates greater than 1E-4 atm·cc/s are large leak rates. Unfortunately, when a leak path becomes active during testing is not known for these diffusion couple experiments. Leak paths that occur either during fabrication or handling or early during heating would be expected to result in large mass losses. However, paths that develop near the end of heating or during cool down would result in only small mass losses. Due to the variation between individual samples and the lack of time-specific data, further conclusions cannot be drawn from the mass loss vs. leak rate plot in Figure 4-18.

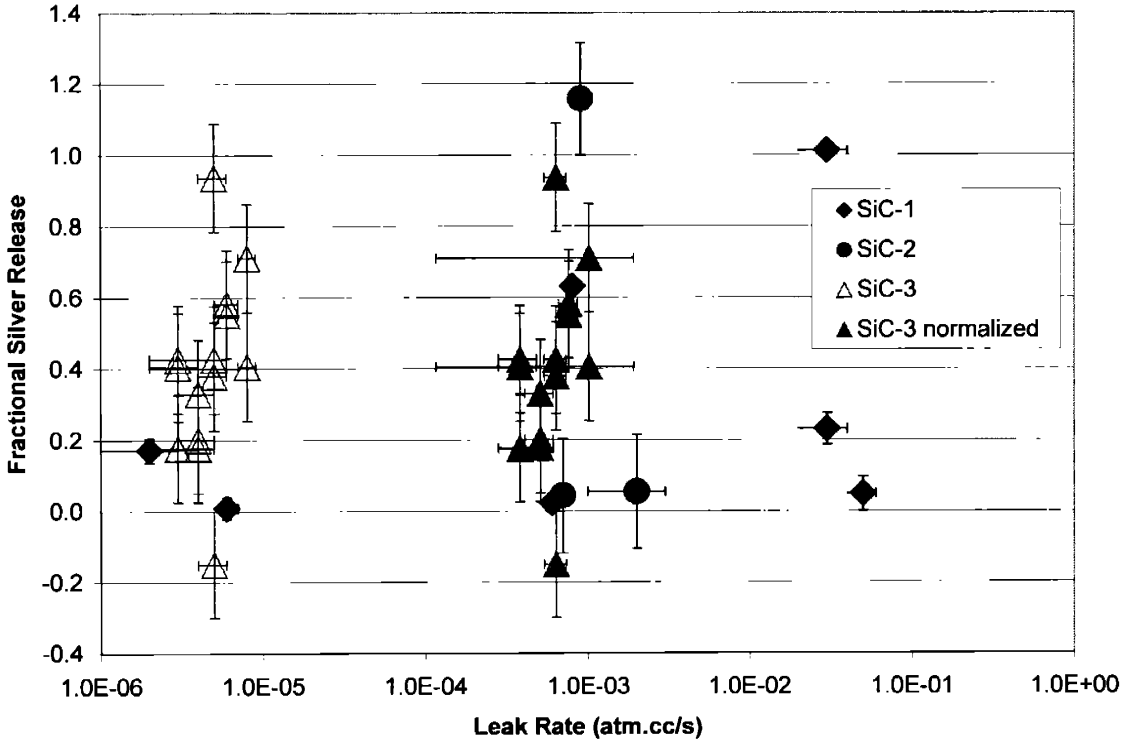

Figure 4-18. Fractional silver mass loss shows no direct correlation with leak rate measurements. In general, all of the leak rates measured after heating were very large and would allow significant mass loss during heating.

4.3.3.3 *Effective Diffusion Coefficient Calculations*

Even though the analysis techniques aimed at observing silver diffusion found no direct evidence of silver diffusion in silicon carbide, it is still instructive to evaluate diffusion coefficients from the spherical diffusion couple mass loss data. The mass loss from the current experiments was converted to effective diffusion coefficients using an analytical expression for release through a thin spherical shell, similar to the procedure used to calculate effective diffusion coefficients in the literature. The diffusion couples have a range of SiC coatings approximately 40-120 μm thick with overall radii on the order of 0.95 cm and qualify as thin spherical shells for the purposes of this analysis. The graphite shell in the SiC-1 and SiC-2 and the SiC shell in the SiC-3 diffusion couples were neglected for this calculation. Considering only the CVD SiC coating on the outside of the diffusion couples, an effective diffusion coefficient was calculated, using Equation (2-19) for different limits of the source silver concentration. The results are shown in Figure 4-19.

Equation (2-19) is the analytical solution for mass release from a thin spherical shell.[6] The diffusion coefficient necessary to produce the observed mass loss can be calculated from the difference in mass as measured before and after the diffusion couple heat treatments (Q_r), the known dimensions for each diffusion couple, and the silver concentration level at different areas in the couple. Three different values of the silver concentration have been considered: the first is the concentration of silver in the molten pool in contact with the silicon carbide at the bottom of the diffusion couples; the second is the limit of detection of XPS, the technique used to measure concentration profiles in the silicon carbide coatings and shells; and the third is the silver concentration in the vapor phase in contact with the silicon carbide in the upper portion of the diffusion couple.

$$Q_r = 4\pi ab(b-a)C_1 \cdot \left[\frac{D \cdot t}{(b-a)^2} - \frac{1}{6} - \frac{2}{\pi^2} \cdot \sum_{n=1}^{\infty} \frac{(-1)^n}{n^2} \exp\left[-\frac{Dn^2\pi^2 t}{(b-a)^2} \right] \right] \quad (4\text{-}3)$$

where Q_r = mass released (g),
a = inner radius of spherical shell (m),
b = outer radius of spherical shell (m),
C_1 = source concentration of silver at $r = a$ (g/m^3),
D = diffusion coefficient of silver in SiC (m^2/s), and
t = duration of heat treatment (s).

Figure 4-19 shows the band of effective diffusion coefficients reported in the literature and discussed in Chapter 2 for comparison to the current data. Diffusion coefficients in the range of 10^{-16} m^2/s to 10^{-14} m^2/s at 1500°C are calculated from the silver concentration at the interface between the molten pool and the SiC at the bottom of the diffusion couple. These values are in the same range as those reported in the literature, but as discussed in section 4.3.1, no silver was observed in the SiC coating at the bottom of the diffusion couple. Therefore, silver release by diffusion according to the rates reported in the literature did not occur in these experiments.

If the silver concentration, however, were just below the XPS detection limit of 100 ppm, XPS would not have measured silver concentration profiles in the SiC coating. If silver diffused through the SiC coating with a source concentration of 100 ppm diffusion coefficients would have had to be in the range of 10^{-14} m^2/s to 2×10^{-10} m^2/s at 1500°C, significantly higher than those previously reported for silver in SiC. If silver diffused through the SiC at the top of the diffusion couples where the source concentration was approximately 1 ppm, the diffusion coefficients necessary to accommodate the observed mass loss would generally be in the range of 10^{-10} m^2/s to 10^{-7} m^2/s at 1500°C. The source concentration of the silver vapor in the upper portion of the diffusion couple, used as C_1 in Equation (2-19), was derived from the equilibrium silver vapor pressure during each experiment.

The calculated diffusion coefficients from the current tests using the silver source concentration values derived from the XPS detection limit of the vapor phase during heating are not consistent with the previously derived diffusion coefficients and the assumptions of grain boundary diffusion. Although the concentration profile measurements using XPS had a detection limit of 100 ppm, it is likely that any silver concentrations near that limit would have been detected either during XPS analysis or during AEM or other measurement techniques. If silver diffused through the SiC coating from the vapor source, the diffusion coefficients would have had to have been between 6 and 7 orders of magnitude greater than those previously accepted to support the observed mass loss. While the results collected so far cannot disprove silver diffusion from the low-concentration vapor source in the upper portion of the diffusion couple, typical diffusion coefficients reported previously in the literature do not support the total amount of silver released during the current experiments. Silver may diffuse in low concentrations, but another mechanism must be active to provide a pathway for the amount of silver loss measured.

It is more likely, especially when considered together with the leak testing results discussed in section 4.3.2, that silver vapor migrated through cracks in the SiC coating.

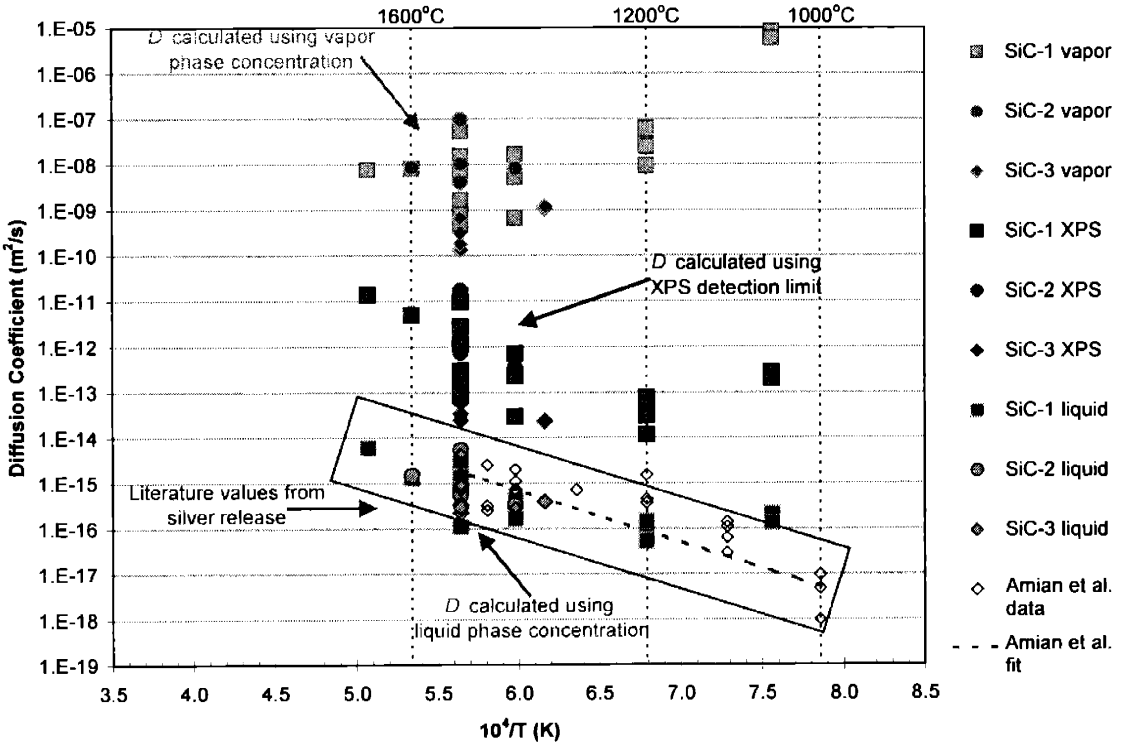

Figure 4-19. Effective diffusion coefficients calculated from diffusion couple mass loss are much greater than those previously reported in the literature.

4.4 STRESS ANALYSIS

Silver clearly escaped from some of the diffusion couples in the current experiments, but no signs of classical diffusion were identified. Silver release via vapor migration through cracks in the SiC coating fits the experimental observations, but a specific crack development sequence has not yet been identified. One possible scenario is that one or more cracks developed during the thermal cycling between fabrication, heating, and cool down due to the mismatch in the coefficients of thermal expansion between the graphite shell and the SiC coating.

A preliminary finite element stress analysis completed at the Idaho National Engineering and Environmental Laboratory indicates that stresses in the diffusion couple can exceed the fracture strength of the silicon carbide coating.[7] The selection of the graphite shells aimed at achieving the best possible match of the coefficient of thermal expansion (CTE) for both the graphite and SiC. Ibiden ET-10 graphite, with approximately 15% porosity, has a CTE equal to 3.8×10^{-6}/°C and the CTE for SiC is 2.9×10^{-6}/°C between room temperature and 100°C and 5.1×10^{-6}/°C at 1200°C. Figure 4-20 shows the stress state for a perfectly spherical diffusion couple, assuming a zero initial stress state during SiC deposition at 1200°C, cooling to room temperature, a heat treatment at 1500°C for 200 h, and a final cool down. The thermal cycling as shown in Figure 4-20 would cause stresses greater than the fracture strength of 480 MPa and could lead to SiC cracking during cooling.[8]

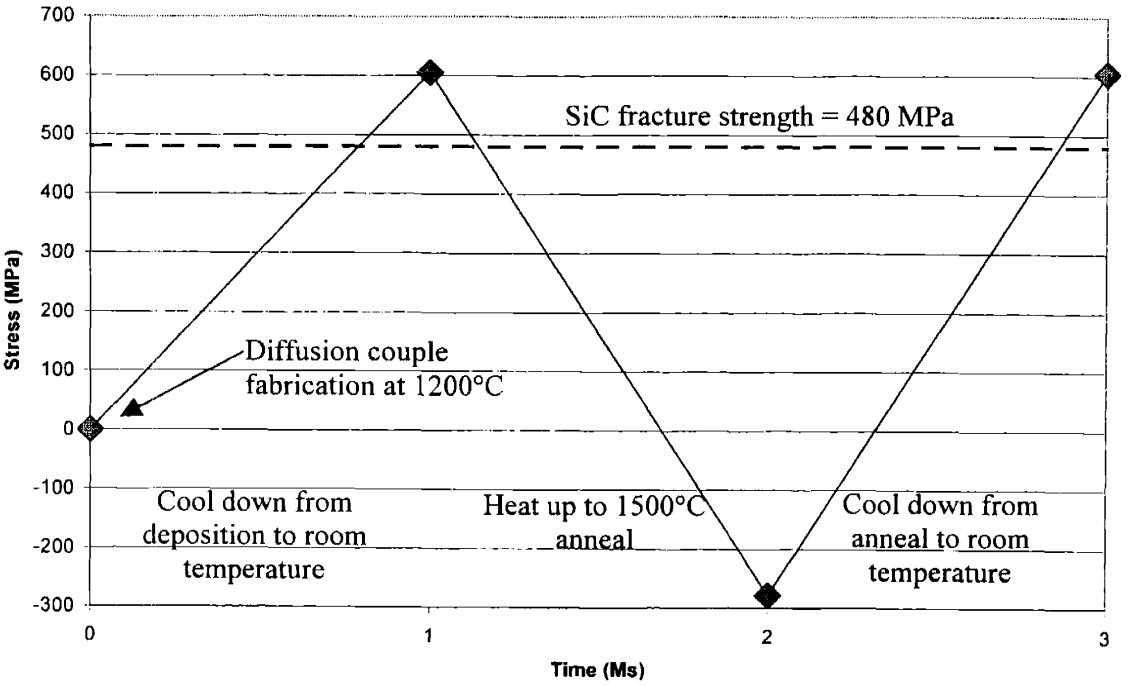

Figure 4-20. Stresses in SiC coating during thermal cycling due to differential thermal expansion between the SiC coating and the graphite shell exceed SiC's yield strength.

Preliminary analysis, though still inconclusive, indicates possible crack development in the SiC coating. AFM (atomic force microscopy) analysis detected no signs of silver in the SiC shell or coatings of two SiC-3 diffusion couples: S09, an unheated sample; and S22 after 500 h at 1500°C. Indications of "nano-cracks", however, were found in the heated sample, S22. Between grains, at a level of detail on the order of nanometers, indications of cracks appear on the order of angstroms wide, as shown in Figure 4-21. Additional AFM work is needed to verify the presence of nano-scale cracks in the SiC coatings, but features such as these may offer a silver transport pathway through SiC.

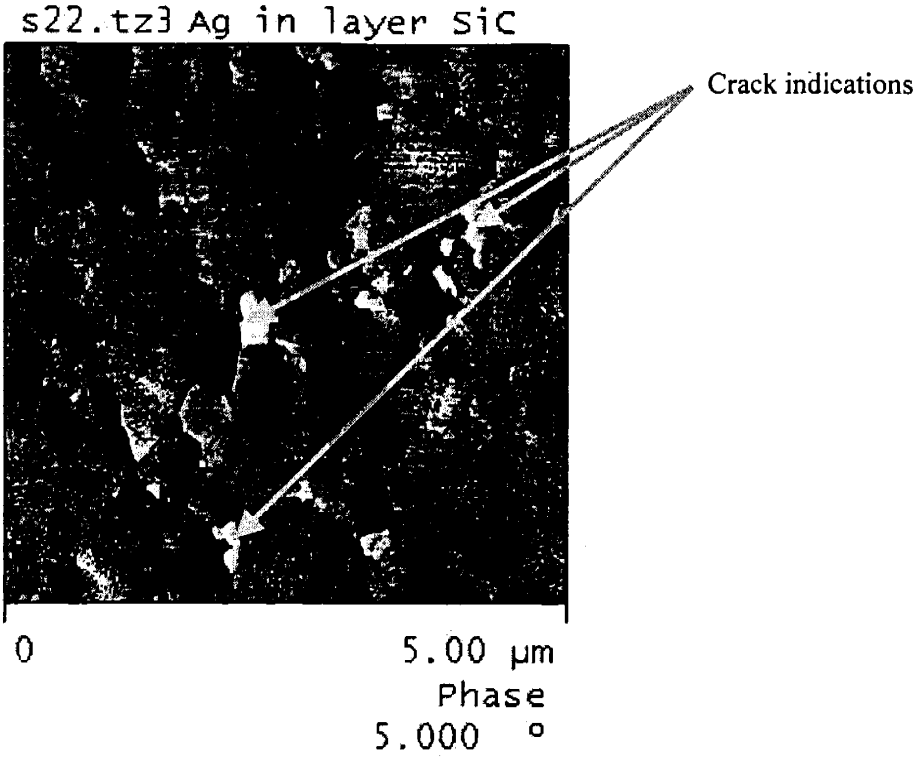

Figure 4-21. AFM analysis reveals nano-crack features in the SiC coating of SiC-3 sample S22 after 500 h at 1500°C.

4.5 VAPOR MIGRATION AND LITERATURE DATA

Results from the current experiments lead to the conclusion that silver release from the silicon carbide coated diffusion couples is likely dominated by vapor migration through cracks in the SiC coating, not classical diffusion as previously thought. If silver cannot diffuse through SiC in the current spherical diffusion couples, then it cannot diffuse through similar SiC coatings in typical coated particle fuel. While this may at first appear contradictory to the results from previous literature reports, a reinterpretation of the literature data suggests some similarity.

As discussed in greater detail in Chapter 2, silver diffusion coefficients have frequently been derived from batch-averaged silver release measurements. When silver release is collected for a large batch of particles during annealing, it is impossible to know individual particle silver release. Gamma counting of individual particles attempts to evaluate fission product inventory of each particle, but this process is time-consuming and has only been completed on small batches.[9] In previous tests, the total amount of silver release from a batch of particles was averaged over all of the particles to arrive at the average release per particle. From these data, diffusion coefficients were calculated assuming identical behavior within the batch. Moreover, the activation energies for this data fell within the range characteristic of grain boundary diffusion processes, lending support to the conclusions of silver diffusion in SiC coatings.

If all of the particles, however, are not assumed to behave identically, as seen by the large variation of fission product inventory measurements in the JAERI tests, other conclusions seem viable.[10] Reported silver mass loss from annealed particle batches varied from about 0.4% to 29% of the total batch inventory.[11] Although these data were equally attributed to all of the

particles in order to calculate diffusion coefficients, the same total mass loss could have been obtained from large vapor migration from just a few particles in each batch. The example using the data reported by Amian and Stöver, discussed in Section 2.4.2, illustrates that complete silver release from just a few particles in a batch could produce the same results that were interpreted as diffusion.

4.6 SUMMARY OF SILVER MIGRATION

Measurements before and after heat treatments show significant silver mass loss from the diffusion couples, but measurements aimed at recording silver concentration profiles in the silicon carbide coatings detected no silver. Leak rate increases after heating strongly suggest mechanical paths for non-diffusive release. Taken together these results lead to the conclusion that silver must have escaped from the diffusion couples through a vapor migration path. Silver diffusion, if it occurs at all in intact silicon carbide, is extremely slow, much slower than previously reported in the literature. Silver release from silicon carbide is controlled by vapor migration through cracks in the silicon carbide.

Had silver diffused from the source of molten silver at the bottom of the diffusion couples, it would have been detected during concentration profile measurements. Silver diffusion from the low-concentration vapor source cannot be ruled out, but diffusion cannot account for the total amount of silver loss measured using the range of diffusion coefficients reported in the literature. Vapor migration through mechanical pathways accounts for the amount of mass loss, the extreme variation between samples, and the increase in leak rates after heating.

As discussed in Chapter 2, a reinterpretation of historic literature data indicates that it is possible that silver releases in previous experiments likely resulted from large inventory losses from a few individual particles rather than small fractional releases assumed due to grain boundary diffusion. Silver release values governed by vapor migration can still exhibit a temperature dependence, not unlike those presented in the literature, due to the vapor pressure driving force. The silver vapor pressure increases with temperature, increasing the driving force for silver release during higher temperature tests. A weak trend between the current experimental data and the product of the vapor pressure and duration of each test is seen in Figure 4-22, but this temperature dependence may account for the temperature trends observed in the literature.

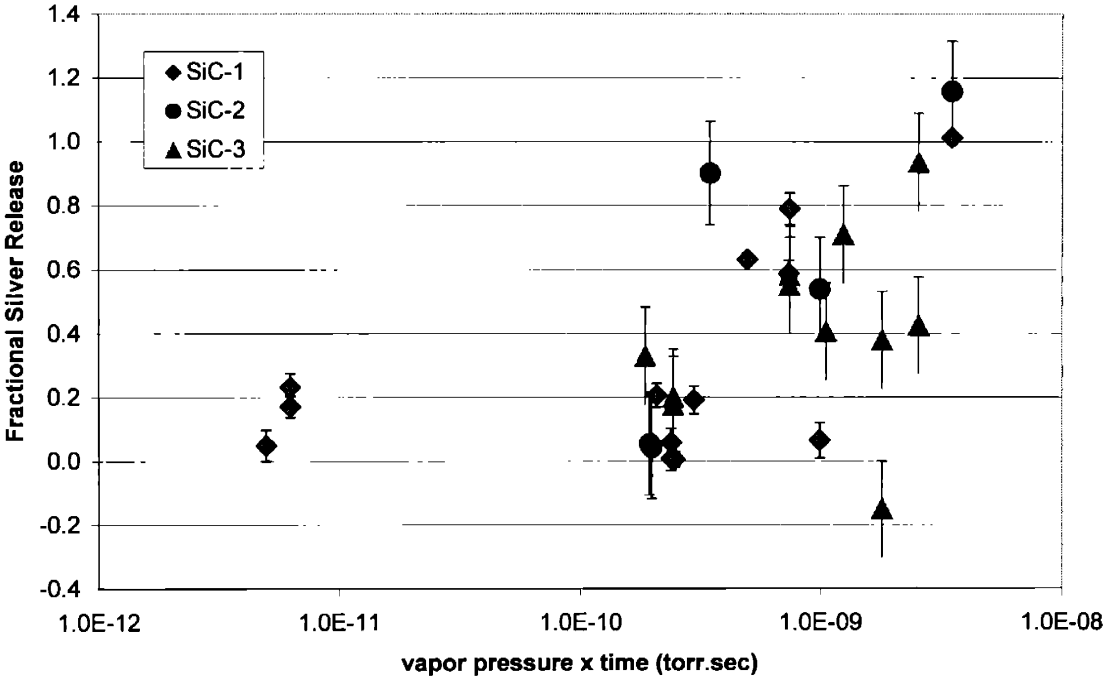

Figure 4-22. Silver fractional release displays a weak trend with the product of vapor pressure and time during anneal.

4.7 CONCLUSIONS AND SIGNIFICANCE

Contrary to previous assumptions in the literature, silver does not diffuse, but rather likely leaks through intact silicon carbide via vapor migration through cracks or flaws. The importance of this new finding is that silver release in high-temperature gas reactors can be prevented by improving silicon carbide quality.

Only some of the diffusion couples released silver and it appears that only some of the coated fuel particles reported in the literature released silver, indicating that vapor migration is not endemic to all silicon carbide, but affects only certain particles. Preliminary findings from the current experiments suggest silicon carbide cracking due to thermal cycling and a possible network of nanometer-sized cracks. If particles afflicted with or prone to crack networks can be removed from the population to be irradiated, silver release can be eliminated.

Additional work is required to identify the exact pathway for silver vapor release and to determine its cause, but these results signify that silver release does not have to be accepted as an undesired side-effect of operating SiC-coated fuel. If silicon carbide can reliably be made without the features leading to crack formation, then silver can be retained inside coated fuel particles. Achieving this goal requires a renewed focus on the development and fabrication of high quality silicon carbide resistant to crack formation. This may also require the development of new quality control techniques to identify faulty or susceptible particles before irradiation.

The results of the current experiments also show that the test methods used to evaluate silver migration need to be carefully reviewed. Care must be taken when applying large batch behavior to individual particles. Particle variation is a natural consequence of the fluidized bed fabrication process and the use of ceramic materials. Ignoring the variation in individual particle properties

and behavior and assuming identical behavior among all particles can produce misleading results. Although large population tests are necessary and provide effective batch data, information on specific transport mechanisms can be missed.

4.8 REFERENCES

[1] D. Lide, *CRC Handbook of Chemistry and Physics*, 71st ed., Boca Raton: CRC Press, 1990.

[2] H. Nabielek, P.E. Brown, P. Offermann, "Silver Release from Coated Particle Fuel," *Nucl. Tech.* **35** (1977) 483-493.

[3] R.D. Webb Company Red Devil Furnace, http://www.rdwebb.com/.

[4] Personal communication with R.D. Webb.

[5] Department of Defense Test Method Standard, Microcircuits, MIL-STD-883E, December 31, 1996.

[6] J. Crank, *The Mathematics of Diffusion*, 2nd ed., London: Oxford University Press, 1975.

[7] G.K Miller, Idaho National Engineering and Environmental Laboratory, Stress Analysis for the Thermal Cycling of a Spherical Diffusion Couple, personal communication, June 2003.

[8] F. Ho, *Material Models of Pyrocarbon and Pyrolitic Silicon Carbide*, CEGA-002820, Rev. 1, General Atomics, July 1993.

[9] R.E. Bullock, "Fission-Product Release During Postirradiation Annealing of Several Types of Coated Fuel Particles," *J. Nucl. Mat.* **125** (1984) 304-319.

[10] K. Minato, et al. HRB-22 Capsule Irradiation Test for HTGR Fuel (JAERI/USDOE Collaborative Irradiation Test), JAERI-Research 98-021, March 1998.

[11] W. Amian, D. Stöver, "Diffusion of Silver and Cesium in Silicon-Carbide Coatings of Fuel Particles for High-Temperature Gas-Cooled Reactors," *Nucl. Tech.* **61** (1983) 475-486.

5. A New View of Silver Transport In SiC

As discussed previously in Chapters 3 and 4, the results of this research strongly suggest that classical diffusion does not govern silver transport in apparently intact SiC. Although the bulk of the previous literature on silver migration in silicon carbide presents results based on the assumption of diffusion, there are still holes in the data and some alternative explanations have been hinted at by other authors, as discussed in Chapter 2. There is no question that coated fuel particles release silver under certain conditions; however, a new description is needed for silver release from fuel particles since it is clear that silver does not diffuse through intact SiC via classical diffusion.

5.1 INTRODUCTION

Data collected during the current experimental program clearly demonstrate that silver does not diffuse through intact silicon carbide. Chapters 3 and 4 detail these findings and Chapter 2 presents a re-interpretation of previous experiments highlighting the questions and doubt regarding the assumption of diffusion as the silver transport mechanism. Silver does not diffuse in silicon carbide, but silver release does indeed occur from both the current spherical diffusion couple and previous coated fuel particle tests. As discussed in Chapter 4, this release is most likely due to vapor transport through mechanical cracks in the SiC layer.

The results of previous experiments, reported in the literature, characterize silver release from coated fuel particles as the result of diffusion. For more than three decades, authors have presented silver release data in the form of Arrhenius diffusion relationships. As discussed in Chapter 2, there have been doubts about the accuracy of solid-state diffusion as the actual mechanism controlling silver migration in SiC with some authors suggesting a "short-circuit" path.

Leak testing results, detailed in Chapter 4, provide evidence that cracks exist in the SiC coating of the current diffusion couples. Although there is very little time data available to evince when cracks developed, the cracks provide a plausible pathway for silver release in the current diffusion couple experiments. Although the exact SiC crack formation scenario may be unique to these diffusion couples due to the large volume of SiC present and the presence of a large discontinuity at the seam of the diffusion couple, the existence of cracks in the SiC layer of the diffusion couples suggests that silver escapes by means of vapor transport through cracks.

If cracks are present in the SiC layer and allow silver vapor to escape, why aren't more fission products released during irradiation or annealing tests? The interaction of all of the layers in the coated fuel particle and the retention of other fission products in those layers, even when the SiC contains cracks, will be discussed in this chapter.

5.2 UNCERTAINTY IN THE LITERATURE

A detailed review of the state of knowledge in the literature regarding silver migration in silicon carbide was presented in Chapter 2. In general, silver release has been discussed in terms of diffusion, but that representation is a useful tool rather than an exact description of the specific mechanism itself.

Numerous authors, while presenting silver release results in the form of Arrhenius diffusion relationships, have suggested that silver release does not follow classical diffusion. Nabielek presented silver release results from fuel particles that did not follow the expected diffusive release and hypothesized rather that the SiC becomes progressively transparent to silver due to traces of free silicon on the SiC grain boundaries.[1] After a thorough review of the state of knowledge of silver release from coated fuel particles in 1992, McCardell et al. pointed out that "the technical community is not in complete agreement on the exact mechanism for silver transport through SiC."[2]

Furthermore, a review of the overall literature data highlights the uncertainty of the silver release mechanism. Within tests containing a single batch of particles that were all manufactured under the same conditions, often in the same batch, silver release values vary from 0% to 100%. Some variations in total release would be expected for a diffusive process due to variations in total SiC thickness in each sample and variations in the specific microstructure and grain orientation within the SiC layers, but those variations would not produce fractional release values spanning the entire possible range from 0% to 100%. Differences in SiC thickness or grain orientation (i.e., total path length) could cause a change in total silver release of a few percent, but clearly do not account for the large variation in release between samples within individual tests or the overall range of diffusion coefficients reported, as seen in Chapter 2.

Unresolved questions also remain regarding the method of data collection from silver release experiments. In many of the experiments silver release was measured for a batch of particles. In many cases, individual fission product inventories were not measured and the silver released was assumed to have been distributed evenly among the particles in the test batches. This assumption has worked reasonably well to characterize batch performance and has provided a convenient tool for comparing test results between different types of fuel and between different researchers at different labs. Measuring release from a batch of particles, however, does not supply any insight into the mechanism responsible for silver migration in individual particles.

In cases where individual fuel particles were measured, the silver release varied widely, in some cases from 0% to 100% in the same batch and test. These types of results run counter to a diffusive release mechanism and suggest that another mechanism is responsible for silver release in some of the samples while the rest retain most of their silver inventories.

5.3 DIFFUSION COUPLE LEAK TESTING REVIEW

There are some doubts expressed in the literature and uncertainties as to the exact mechanism or mechanisms responsible for silver release from coated fuel particles. Classical diffusion does not explain the current experimental results or the results previously reported in the literature. Silver doesn't diffuse through intact SiC, but clearly escaped from the diffusion couples in the current experiments. Chapter 4 includes a more detailed description and discussion of the leak testing results on the diffusion couples, but a review of those results is warranted here.

Silver did not diffuse through the spherical diffusion couples, as presented in Chapter 4, but silver release did certainly occur. Leak testing of the diffusion couples clearly indicates the presence of cracks (mechanical paths) in the SiC coating of many of the diffusion couples. Although leak rates are not available for all of the diffusion couples, these mechanical paths would certainly provide a pathway for silver vapor migration through the diffusion couples during heating.

Additionally, where leak rates are available both before and after heating, they show that some of the samples definitely undergo a transition from low to high leak rates during heating.

These leak rates are proof of available mechanical pathways open to vapor transport. Leak testing was performed with helium gas, a gas with atoms much smaller than silver's, but the results clearly identify mechanical, not chemical, paths through the SiC coating that would allow vapor migration and release. Therefore, the next step in the study of silver migration through SiC is to consider vapor flow as the mechanism for silver release. Vapor flow modeling, discussed in the following section, can be used to estimate crack sizes in the current diffusion couples and also in typical coated fuel particles.

5.4 VAPOR FLOW MODELING

5.4.1 Background

Basic vapor flow modeling and some simplifying assumptions can be used to estimate the crack size required to accommodate the observed silver loss in the current diffusion couple experiments and in previous coated fuel particle tests. All cracks were assumed to be straight tubes with circular cross-sections such that the length of the crack was equal to the SiC coating thickness. In reality, the crack paths will likely follow tortuous routes and will not have perfectly circular cross-sections. Using these assumptions, however, allows an initial estimate of the size of the crack paths with minimal introduction of unknown quantities (e.g., tortuosity factors) and allows a comparison of the crack sizes between different sets of experiments.

Different regimes govern vapor flow depending on the system pressure and channel size. At very low pressures, the mean free path of the gas molecules is much larger than dimensions of the vacuum enclosure. Under these conditions, the gas molecules undergo collisions primarily with the walls of the enclosure rather than with other molecules; this is known as molecular flow. At atmospheric pressures, the mean free path of gas molecules is very small relative to the structure through which they're flowing. In this case, known as viscous flow, the gas molecules undergo collisions primarily with other gas molecules rather than with the walls and the gas viscosity limits the flow. At pressures in between, both viscous and molecular phenomena contribute to gas flow in the transition flow regime. For the data sets analyzed here, only molecular flow was encountered.

Since silver did not diffuse out of the diffusion couples, as discussed in Chapter 4, the silver release and leak rate results were reexamined using vapor flow theory. In addition, the results of a typical coated fuel particle experiment were reevaluated using vapor flow theory. Results of these calculations, shown in the following sections, indicate that silver vapor flow through SiC cracks is a plausible migration mechanism.

During molecular flow, the mean free path of the gas molecules is much larger than the diameter of the tube in which they're flowing; the movement of the molecules is dominated by collisions with the tube walls rather than with other molecules.

The conductance of a gas governed by molecular flow is defined as:[3]

$$C_{molecular} = \frac{1}{6}\sqrt{\frac{2\pi RT}{aw}}\frac{d^3}{L} \tag{5-1}$$

where $C_{molecular}$= conductance (liter/sec),
R = gas constant (8.314 J/mol·K),
T = absolute temperature (K),
d = crack diameter (m),
aw = atomic weight of the gas (107.87 g/mol for silver), and
L = length of the crack tube (assumed equal to the thickness) (m).

To convert from conductance to mass loss, a value measured during the current diffusion couple experiments, the time of the experiment and the molar volume are also needed. The molar volume is calculated from the ideal gas law and is given by:

$$v_{molar} = \frac{RT}{P} \tag{5-2}$$

where v_{molar} = molar volume (m^3/mol),
R = gas constant (8.314 J/mol·K),
T = absolute temperature (K), and
P = pressure (Pa).

For the molar volume as defined by Equation (5-2), the mass loss over a specified time, t, due to molecular flow is given by:

$$Q_{molecular} = \frac{C_{molecular}\, t}{v_{molar}} aw \tag{5-3}$$

where $Q_{molecular}$= mass loss (g),
$C_{molecular}$= laminar flow conductance (liter/sec),
t = time (sec),
v_{molar} = molar volume (m^3/mol), and
aw = atomic weight of the gas (g/mol).

The molecular flow equation attributed to Knudsen applies to pipes of circular cross-section. For pipes of equal cross-sectional areas, pipes with non-circular cross-sections will experience lower conduction than those with circular cross-sections.[4] More details of vapor flow modeling are presented in Appendix B.

5.4.2 Silver Mass Loss from Diffusion Couples

As discussed in Chapter 4, there was no evidence of silver diffusion in the silicon carbide shells or outer coatings in the spherical diffusion couples. Silver did, however, escape from the diffusion couples. There were no signs of any interaction between the diffusion couples and the pools of molten silver at the bottom of the couples during heating. Vapor migration of silver through openings in the SiC layer, therefore, is the only plausible mechanism resulting in silver release.

The crack diameter necessary to account for the mass of silver released can be calculated from the equations presented in Section 5.4.1 and the temperatures, times, and pressures of the diffusion couple experiments. This procedure was also applied to the helium leak testing results on the diffusion couples, presented in Section 5.4.3, and also to mass loss data from the JAERI (Japanese Atomic Energy Research Institute) HRB-22 capsule irradiation and heating test, discussed in Section 5.4.4.

The graphite substrate shell is ignored for the calculations on the SiC-1 and SiC-2 diffusion couples. The graphite layer consists of interconnected porosity, providing a direct path for silver vapor to reach the inner surface of the SiC coating in the diffusion couples. The pressure inside the SiC layers is simply the equilibrium vapor pressure of silver at the heat treatment temperature.

At all heating temperatures, there is plenty of excess silver available; only 2×10^{-5} g of silver is required to maintain vapor/liquid equilibrium inside the diffusion couples and approximately 0.12 g to 0.50 g of silver was loaded into each diffusion couple. One SiC-1 sample and one SiC-2 sample experienced fractional releases greater than 100% and did not maintain silver equilibrium throughout the heat treatment. All calculations assumed a single, straight crack with circular cross-section and a length equal to the thickness of the SiC layer. The SiC thickness was calculated from the measured weight gain of the diffusion couples after CVD deposition of the SiC layer.

The same assumptions were used for calculations on the SiC-3 diffusion couples with SiC substrate shells with an outer CVD SiC coating. The SiC substrate shell, however, was not porous like the graphite shell in the SiC-1 and SiC-2 diffusion couples and it was less likely that a crack would develop through the entire 800 μm thickness of the SiC substrate shell. The only release path, therefore, for the silver vapor was through the outer SiC coating.

There was a significant gap between the two SiC substrate shells, as discussed and shown in Section 4.3.3.2. In this area, around the entire diffusion couple, silver vapor had direct access to the outer SiC coating. Any cracks or connected mechanical paths in the SiC outer coating near the seam would result in silver release. In the SiC-3 couples, only silver vapor near the seam in the inner shell could easily get to the outer SiC coating. Only cracks in the outer SiC coating near the seam area produced silver release, resulting in lower overall mass loss compared to the SiC-1 and SiC-2 diffusion couples.

The seam in the SiC-1 and SiC-2 diffusion couples between the graphite substrate shells did not significantly contribute to the overall silver release because the graphite shells were porous and allowed unimpeded silver migration to the SiC coating. The graphite substrate shells also formed a closer fit with each other, presenting only a small gap at the seam. In the SiC-1 and SiC-2 diffusion couples with SiC coatings over a graphite hollow shell, the silver vapor had ample access to the SiC coating through the porous graphite shell. At the seam location silver vapor had direct access to the SiC coating, but since the graphite shell did not significantly impede silver vapor migration the presence of a gap between the graphite substrate shells did not change the calculations.

The conductance and mass loss equations require the silver vapor pressure inside the spherical diffusion couple. At the heating temperatures used for the diffusion couple experiments, the silver existed as a vapor in equilibrium above its liquid. In all but two cases, there was sufficient silver inside the diffusion couple to maintain equilibrium between the gas and the liquid during the entire heat treatment. The equilibrium pressure for silver vapor above its liquid is given by:[5]

$$p_{silver} = 2.131 \times 10^{8} \exp\left(-3.054K \frac{10^{4}}{T}\right) \quad (5\text{-}4)$$

where p_{silver} = equilibrium silver vapor pressure (torr), and
T = absolute temperature (K).

As mentioned in Chapter 2, graphitic materials do not act as barriers to silver migration. The graphite layer in the diffusion couples (types SiC-1 and SiC-2) had 13% porosity and was easily penetrated by the silver vapor. One heating experiment with a diffusion couple with a spot of exposed graphite approximately 0.16 cm in diameter, sample Ag15, resulted in significant mass loss in just 2 h at 1500°C. If the silver loss occurred primarily through the bare graphite location, then the effective transport coefficient for silver vapor through the graphite shells in the diffusion couples was roughly 0.5 cm^2/s, resulting in nearly instantaneous transport of silver across the graphite shell. Therefore, the graphite shell is ignored during the crack size calculations and only transport through the SiC outer coating is considered.

The crack size calculations include the assumptions that the crack path is a straight tube with a circular cross-section such that the length of the crack path is equal to the SiC coating thickness. Additional assumptions include an active and accessible crack path during the entire heat treatment (i.e., silver is uniformly released during the heat treatment).

The molecular flow model was used to calculate the crack diameters for all of the spherical diffusion couples, then the Knudsen number of the resulting crack diameter and silver mean free path was checked. For all of the cases, the Knudsen number was well above the limit for molecular flow, confirming the use of the molecular flow model. Appendix A includes further details for calculating the Knudsen number and the flow regime.

Table 5-1 through Table 5-3 list the relevant heating parameters and the calculated crack diameters from the three sets of spherical diffusion couple tests. The calculated crack diameters mostly fall in the range from 3 μm to 20 μm with one sample near 30 μm and two samples near 50 μm. These crack diameters may seem rather large and easy to detect, but if multiple cracks are present in the sample, a likely event given the large surface area of the diffusion couples, then the average crack diameter will be smaller. The crack diameter calculated for 20 identical cracks is also listed in Table 5-1 through Table 5-3. These crack diameters vary from about 1μm to 4 μm with one sample near 7 μm and two greater than 10 μm. Although these dimensions are detectable under optical microscopy cracks may not be noticed if they are not perfectly aligned with the cross-section that is being viewed. It is possible, therefore, that cracks of the order of those listed in Table 5-1 through Table 5-3 would not have been detected during investigation with optical microscopy.

Table 5-1. SiC-1 heating parameters and calculated crack diameters.

Sample ID	Heating Temperature (°C)	Heating Time (h)	SiC Thickness (μm)	Mass Loss (g)	Calculated Crack Diameter (μm)	Calculated Crack Diameter for 20 Equal Cracks (μm)
10	1050	1000	65.1	0.0319	54.8	12.1
24	1050	1000	49.6	0.0300	49.0	11.0
28	1200	1760	55.4	0.0083	12.8	2.7
30	1200	1760	53.7	0.0075	12.2	2.7
56*	1500	200	74.6	0.0060	8.4	1.8
57	1500	500	73.2	0.1913	19.4	4.2
63**	1600	550	61.9	0.3297	15.8	3.3

* 0.0000 g initial silver loading (control sample)
** 101% mass loss (of initial silver load)

Table 5-2. SiC-2 heating parameters and calculated crack diameters.

Sample ID	Heating Temperature (°C)	Heating Time (h)	SiC Thickness (μm)	Mass Loss (g)	Calculated Crack Diameter (μm)	Calculated Crack Diameter for 20 Equal Cracks (μm)
37	1500	80	39.4	0.0110	11.2	2.5
38	1400	224	41.9	0.0138	12.2	2.7
39	1500	400	39.9	0.1360	15.3	3.4
40	1500	140	79.4	0.2280	32.3	7.2
53*	1600	550	72.2	0.3009	16.2	3.6

* Significant mass loss (116% of initial silver load) violates the equilibrium assumption

Table 5-3. SiC-3 heating parameters and calculated crack diameters.

Sample ID*	Heating Temperature (°C)	Heating Time (h)	SiC Thickness (μm)	Mass Loss (g)	Calculated Crack Diameter (μm)	Calculated Crack Diameter for 20 Equal Cracks (μm)
S10-1	1500	300	110.2	0.0022	6.0	1.3
S10-2	1500	725	110.2	0.0000	0.0	0.0
S10	**1500**	**1025**	**110.2**	**0.0017**	**3.6**	**0.7**
S11-1	1500	300	116.7	0.0023	6.2	1.3
S11-2	1500	725	116.7	0.0015	4.0	0.9
S11	**1500**	**1025**	**116.7**	**0.0037**	**4.8**	**1.1**
S12-1	1350	500	112.3	0.0007	5.8	1.3
S12-2	1350	1000	112.3	0.0007	4.6	0.9
S12	**1350**	**1500**	**112.3**	**0.0016**	**5.3**	**1.1**
S13-1	1350	500	109.7	0.0008	6.0	1.3
S13-2	1350	1000	109.7	0.0007	4.6	0.9
S13	**1350**	**1500**	**109.7**	**0.0017**	**5.3**	**1.1**
S22-1	1500	75	63.0	0.0013	6.6	1.3
S22-2	1500	425	63.0	0.0016	4.0	0.7
S22	**1500**	**500**	**63.0**	**0.0028**	**4.5**	**0.9**

* Each sample was heated twice. For example, S10-1 represents the first heat treatment, S10-2 represents the second, and S10 is the combined heating and mass loss data for sample S10.

5.4.3 Helium Leak Testing of Diffusion Couples

Helium leak testing, performed on many of the spherical diffusion couples and described in more detail in Chapter 4, provides additional information on the presence of cracks in the silicon carbide coating. Leak testing techniques measure the presence of mechanical cracks. Since silicon carbide is not permeable to helium, this type of testing detects mechanical cracks present in the diffusion couples.

A procedure similar to the one described above can be used to calculate the crack diameter from helium leak testing results on the diffusion couples after heating. Since the leak testing results are in the form of leak rates for each sample, the leak rate model for transition flow, Equation (5-3), can be used directly to determine the crack diameter. Again, assumptions of a straight crack with a circular cross-section and a length equal to the SiC coating thickness were employed.

As shown in Table 5-4 through Table 5-6, the crack diameters as calculated from the helium leak testing data on the spherical diffusion couples are roughly one order of magnitude smaller than those calculated from the silver mass loss.

Table 5-4. SiC-1 calculated crack diameters from leak testing.

Sample ID	Mass Loss (g)	Crack Diameter from Silver Mass Loss(μm)	Crack Diameter from Helium Leak Testing (μm)
10	0.0319	54.8	5.3
15	0.0061	37.1	6.1
24	0.0300	49.0	0.34
28	0.0083	12.8	1.8
30	0.0075	12.2	0.49
56*	0.0060	8.4	1.5
57	0.1913	19.4	2.1
63**	0.3297	15.8	5.3

* 0.0000 g initial silver loading (control sample)
** 101% mass loss (of initial silver load)

Table 5-5. SiC-2 calculated crack diameters from leak testing.

Sample ID	Mass Loss (g)	Crack Diameter from Silver Mass Loss(μm)	Crack Diameter from Helium Leak Testing (μm)
37	0.0110	11.2	1.7
38	0.0138	12.2	2.3
39	0.1360	15.3	N/A
40	0.2280	32.3	N/A
53*	0.3009	16.2	2.2

* significant mass loss (116% of initial silver load) violates silver vapor equilibrium assumption
No leak testing data available for samples Ag39 and Ag40

Table 5-6. SiC-3 calculated crack diameters from leak testing.

Sample ID	Mass Loss (g)	Crack Diameter from Silver Mass Loss(μm)	Crack Diameter from Helium Leak Testing (μm)
S10-1	0.0022	6.0	0.60
S10-2	0.0000	0.0	0.57
S10	**0.0017**	**3.6**	**0.57**
S11-1	0.0023	6.2	0.61
S11-2	0.0015	4.0	0.58
S11	**0.0037**	**4.8**	**0.58**
S12-1	0.0007	5.8	0.54
S12-2	0.0007	4.6	0.49
S12	**0.0016**	**5.2**	**0.49**
S13-1	0.0008	6.0	0.53
S13-2	0.0007	4.6	0.49
S13	**0.0017**	**5.3**	**0.49**
S22-1	0.0013	6.6	0.45
S22-2	0.0016	4.0	0.56
S22	**0.0028**	**4.5**	**0.56**

* Each sample was heated twice. For example, S10-1 represents the first heat treatment, S10-2 represents the second, and S10 is the combined heating and mass loss data for sample S10.

In all but two cases, the Knudsen number for helium flow through the calculated crack diameter at room temperature and 80 psi (the soaking over-pressure) was in the intermediate regime. For two cases, the Knudsen number was very close to the limit between intermediate and laminar flow.

5.4.4 Silver Mass Loss from Coated Fuel Particles

JAERI irradiated fuel elements with typical coated fuel particles in the HRB-22 capsule at ORNL (Oak Ridge National Laboratory). Some of the fuel elements were deconsolidated after heating and individual particles were removed and heated. The third accident condition test (ACT-3) was heated at 1700°C for 270 h. The activity of each particle was measured before and after heating. In addition, deposition cups inserted in the furnace were removed and counted periodically during heating to monitor fission product release.

The initial mean silver activity per particle was 1.04 μCi before the ACT-3 heating test. The mean mass of silver per particle before the heating test can be calculated from the initial mean activity and the decay constant for ^{110m}Ag. The relative change in activity per particle was reported after the test. Therefore, the final activity and the final mass of silver per particle can be calculated by Equation (5-5):

$$m_{Ag} = \frac{A}{\lambda_{Ag-110m}} \frac{aw_{Ag}}{N_A} \tag{5-5}$$

where m_{Ag} = silver mass (g),
A = silver activity (Bq),
λ = ^{110m}Ag decay constant (s^{-1}),

aw_{Ag}= silver atomic weight (110 g/mol), and
N_A = Avogadro's number (6.02×10^{23} atom/mol).

The mass loss for each particle during the heat treatment can then be derived from the change in activity as shown in Equation (5-6). The fractional mass loss for each of the 25 particles in ACT-3 is shown in Figure 5-1.

$$\Delta m_{Ag} = \frac{A_{initial} - A_{final}}{\lambda_{Ag-110m}} \frac{aw_{Ag}}{N_A} \tag{5-6}$$

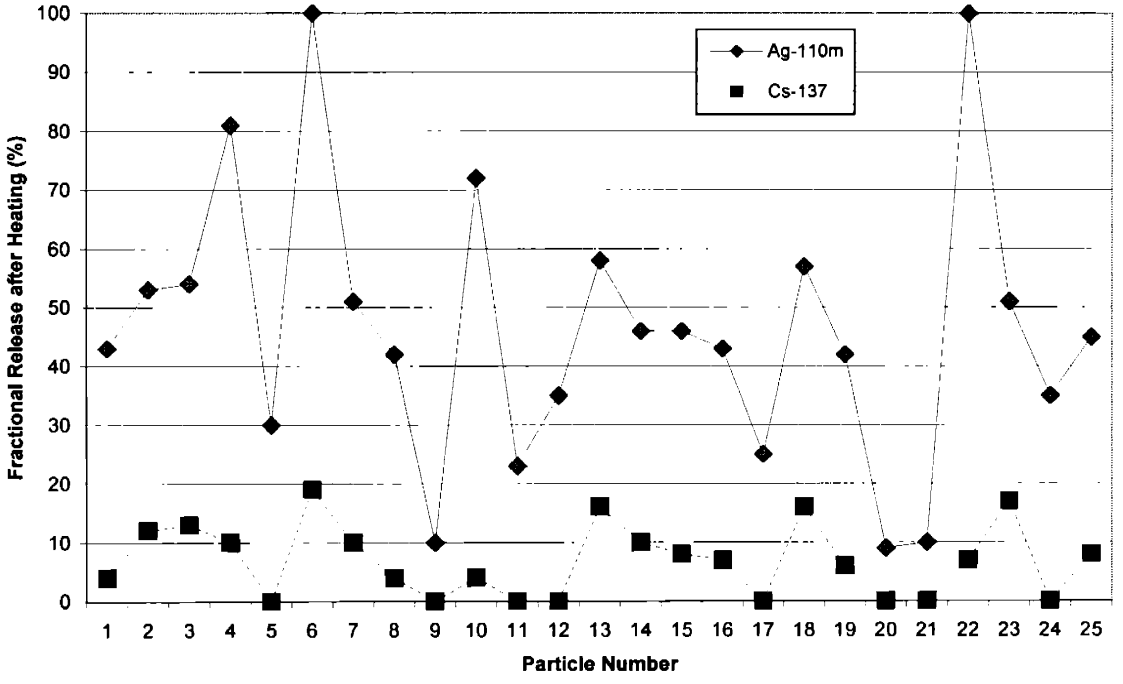

Figure 5-1. Significant variation in fission product fractional release occurs among the 25 heated particles in ACT-3.

The crack diameter in the coated fuel particles was calculated using the same procedure used in Section 5.4.1 to calculate the crack diameters from silver mass loss in the diffusion couples. The silver mass loss was calculated from the change in activity, as shown in Equation (5-6), using the equilibrium silver vapor pressure at the heating temperature and assuming the length of the crack path equal to the SiC thickness. The calculated crack diameters are listed in Table 5-7.

Table 5-7. HRB-22 silver loss and calculated crack diameters.

ID	Silver Mass Loss (10^{-10} g)	Calculated Crack Diameter	
		(μm)	(nm)
1	0.924	0.019	19.1
2	1.139	0.020	20.4
3	1.161	0.021	20.6
4	1.741	0.024	23.6
5	0.645	0.017	16.9
6	2.15	0.025	25.3
7	1.096	0.020	20.2
8	0.903	0.019	18.9
9	0.215	0.012	11.7
10	1.548	0.023	22.6
11	0.494	0.015	15.5
12	0.752	0.018	17.8
13	1.247	0.021	21.1
14	0.989	0.020	19.5
15	0.989	0.020	19.5
16	0.924	0.019	19.1
17	0.537	0.016	15.9
18	1.225	0.021	21.0
19	0.903	0.019	18.9
20	0.193	0.011	11.3
21	0.215	0.012	11.7
22	2.15	0.025	25.3
23	1.096	0.020	20.2
24	0.752	0.018	17.8
25	0.967	0.019	19.4

The calculated crack diameters for the JAERI ACT-3 coated fuel particles are extremely small. Features of this size would not have been visible during normal post-irradiation examination. Optical microscopy or scanning electron microscopy would likely not have revealed cracks on the order of 20 nm or less, especially if the crack was not aligned with the cross-sectional plane being viewed.

5.4.5 Crack Size Conclusions

A simple calculation of crack sizes in the silicon carbide layers of the current diffusion couples and typical coated fuel particles using the observed mass loss show that vapor transport through cracks can account for silver release. This explanation allows for some diffusion couples or some fuel particles to lose significant fractions of their silver inventory through cracks while other samples remain intact and retain their inventory. Due to the relatively small size of the estimated cracks, they would be difficult to detect by standard optical microscopy of polished cross-sections.

5.5 OTHER FISSION PRODUCT BEHAVIOR

The previous sections have shown that vapor migration through small cracks in the SiC coating provides a viable mechanism for silver release from both the current diffusion couple experiments and previous typical coated fuel particle tests. The SiC coating, however, also acts as a barrier for other fission products and cracks existing through the SiC coating might also be expected to release some of the other fission products as well. The summary of fission product interactions in the layers of coated fuel particles and the surrounding fuel element materials provides evidence that cracks in the SiC resulting in silver release would not necessarily increase the release of other fission products. Silver vapor migration through SiC cracks is, therefore, a viable explanation for silver release.

Catastrophic failure of the TRISO coatings or through-coating cracks that extend through the IPyC-SiC-OPyC system will certainly result in significant fission product release of both gases and metallic fission products. Minor flaws in a single layer, however, may allow preferential release of only certain fission products. Retention of fission products in layers other than the SiC layer may prevent release even if cracks are present in the SiC. The role of all of the layers in the coated fuel particle needs to be examined to understand the effect cracks in the SiC layer would have on the overall fission product release.

The key fission products of interest for release and the ones most frequently measured during testing include the fission gases krypton and xenon and the solid fission product cesium. These fission products are discussed below.

5.5.1 Fission Gases

Intact pyrocarbon layers are effectively impermeable to fission gases during normal operating conditions.[2] The SiC layers also provide holdup of the fission gases, but as long as at least one of the PyC layers remains intact, the particle will retain the fission gases. Therefore, small cracks in the SiC layer that permit the escape of silver will not result in an increased krypton or xenon release as long as the PyC layers remain intact.

5.5.2 Cesium

Many of the layers in a typical coated fuel particle retain cesium better than silver. Therefore, even if cracks are present in the SiC layer, allowing silver release, cesium release may be decreased or delayed due to increased retention in the particle relative to silver.

In general, cesium has been reported to diffuse more slowly than silver out of UO_2 fuel kernels.[6, 7] This increased retention of cesium in the fuel kernel will decrease the amount of fractional release of cesium relative to silver and will also delay the time to breakthrough of cesium relative to silver. Also aiding retention of cesium is the formation of stable compounds in the kernel such as $CsMoO_4$.[8]

Although the pyrocarbon layers do not do a great job of retaining the solid fission products compared to the SiC layer, they do provide more retention for cesium than for silver.[6, 7] Additionally, cesium experiences some sorption in the matrix graphite in fuel elements.[2, 9] Therefore, cesium released from fuel particles into the matrix will be, at least partially, adsorbed onto the graphite. Silver is not retained by any of the PyC layers or the matrix graphite. Where reported, the diffusion coefficients for silver in PyC and matrix graphite are all lower for cesium than for silver, indicating greater cesium retention in those materials.

Greater retention of cesium by PyC layers also means that if cesium does migrate through the SiC layer, even if through cracks as proposed for silver release, additional holdup by the OPyC layer will decrease the amount of cesium released from the fuel particle and will also delay the breakthrough time for cesium relative to that for silver.[2]

Concentration profiles measured through fuel particles typically show cesium mainly in the kernel and buffer with steep concentration gradients through the IPyC layer indicating retention in that layer.[2] A crack in the SiC will result in silver release, but retention in the PyC layers and matrix graphite will lessen the amount of cesium that escapes.

5.6 CRACK FORMATION POSSIBILITIES

Although cracks in the SiC coating provide a good explanation for the wide variations in silver release, cracks have not yet been positively identified or observed and remain a hypothesis at this time. However, the formation of microscopic-scale cracks in the SiC coating may not be surprising given the residual stresses remaining in SiC after fabrication and the individual grain behavior during thermal cycling.

For the current diffusion couples, an additional stress factor not present in typical coated fuel particles is the seam. The seam is an asymmetrical feature and may promote crack growth around the circumference of the diffusion couples. Additionally, the differential thermal expansion between the graphite substrate shell and the SiC coatings can lead to cracking. Finite element calculations of a typical diffusion couple, neglecting the discontinuity of the seam, indicate that the stress in the diffusion couple could exceed the fracture strength of the SiC due to differential thermal expansion after fabrication, as shown in Figure 5-2.

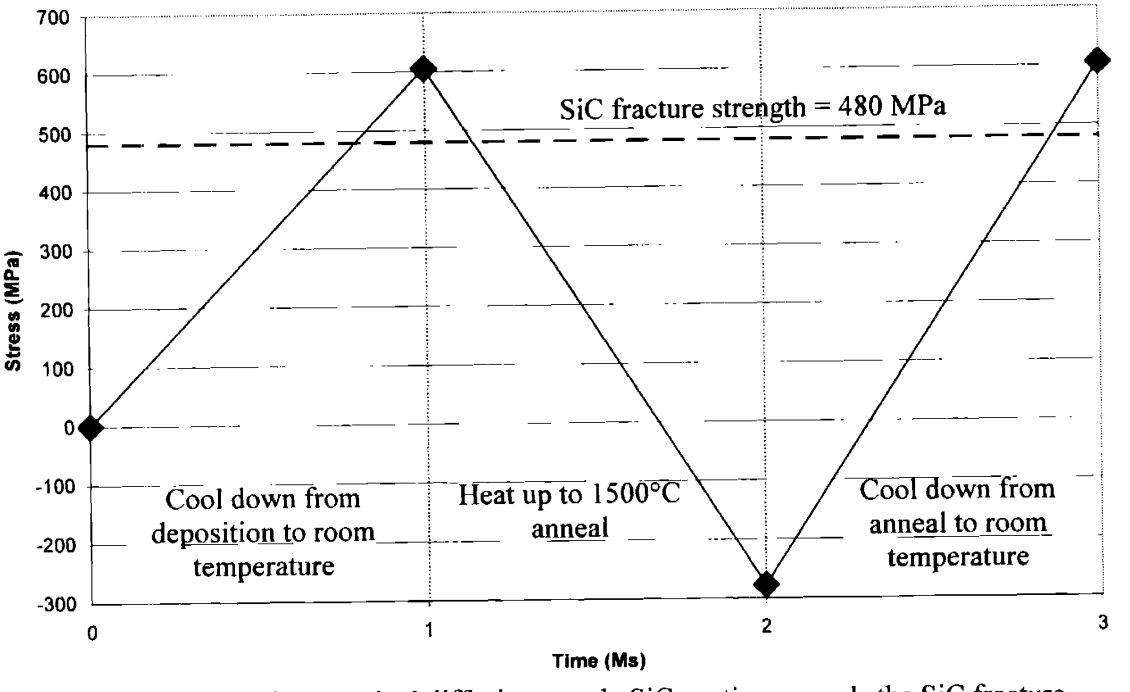

Figure 5-2. Stress state in a nominal diffusion couple SiC coating exceeds the SiC fracture strength during thermal cycling. (Initial zero stress state occurs during CVD deposition at 1200°C)

5.7 CONCLUSIONS

With the variation in the fission product release data, diffusion clearly does not explain the range of silver release. Further, it is unlikely that one mechanism can describe all observed results. Within a single batch, some particles appear to undergo catastrophic failure, releasing most of their fission product inventories in a short time, while others lose only small fractions, if any at all, over long heat treatments.

Crack sizes based on observed silver mass loss from both the current diffusion couples and typical coated fuel particles and from leak testing results on the diffusion couples offer a reasonable and plausible explanation of silver release. Furthermore, this proposed mechanism is also consistent with other fission product behavior in coated fuel particles.

5.8 REFERENCES

[1] H. Nabielek, *The Mechanism of Silver Retention in Coated Particle Fuel*, Dragon Project Technical Report DTN/801, April 1976.

[2] R.K. McCardell et al., *NP-MHTGR Fuel Development Program Plan*, Idaho National Engineering and Environmental Laboratory EGG-NPR-8971, Rev. C., September 1992, Appendix A.

[3] Alcatel Vacuum Technology (catalog), France.

[4] Varian Proceedings, Leak Detection Seminar/Workshop. June 2-4, 1976.

[5] I. Barin, O. Knacke, O. Kubaschewski, *Thermochemical Properties of Inorganic Substances: Supplement*, New York: Springer-Verlag, 1977.

[6] R.C. Martin, Compilation of Fuel Performance and Fission Product Transport Models and Database for MHTGR Design, ORNL/NPR-91/6, 1993 (Chapter 5).

[7] International Atomic Energy Agency, Fuel performance and fission product behaviour in gas cooled reactors, IAEA-TECDOC-978, 1997.

[8] J. McFarlane et al., "Chemical Speciation of Iodine Source Term to Containment," *Nucl. Tech.* **138** (2002) 162-178.

[9] W. Schenk, D. Pitzer, H. Nabielek, "Fission Product Release Profiles from Spherical HTR Fuel Elements at Accident Temperatures," Jül-2234, September 1988.

6. Conclusions

Although silver release from various coated fuel particle designs has been observed for decades, its exact transport path has yet to be identified. One of the goals of the work described in this dissertation was to observe silver diffusion, the assumed mechanism governing silver transport through and release from silicon carbide by measuring characteristic concentration profiles.

Many authors have reported diffusion coefficients to explain silver release observations. These values represent average batch behavior, but do not address the variability within batch populations. Identifying the exact path and cause of silver transport in silicon carbide is hampered by the small feature size of the potential cracks or flaws and the relatively small number of flawed particles.

The results of this work show that SiC is not intrinsically permeable to silver. Rather, silicon carbide can be fabricated such that silver does not diffuse at any appreciable rate. Although these findings are remarkably different than those initially expected, they do provide hope that silver transport through and release from silicon carbide coatings can be prevented.

6.1 KEY FINDINGS

As stated earlier, the goals of this work were to observe silver diffusion in silicon carbide and to measure the resulting silver concentration profiles. Two different types of experiments with different silver concentration ranges showed no evidence of silver diffusion through silicon carbide. The results of the experiments described in this dissertation indicate that silver release from silicon carbide is dominated by vapor migration through physical cracks.

(1) A reassessment of the literature, detailed in Chapter 2, highlights variations in silver release and reported diffusion coefficients in excess of that expected for a grain boundary diffusion mechanism. Although variations in silver release would be expected from a grain boundary diffusive process, diffusion does not account for the variations observed in individual particles and even between batches. The range of diffusion coefficients reported in the literature spans almost 2 orders of magnitude. If the size of that range were the result of differences in exact path length between particles, due to SiC thickness and microstructure, the total path length would have to change by a factor of roughly 13 for an effective path length of 470 μm through a 35 μm thick coating. Silver traveling along SiC grain boundaries, as suggested in the literature, would follow a meandering path through a 35 μm thick SiC layer, but total path lengths on the order of 400-500 μm are not plausible. The population of silver release results reported in the literature is not consistent with solid-state diffusion, either grain boundary or trans-granular.

(2) Silver did not diffuse in silicon carbide in ion-implanted samples, even along the abundant grain boundary area in the recrystallized and original SiC. The silver concentration profile should have been completely depleted during heating according to the diffusion coefficients reported in the literature. No change in the silver concentration profile, however, was observed. Based on the measured silver concentration profiles, the diffusion coefficient for silver in SiC must be less than 5×10^{-21} m^2/s at 1500°C. The microscopic distribution of silver changed from a fairly homogeneous mixture in amorphous silicon carbide after implantation to discrete precipitates between recrystallized SiC grains after heating. At the heating

temperature of 1500°C, the vacancies and vacancy loops created during the implantation were sufficiently mobile to prevent the trapping of silver. Pockets of unit-activity silver provided ideal sources for diffusion along grain boundaries, but no silver diffusion was observed. The results of the ion implantation experiments indicate that silicon carbide can be manufactured to resist silver migration.

(3) Diffusion did not govern silver release from the spherical diffusion couples. The diffusion couple experiments resulted in a range of silver release from 0% to 100%. Although the silicon carbide coating thickness varied significantly in the diffusion couples (from approximately 40 μm to greater than 100 μm), the release results are not explained by a diffusive mechanism. Furthermore, the diffusion coefficients necessary to account for the silver mass loss from the silver vapor source at the top of the diffusion couples would have had to be about 6 orders of magnitude greater than those reported in the literature. Although the diffusion couple experiments did indeed produce silver mass loss, silver migration was not controlled by diffusion on the scale of that reported in the literature.

(4) Increased helium leak rates after heating prove the presence of cracks in the SiC coating on the diffusion couples. Cracks in the silicon carbide coating could have provided a pathway for silver vapor escape. Crack sizes in the diffusion couples calculated from simplified vapor flow models are on the order of 1-10 μm. Features of this dimension would not likely have been observed during analysis due to their small size and random orientation within the sample.

(5) Vapor migration through cracks is proposed to dominate silver release from silicon carbide. Only silver vapor had access to the SiC coating, via migration through the graphite porosity, during heating. Molten silver, at the bottom of the diffusion couples, did not penetrate the graphite shell and, therefore, could not have resulted in silver release. A vapor migration mechanism is consistent with the results and observations of the current experimental program and is also consistent with results and observations reported in the literature. Vapor migration through mechanical cracks explains why some particles, those with cracks, release large fractions of their silver inventories while other particles, those without cracks, retain all of their silver. Diffusion cannot account for this broad variation in fractional release results. Given the properties of the other coated fuel particle layers, vapor migration is also consistent with other observed fission product behavior. The presence of small cracks in the SiC layer will not result in large releases for other fission products, for example cesium and krypton, due to their retention in the other layers. The PyC layers retain krypton, xenon, and the noble fission gases; as long as either the IPyC or the OPyC is intact, the noble fission gases will be retained in the particle, even if the SiC layer is damaged. Although the SiC improves cesium retention (relative to the PyC layers), the graphite materials, both within and surrounding the fuel particles, aid in retention. Therefore, cesium release through SiC cracks will be lower than silver release.

6.2 RECOMMENDATIONS FOR FUTURE WORK

Although the work detailed in this dissertation provides a major step forward in understanding silver transport in silicon carbide, much work remains to identify silver's exact pathway and the specific conditions leading to crack formation. In order to improve coated fuel particle performance, relative to silver release, attention needs to focus on silicon carbide integrity.

It is not yet known, however, what characteristics may promote cracking or what features, if any, may act as a seed for cracking in SiC. It is clear that not all particles develop cracks and release silver. Successful particles are fabricated and can retain silver during operation. Additional work needs to focus on developing a better understanding of SiC fabrication and what parameters influence cracking and subsequent vapor release.

The experiments described in this dissertation were performed with CVD silicon carbide materials with properties similar to those of typical coated fuel particles. The diffusion couples, however, were much larger than typical coated fuel particles and have approximately 37,000 times more SiC volume than a fuel particle. This large volume significantly increases the probability of obtaining a critical flaw, which may act as a seed for crack formation. Future investigations should, therefore, focus on typical coated fuel particles to eliminate volume effects that may increase the presence of cracks.

Given the small size of the calculated cracks in the SiC coating and their random orientation, observing such features during normal cross-section optical microscopy is highly unlikely. Other techniques or metrics are, therefore, needed to provide evidence of the presence of cracks. Leak testing, as performed on the diffusion couples and described in Chapter 4, is one possible technique. Care must be taken to select a technique that can measure the small number of leaks present in a typical batch of coated fuel particles. The leak testing described in Chapter 4 measured the helium release from large diffusion couples after soaking. It takes about 37,000 typical coated fuel particles to equal the same free volume as a single diffusion couple. A crack in a single particle may not be detected during leak testing because gas release may be too small to register above the noise level. It may be harder, therefore, to identify individual cracked particles due to their limited volume. This technique may still be useful though for analysis of batches of particles and for investigating the effects of thermal cycling or irradiation on overall leak rates. Additional work is needed to determine methods to identify and quantify cracks in SiC coatings. A non-destructive technique capable of 3-D imaging and high resolution is needed to directly observe small cracks in SiC coatings.

A simplified, bulk material stress analysis, discussed in Section 4.4, indicates that stresses inside the spherical diffusion couples may have exceeded SiC fracture strengths. A detailed, grain-level stress analysis, however, is needed to understand the stress state and behavior of individual SiC grains. Research on microstructural stress networks in polycrystalline materials with anisotropic properties reveals significant stresses between grains.[1] Additional work is required to develop a better understanding of the relationship between SiC coating parameters and the microstructural stress state that may contribute to cracking.

In addition to thermal cycling, irradiation effects may promote cracking in the silicon carbide coatings. Irradiation-induced swelling changes the stress state within the particles during irradiation and may lead to increased cracking probabilities. Furthermore, irradiation damage in the silicon carbide may create or exacerbate a crack, leading to a vapor transport path.

This work has shown that silver release does not result from classical diffusion through intact silicon carbide, but rather is dominated by vapor transport through cracks. Silicon carbide can be fabricated that does not release silver. Zirconium carbide is under investigation as a possible alternative to silicon carbide as a fission product barrier.[2,3] Very little work has been completed on silver release from ZrC coatings. Additional experiments should be conducted to understand the susceptibility of ZrC to cracking to determine whether or not silver diffuses in ZrC.

6.3 REFERENCES

[1] E.R. Fuller, Jr., "Microstructural Stresses: Networks, Structural Reliability, and Antiquity Preservation," 106th Annual Meeting of the American Ceramic Society, Indianapolis, IN, April 21, 2004.

[2] G.H. Reynolds, J.C. Janvier, J.L. Kaae, J.P. Morlevat, "Irradiation Behavior of Experimental Fuel Particles Containing Chemically Vapor Deposited Zirconium Carbide Coatings," *J. Nucl. Mat.* **72** (1976) 9-16.

[3] R.E. Bullock, "Fission-Product Release During Postirradiation Annealing of Several Types of Coated Fuel Particles," *J. Nucl. Mat.* **125** (1984) 304-319.

A. Diffusion Couple Data

The following tables list the heat treatment and fabrication data for the diffusion couple experiments discussed in Chapter 4. Two different fixtures, shown in Figure A-1 and noted as "clamp" and "plate" in the following tables, were used to hold the diffusion couples during SiC coating.

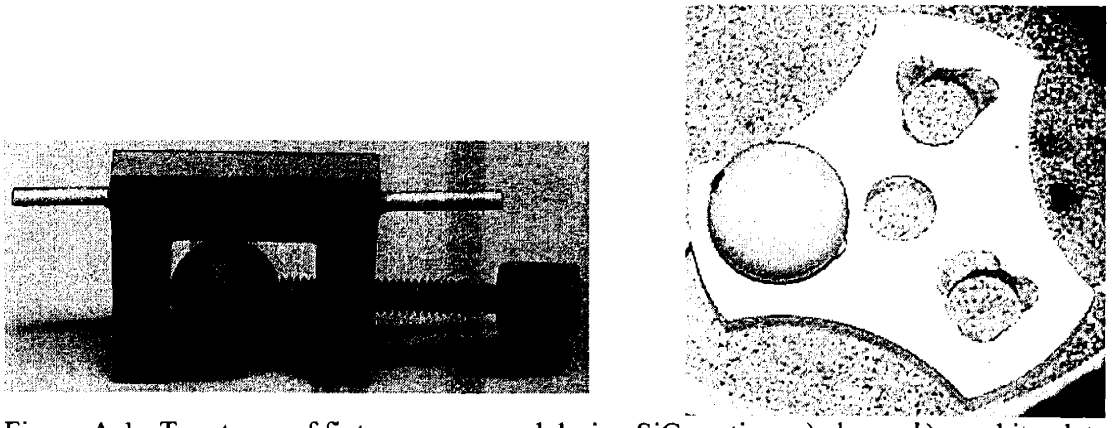

Figure A-1. Two types of fixtures were used during SiC coating: *a*) clamp, *b*) graphite plate.

A.1 SiC-1

Table A-1. SiC-1 Diffusion Couple Annealing Data.

	Anneal				
ID	Temp (°C)	Time (hrs)	Start Date	End Date	Notes
8	1500	24	7/14/00	7/15/00	
9	1400	43.8	7/19/00	7/21/00	
10	1050	1000	7/12/01	8/26/01	
11	1700	50	11/15/01	11/17/01	
12					as-fabricated, not heated
13	1400	276	7/17/01	7/29/01	
14	1500	300	11/15/01	11/30/01	
15	1500	2	8/31/01	8/31/01	bare graphite spot
16					
17	1500	400	10/23/01	11/6/01	control sample, sectioned before heat
19					missing button
20	1500	120	1/17/01	1/22/01	
21	1400	240	1/24/01	2/3/01	
22					missing button
23	1400	276	7/17/01	7/29/01	
24	1050	1000	7/12/01	8/26/01	
28_1	1200	643	7/30/01	8/26/01	1st heat treatment
28_2	1200	1117	12/11/01	1/27/02	2nd heat treatment
28	1200	1760			cumulative
29_1	1500	24			1st heat treatment
29_2	1200	400	2/20/01	3/12/01	2nd heat treatment
30_1	1200	643	7/30/01	8/26/01	1st heat treatment
30_2	1200	1117	12/11/01	1/27/02	2nd heat treatment
30	1200	1760			cumulative
32	1500	100	7/12/01	7/17/01	
33	1500	100	7/12/01	7/17/01	
56	1500	200	2/28/02	3/8/02	control sample, no silver
57	1500	200	2/28/02	3/8/02	
58					
59					
60					
61					
62					
63	1600	550	2/1/02	2/24/02	
64					

Table A-2. SiC-1 Diffusion Couple Mass Loss and Leak Testing Data.

		Mass Loss					Leak Testing	
ID	Initial Ag Mass (gm)	Mass before anneal (gm)	Mass after anneal (gm)	dM Total (gm)	dM / initial Ag mass	dM / total mass	pre (atm.cc /sec)	post (atm.cc /sec)
8	0.1366	1.7734	n/a					
9	0.1297	1.7511	n/a					
10	0.1378	1.7728	1.7409	0.0319	0.2315	0.0180		3.0E-02
11	0.1441	1.7672	1.6826	0.0846	0.5871	0.0479		
12	0.1405							
13	0.1358	1.7634	1.7555	0.0079	0.0582	0.0045		
14	0.1219	1.7615	1.6652	0.0963	0.7900	0.0547		
15	0.1249	1.7401	1.7340	0.0061	0.0488	0.0035		1.0E-03
16	0.1289						2.5E-02	
17	0.1090	1.3471	1.3400	0.0071	0.0651	0.0053		
19	0.1294						8.0E-03	
20	0.1383	1.6834	1.6569	0.0265	0.1916	0.0157		
21	0.1615	1.6989	1.6656	0.0333	0.2062	0.0196		
22	0.1700						4.0E-02	
23	0.1581	1.7213	1.7200	0.0013	0.0082	0.0008		
24	0.1750	1.7466	1.7166	0.0300	0.1714	0.0172		2.0E-06
28_1	0.2363	1.8527	1.8460	0.0067	0.0284	0.0036		
28_2	0.2363	1.8497	1.8444	0.0053	0.0224	0.0029		5.0E-04
28	0.2363	1.8527	1.8444	0.0083	0.0351	0.0045		
29_1	0.2363	n/a						
29_2	0.2038	1.8318	n/a					
30_1	0.2029	1.8062	1.7996	0.0066	0.0325	0.0037		
30_2	0.2029	1.8005	1.7987	0.0018	0.0089	0.0010		5.0E-06
30	0.2029	1.8062	1.7987	0.0075	0.0370	0.0042		
32	0.2737	1.9797	1.9781	0.0016	0.0058	0.0008		
33	0.2497	1.9973	1.9959	0.0014	0.0056	0.0007		
56	0.0000	1.6924	1.6864	0.0060		0.0035	5.0E-07	2.0E-04
57	0.3029	1.9801	1.7888	0.1913	0.6316	0.0966	5.0E-07	8.0E-04
58	0.3009						5.0E-07	
59	0.2751						5.0E-07	
60	0.2859						5.5E-07	
61	0.2693						5.0E-07	
62	0.2683						1.5E-05	
63	0.3256	1.9622	1.6325	0.3297	1.0126	0.1680		2.5E-02
64	0.3115						5.0E-07	

Table A-3. SiC-1 Diffusion Couple SiC Coating Data.

	SiC Coating				
ID	CVD fixture	SiC Coating Date	Total Mass (gm)	SiC Mass (gm)	SiC thick (μm)
8	clamp	3/00	1.7734	0.2377	64.5
9	clamp	3/00	1.7511	0.2323	63.1
10	clamp	3/00	1.7730	0.2399	65.1
11	clamp	3/00	1.7676	0.2246	61.0
12	clamp	3/00	1.7270	0.1929	52.4
13	clamp	3/00	1.7636	0.2176	59.1
14	clamp	5/00	1.7606	0.2323	63.1
15	clamp	5/00	1.7599	0.2357	64.0
16	clamp	5/00	1.7725	0.2368	64.3
17	clamp	10/00	1.6337	0.1275	34.7
19	clamp	10/00	1.6500	0.1281	34.9
20	clamp	10/00	1.6834	0.1402	38.2
21	clamp	10/00	1.7014	0.1405	38.2
22	clamp	10/00	1.6856	0.1203	32.8
23	plate	10/00	1.7211	0.1686	45.8
24	plate	10/00	1.7463	0.1824	49.6
28_1	plate	2/01	1.8525	0.2038	55.4
28_2	plate	2/01	1.8525	0.2038	55.4
28	plate	2/01	1.8525	0.2038	55.4
29_1	plate	2/01	1.8318	0.2132	57.9
29_2	plate	2/01	1.8318	0.2132	57.9
30_1	plate	2/01	1.8060	0.1978	53.7
30_2	plate	2/01	1.8060	0.1978	53.7
30	plate	2/01	1.806	0.1978	53.7
32	plate	5/01	1.9972	0.3061	82.9
33	plate	5/01	1.9796	0.3089	83.7
56	plate	11/01	1.6922	0.2750	74.6
57	plate	11/01	1.9800	0.2701	73.2
58	plate	11/01	1.9574	0.2519	68.3
59	plate	11/01	1.9040	0.2206	59.9
60	plate	11/01	1.9034	0.2037	55.3
61	plate	11/01	1.8948	0.2114	57.4
62	plate	12/01	1.8974	0.2208	60.0
63	plate	12/01	1.9602	0.2280	61.9
64	plate	12/01	1.9701	0.2383	64.7

Table A-4. SiC-1 Diffusion Couple Fabrication Data.

	Sample Fabrication / Silver Data										
ID	Silver Coating Date	Silver Source	Shell Mass (gm)	Male Mass (gm)	M + Ag (gm)	M + Ag + F (gm)	Ag Mass (gm)	Female Mass (gm)	Female Mass (gm)	F + Ag Mass (gm)	F Ag Mass (gm)
8	2/1/00	sputter	1.3604	0.7091	0.7737	1.4970			0.6513	0.7233	0.0720
9	2/1/00	sputter	1.3504	0.7095	0.7758	1.4801			0.6409	0.7043	0.0634
10	2/2/00	sputter	1.3568	0.7147	0.7852	1.4944			0.6421	0.7094	0.0673
11	2/2/00	sputter	1.3603	0.7091	0.7813	1.5043			0.6512	0.7231	0.0719
12	2/2/00	sputter	1.3550	0.7073	0.7788	1.4954			0.6477	0.7167	0.0690
13	2/2/00	sputter	1.3715	0.7114	0.7841	1.5073			0.6601	0.7232	0.0631
14	3/23/00	sputter	1.3677	0.7107	0.7724	1.4896			0.6571	0.7173	0.0602
15	3/23/00	sputter	1.3607	0.7085	0.7688	1.4855			0.6522	0.7168	0.0646
16	3/23/00	sputter	1.3680	0.7121	0.7788	1.4970			0.6560	0.7182	0.0622
17	3/23/00	sputter	1.3584	0.7034	0.7679	1.4675			0.6551	0.6996	0.0445
19	3/23/00	sputter	1.3537	0.7137	0.7824	1.4832			0.6401	0.7008	0.0607
20	3/23/00	sputter	1.3665	0.7131	0.7837	1.5045			0.6533	0.7210	0.0677
21	5/3/00	sputter	1.3606	0.7073	0.7929	1.5222			0.6534	0.7293	0.0759
22	5/3/00	sputter	1.3566	0.7036	0.7856	1.5266			0.6531	0.7411	0.0880
23	5/3/00	sputter	1.3558	0.7160	0.7966	1.5138			0.6398	0.7173	0.0775
24	5/3/00	sputter	1.3501	0.7110	0.7997	1.5252			0.6392	0.7255	0.0863
28_1	2/7/01	powder	1.4125	0.7292	0.9655	1.6487	0.2363	0.6832			
28_2	2/7/01	powder	1.4125	0.7292	0.9655	1.6487	0.2363	0.6832			
28	2/7/01	powder	1.4125	0.7292	0.9655	1.6487	0.2363	0.6832			
29_1	2/7/01	powder	1.4148	0.7219	0.9257	1.6186	0.2038	0.6929			
29_2	2/7/01	powder	1.4148	0.7219	0.9257	1.6186	0.2038	0.6929			
30_1	2/7/01	powder	1.4054	0.7238	0.9267	1.6082	0.2029	0.6815			
30_2	2/7/01	powder	1.4054	0.7238	0.9267	1.6082	0.2029	0.6815			
30	2/7/01	powder	1.4054	0.7238	0.9267	1.6082	0.2029	0.6815			
32	3/16/01	powder	1.4166	0.7248	0.9985	1.6911	0.2737	0.6926			
33	3/16/01	powder	1.4210	0.7280	0.9777	1.6707	0.2497	0.6930			
56	11/13/01	powder		0.7257		1.4172		0.6915			
57	11/13/01	powder		0.7221	1.0250	1.7099	0.3029	0.6849			
58	11/13/01	powder		0.7241	1.0250	1.7055	0.3009	0.6805			
59	11/13/01	powder		0.7238	0.9989	1.6834	0.2751	0.6845			
60	11/13/01	powder		0.7206	1.0065	1.6997	0.2859	0.6932			
61	11/13/01	powder		0.7313	1.0006	1.6834	0.2693	0.6828			
62	11/15/01	powder		0.7263	0.9946	1.6766	0.2683	0.682			
63	11/15/01	powder		0.7271	1.0527	1.7322	0.3256	0.6795			
64	11/15/01	powder		0.7281	1.0396	1.7318	0.3115	0.6922			

A.2 SiC-2

Table A-5. SiC-2 Diffusion Couple Annealing Data.

	Anneal					
ID	Temp (°C)	Time (hr)	Start Date	End Date	Furnace	Notes
Ag34						no silver
Ag35						no silver
Ag37	1500	80	9/14/01	9/17/01	W4 plate	
Ag38	1400	224	9/14/01	9/23/01	W5 plate	
Ag39	1500	400	10/23/01	11/6/01	W5 plate	
Ag40	1500	140	10/12/01	10/18/01	W4 plate	
Ag50						free Si in SiC
Ag51						free Si in SiC
Ag52						free Si in SiC
Ag53	1600	550	2/1/02	2/25/02	W5 plate	
Ag54						
Ag55						

Table A-6. SiC-2 Diffusion Couple Mass Loss and Leak Testing Data.

	Mass Loss						Leak Testing	
ID	Initial Ag Mass (gm)	Mass before anneal (gm)	Mass after anneal (gm)	dM Total (gm)	dM / initial Ag mass	dM / total mass	pre (atm.cc /sec)	post (atm.cc /sec)
Ag34	0.0000						5.0E-07	
Ag35	0.0000							
Ag37	0.2530	1.8084	1.7974	0.0110	0.0435	0.0061		7.0E-04
Ag38	0.2545	1.8190	1.8052	0.0138	0.0542	0.0076		2.0E-03
Ag39	0.2525	1.8092	1.6732	0.1360	0.5386	0.0752		
Ag40	0.2530	1.9577	1.7297	0.2280	0.9012	0.1165		
Ag50	0.2863							
Ag51	0.2852							
Ag52	0.2836							
Ag53	0.2600	1.9339	1.6330	0.3009	1.1573	0.1556		9.0E-04
Ag54	0.2705						3.0E-02	
Ag55	0.3300						8.0E-04	

Table A-7. SiC-2 Diffusion Couple SiC Coating Data.

	SiC Coating				
ID	SiC Fixture	SiC Coating Date	G + Ag + SiC Mass (gm)	SiC Mass (gm)	SiC thick (um)
Ag34	plate	7/01	1.6065	0.2044	55.5
Ag35	plate	7/01	1.6028	0.1927	52.4
Ag37	plate	8/01	1.8084	0.1448	39.4
Ag38	plate	8/01	1.8190	0.1541	41.9
Ag39	plate	8/01	1.8092	0.1466	39.9
Ag40	plate	9/01	1.9579	0.2929	79.4
Ag50	plate	10/01	1.8321	0.1308	35.6
Ag51	plate	10/01	1.8188	0.1194	32.5
Ag52	plate	10/01	1.8570	0.1703	46.3
Ag53	plate	11/01	1.9343	0.2663	72.2
Ag54	plate	11/01	1.8859	0.2019	54.9
Ag55	plate	11/01	1.8806	0.1329	36.2

Table A-8. SiC-2 Diffusion Couple Fabrication Data.

	Sample Fabrication / Silver Data							
ID	Silver Source	Silver Date	Shell Mass (gm)	Male Mass (gm)	M + Ag Mass (gm)	M + Ag + F (gm)	Ag Mass (gm)	Female Mass (gm)
Ag34	none		1.4021					
Ag35	none		1.4101					
Ag37	powder	7/24/01	1.4107	0.7202	0.9732	1.6636	0.2530	0.6904
Ag38	powder	7/24/01	1.4106	0.7299	0.9844	1.6649	0.2545	0.6805
Ag39	powder	7/24/01	1.4103	0.7227	0.9752	1.6626	0.2525	0.6874
Ag40	powder	7/24/01	1.4122	0.7214	0.9744	1.6650	0.2530	0.6906
Ag50	powder	9/18/01	1.4154	0.7232	1.0095	1.7013	0.2863	0.6918
Ag51	powder	9/18/01	1.4144	0.7295	1.0147	1.6994	0.2852	0.6847
Ag52	powder	9/18/01	1.4035	0.7290	1.0126	1.6867	0.2836	0.6741
Ag53	powder	10/23/01	1.4081	0.7190	0.9790	1.6680	0.2600	0.6890
Ag54	powder	10/23/01	1.4136	0.7212	0.9917	1.6840	0.2705	0.6923
Ag55	powder	10/23/01	1.4177	0.7362	1.0662	1.7477	0.3300	0.6815

A.3 SiC-3

Table A-9. SiC-3 Diffusion Couple Annealing, Mass Loss, and Leak Testing Data.

	Anneal				Mass Loss					Leak Testing	
ID	Temp (°C)	Time (hr)	Start Date	End Date	Initial Ag Mass (gm)	Mass before anneal (gm)	Mass after anneal (gm)	dM Total (gm)	dM / initial Ag mass	pre (atm.cc /sec)	post (atm.cc /sec)
S09					0.5153					8.0E-05	
S10	1500	300	7/18/02	7/31/02	0.5072	3.4318	3.4296	0.0022	0.0043	8.0E-07	6.0E-06
	1500	725	8/23/02	9/22/02	0.5072	3.4295	3.4301	-0.0006	-0.0012		5.0E-06
	1500	1025			0.5072	3.4318	3.4301	0.0017	0.0034	8.0E-07	5.0E-06
S11	1500	300	7/18/02	7/31/02	0.5019	3.3225	3.3202	0.0023	0.0046	5.0E-07	5.0E-06
	1500	725	8/23/02	9/22/02	0.5019	3.3203	3.3188	0.0015	0.0030		5.0E-06
	1500	1025			0.5019	3.3225	3.3188	0.0037	0.0074	5.0E-07	5.0E-06
S12	1350	500	7/18/02	8/8/02	0.5024	3.4130	3.4123	0.0007	0.0014	7.0E-07	3.0E-06
	1350	1000	9/24/02	11/5/02	0.5024	3.4121	3.4114	0.0007	0.0014		3.0E-06
	1350	1500			0.5024	3.4130	3.4114	0.0016	0.0032	7.0E-07	3.0E-06
S13	1350	500	7/18/02	8/8/02	0.5064	3.4841	3.4833	0.0008	0.0016	7.0E-07	3.0E-06
	1350	1000	9/24/02	11/5/02	0.5064	3.4831	3.4824	0.0007	0.0014		3.0E-06
	1350	1500			0.5064	3.4841	3.4824	0.0017	0.0034	7.0E-07	3.0E-06
S22	1500	75	4/22/02	4/25/02	0.5007	3.3326	3.3313	0.0013	0.0026	6.5E-07	4.0E-06
	1500	425	6/26/02	7/15/02	0.5007	3.3314	3.3298	0.0016	0.0032		8.0E-06
	1500	500			0.5007	3.3326	3.3298	0.0028	0.0056	6.5E-07	8.0E-06

Table A-10. SiC-3 Diffusion Couple SiC Coating and Fabrication Data.

	SiC Coating					Sample Fabrication / Silver Data					
ID	SiC Coating Date	Total Coated Mass (gm)	SiC Mass (gm)	SiC thick (μm)	Silver Date	Male Shell Mass (gm)	Male + Ag Mass (gm)	Male + Ag + Female (gm)	Ag Mass (gm)	Female Mass (gm)	+ SiC in seam (gm)
S09	7/1/02	3.3911	0.3345	90.5	6/7/02	1.3264	1.8417	3.0566	0.5153	1.2149	3.0614
S10	6/14/02	3.2370	0.2106	57.2	6/13/02	1.3324	1.8396	3.0264	0.5072	1.1868	3.0289
S11	6/14/02	3.1231	0.2302	62.5	6/13/02	1.3182	1.8201	2.8929	0.5019	1.0728	2.8962
S12	6/14/02	3.2126	0.2126	57.7	6/13/02	1.3567	1.8591	3.0000	0.5024	1.1409	3.0033
S13	6/14/02	3.2815	0.2013	54.7	6/13/02	1.3393	1.8457	3.0802	0.5064	1.2345	3.0849
S22	4/2/02	3.3326	0.2322	63.0	3/28/02	1.3321	1.8328	3.1004	0.5007	1.2676	

Table A-11. SiC-3 Diffusion Couple Additional SiC Coating Data.

	Additional SiC Coating Data					
ID	SiC Coating Date	Total Coated Mass (gm)	Previous Coated Mass (gm)	added SiC Mass (gm)	added SiC thickness (μm)	total SiC thick (μm)
S09	7/2/02	3.6049	3.3911	0.2138	58.1	148.6
S10	6/17/02	3.4319	3.2370	0.1949	53.0	110.2
S11	6/17/02	3.3226	3.1231	0.1995	54.2	116.7
S12	6/17/02	3.4133	3.2126	0.2007	54.5	112.3
S13	6/17/02	3.4841	3.2815	0.2026	55.0	109.7
S22	n/a					

B. Vapor Flow Modeling

B.1 FLOW REGIMES

The Knudsen number is the ratio of the mean free path of a molecule to a characteristic dimension of the channel, usually the tube diameter, through which the gas is flowing. The Knudsen number describes the limits between molecular, intermediate, and laminar flow and is defined by:[1]

$$Kn = \frac{\lambda}{d} \tag{B-1}$$

where Kn = Knudsen number,
λ = mean free path (m), and
d = channel diameter (m).

The Reynolds number is the ratio fo inertial to viscous forces and is used, among other things, to establish the limit between turbulent and laminar flow. The Reynolds number is defined by the following equation:[2]

$$\mathrm{Re} = \frac{\rho\, v\, d}{\eta} \tag{B-2}$$

where Re = Reynolds number,
v = velocity (cm/s),
ρ = gas density (g/cm^3),
d = channel diameter (cm), and
η = viscosity (poise).

For flow in a circular duct the transport is considered turbulent for Re > 2100 and laminar for Re < 1100.

Table B-1 lists the different gas states, flow regimes, and applicable dimensionless number limits.

Table B-1. Conditions for the different flow regimes.[1,2]

Gas State	Flow Regime	Condition
viscous	turbulent	Re > 2100
	laminar	Re < 1100 Kn < 0.01
transition	intermediate	0.01 < Kn < 1
rarefied	molecular	Kn > 1

In order to calculate the Knudsen number for a specified gas and flow channel, the mean free path of a molecule in the gas is required. For a gas governed by the ideal gas law, the mean free path of a molecule is given by:[3]

$$\lambda = \frac{R\,T}{\sqrt{2}\,\pi\,d^2\,N_A\,P} \tag{B-3}$$

where λ = mean free path (m),
R = universal gas constant (8.314 J/mol-K),
T = absolute temperature (K),
d = molecular diameter (m),
N_A = Avogadro's number (6.02×10^{23} atoms/mol), and
P = pressure (Pa).

From the Smithsonian Physical Tables, the atomic radii for helium and silver are 0.93 and 1.44 Å, respectively.[4] Using these values, the mean free path of helium and silver can be calculated at any temperature and pressure. Then, for a given crack tube diameter, the Knudsen number can be calculated and the flow regime determined.

The flow equations for viscous, molecular, and transition flow are described in the following sections.

B.2 VISCOUS FLOW

At moderate pressures the gas molecules undergo collisions primarily with other gas molecules rather than with the walls of the flow channel; gas viscosity limits flow. Turbulent flow is not usually experienced in leak flow and will not be considered here. For the viscous state, laminar flow is described as follows.

The conductance of a gas governed by laminar flow is:[5]

$$C_{\text{laminar}} = \frac{\pi}{8}\left(\frac{d}{2}\right)^4 \frac{P_{avg}}{\eta\,L} \tag{B-4}$$

where C = conductance (10^4 liter/sec),
d = crack diameter (m),
P_{avg} = average of the upstream and downstream pressures (Pa),
η = viscosity of the gas (poise), and
L = length of the crack tube (m).

To convert from conductance to mass loss, a value measured (or derived) from experiments, the time of the experiment and the molar volume are also needed. The molar volume is calculated from the ideal gas law and is given by:

$$v_{molar} = \frac{R\,T}{P} \tag{B-5}$$

where v_{molar} = molar volume (m^3/mol),
R = gas constant (8.314 J/mol·K),
T = absolute temperature (K), and
P = pressure (Pa).

The following equation converts conductance to mass loss:

$$Q_{\text{laminar}} = \frac{C_{\text{laminar}}\, t}{v_{molar}} aw \qquad \text{(B-6)}$$

where $Q_{laminar}$ = mass loss (g),
$C_{laminar}$ = laminar flow conductance (liter/sec),
t = time (sec),
v_{molar} = molar volume (m^3/mol), and
aw = atomic weight of the gas (g/mol).

B.3 MOLECULAR FLOW

At very low pressures, the mean free path of the gas molecules is much larger than the dimensions of the vacuum enclosure. Under these conditions, the gas molecules undergo collisions primarily with the walls of the flow channel rather than with other molecules; this is molecular flow.

The conductance of a gas governed by molecular flow is defined as:[5]

$$C_{molecular} = \frac{1}{6}\sqrt{\frac{2\pi RT}{aw}}\frac{d^3}{L} \qquad \text{(B-7)}$$

where $C_{molecular}$= conductance (liter/sec),
R = gas constant (8.314 J/mol·K),
T = absolute temperature (K),
d = crack diameter (m),
aw = atomic weight of the gas (107.87 g/mol for silver), and
L = length of the crack tube (assumed equal to the thickness) (m).

Using the molar volume as defined by equation (B-5), the mass loss over a specified time, t, due to molecular flow is given by:

$$Q_{molecular} = \frac{C_{molecular}\, t}{v_{molar}} aw \qquad \text{(B-8)}$$

where $Q_{molecular}$= mass loss (g),
$C_{molecular}$= laminar flow conductance (liter/sec),
t = time (sec),
v_{molar} = molar volume (m^3/mol), and
aw = atomic weight of the gas (g/mol).

The molecular flow equation attributed to Knudsen applies to pipes of circular cross-section. For pipes of equal cross-sectional areas, pipes with non-circular cross-sections will experience lower conduction than those with circular cross-sections.[1]

B.4 TRANSITIONAL FLOW

Transitional flow occurs for gas states between laminar and molecular, where both phenomena contribute to the flow. The leak rate for transitional flow is a combination of both the laminar and molecular flow equations:[1]

$$Q_{transition} = \frac{\pi}{8}\left(\frac{d}{2}\right)^4 \frac{P_{avg}}{\eta L}(P_1 - P_2) + \frac{\sqrt{2\pi}}{6}\sqrt{\frac{RT}{aw}}\frac{d^3}{L}(P_1 - P_2) \qquad \text{(B-9)}$$

where
- $Q_{transition}$ = leak rate (atm·cm^3/sec),
- d = crack diameter (m),
- P_{avg} = average pressure (Pa),
- P_1 = upstream pressure (Pa),
- P_2 = downstream pressure (Pa),
- η = viscosity (poise),
- L = length of the crack tube (assumed equal to the SiC thickness) (m),
- R = gas constant (8.314 J/mol·K),
- T = absolute temperature (K), and
- aw = atomic weight of the gas (107.87 g/mol for silver).

B.5 REFERENCES

[1] Varian Proceedings, Leak Detection Seminar/Workshop. June 2-4, 1976.

[2] A. Roth, Vacuum Technology, North-Holland Publishing Company, New York, 1976.

[3] Mean Free Path, Molecular Collisions, http://hyperphysics.phy-astr.gsu.edu/hbase/kinetic/menfre.html

[4] Knovel online databases: Smithsonian Physical Tables.

[5] Alcatel Vacuum Technology (catalog), France.